

# Optical Wavelength Multicasting Technique for Wavelength Division Multiplexing and Optical Time Division Multiplexing Networks



**Nguyen Quang Nhu Quynh**

Department of Communication Engineering and Informatics

The University of Electro-Communications, Tokyo, Japan.

A dissertation submitted for the Degree of

*Doctor of Philosophy*

March 2016

# **Optical Wavelength Multicasting Technique for Wavelength Division Multiplexing and Optical Time Division Multiplexing Networks**

**Approved by the supervisory committee**

**Professor Kishi Naoto, Supervisor**

**Professor Oki Eiji, Sub-Supervisor**

**Professor Ueno Yoshiyasu**

**Professor Nishioka Hajime**

**Associate Professor Matsuura Motoharu**

**Copyright © 2016 NGUYEN QUANG NHU QUYNH**

**All rights reserved**

## 光波長分割多重及び光時分割多重ネットワークにおける光波長マルチキャスト技術

グエン クアン ニュー クイン

光波長分割多重(WDM: Wavelength Division Multiplexing)伝送方式と光時分割多重(OTDM: Optical Time Division Multiplexing)伝送方式の柔軟性と効率が改善するために、波長マルチキャスト技術を利用したいいくつかの機能が開発される。本論文では、高非線形ファイバ(HNLF: highly nonlinear fiber)での四光波混合(FWM: Four-wave mixing)を利用した波長マルチキャスト技術について実現を行い、WDMとOTDMネットワークに応用した。

最初にNRZ(nonreturn-to-zero)-to-RZ(return-to-zero)波形変換器と波長マルチキャストのパルス幅可変の実現を行う。4マルチキャストRZデータ信号のパルス幅可変は12.17~4.68 psとなった。

2番目は実時間に任意の信号波形処理するため、波長マルチキャスト技術を用いたNRZとRZ OOK(on-off-keying)信号の全光サンプリングが着目された。4チャンネルピコ秒パルス生成し、波長マルチキャストにより4チャンネルデータ信号ができ、40 GSample/sとなって、似合いの元の波形が復元された。

位相変調信号に拡張するため、10 Gb/s インラインRZ-DPSK(differential phase shift keying)信号のラマン増幅器の圧縮の実現が行う。20 ps RZ-DPSK信号は30kmの標準シングモードファイバ(SSMF)に伝送してからパルス幅の12.7 psと3.2 psまで圧縮する。インライン4×10 Gb/s RZ-DPSKはラマン増幅器のパルス圧縮とHNLFを用いた波長マルチキャストの実現を行う。4×10 Gb/s RZ-DPSKを圧縮されてから二つの連続波(CW: continuous wave)信号をHNLFに入力した。マルチキャスト信号のパルス幅12.5 psと4.27 psの間に可変ができる。

最後にOTDMとWDMネットワークのゲートウェイでOTDM-to-WDM変換器が要求される。20 Gb/s OTDM RZ-DPSKチャンネルから2×10 Gb/s WDM RZチャンネルに変換の実現が行う。一つのOTDM信号は二つWDMチャンネルに変換できた。

# Abstract

The capacity of optical communication systems has shown an incredibly thriving growth from their inception to the last several decades. From the observations in traffic demand, the objectives of this thesis are to develop some key functions for improving the flexibility and efficiency of wavelength division multiplexing (WDM) and optical division multiplexing (OTDM) networks by using wavelength multicasting technique.

Practically, at a photonic gateway, for the interconnection between WDM and OTDM networks, a nonreturn-to-zero (NRZ)-to-return-to-zero (RZ) waveform conversion is necessary due to the popular utilization of NRZ and RZ formats in WDM and OTDM networks, respectively. Moreover, if the waveform conversion combines with wavelength multicasting, multiple RZ signals will be generated, resulting in an increase of the throughput of network and the flexibility of wavelength assignment. A desirable stage after these conversions is to aggregate the higher bit-rates OTDM signals based on these lower bit-rates multicast RZ signals. The pulsewidth is one of the parameters to determine the bit-rates of OTDM signals. Therefore, to achieve the aggregate OTDM signals with flexible bit-rates adapting to specific network demand, it is necessary to manage the pulsewidth in a wide tuning range. In the first work, a NRZ data signal is injected into a highly nonlinear fiber (HNLF)-based four-wave mixing (FWM) switch with four RZ clocks compressed by a Raman amplification-based multiwavelength pulse compressor (RA-MPC). The pulsewidth of four multicast RZ signals is adjusted in a continuously large range from 12.17 to 4.68 ps

by changing Raman pump power of RA-MPC.

In addition, the sampling of optical signal waveform is necessary to monitor signals in optical network. The signals can always be analyzed off-line by capture-and-process-later techniques. However, it is challenging that these techniques are not compatible with instantaneous amplitude changes of signals as well as capturing the details and singular manners such as transient events which need real-time processing. Therefore, in the second work, an effort to characterize the waveform of signal in real-time using wavelength multicasting technique with multiwavelength sampling short-width pulses which are on the order of a few picoseconds is implemented. Using the short pulsewidths of the sampling pulses, it is possible to sample the signal precisely because its waveform does not change significantly in the sampling time. An all-optical waveform sampling of NRZ and RZ on-off-keying (OOK) signals is focused. The 4x10 GHz WDM sampling pulses are compressed with the pulsewidth which are less than 3 ps by RA-MPC and then interact with the input signal under test using FWM effect in an HNLF. Four obtained sampled signals result in a sampling rate of 40 GSample/s, therefore, the reconstructed waveforms are well-matched with the input signal waveforms.

Moving to the phase-modulated signals, especially RZ-differential phase shift keying (DPSK) signal, it is attractive for RZ-DPSK signal due to its robust tolerance to the effects of some fiber nonlinearities, and the support of high spectral efficiency. Moreover, all-optical pulse compression has been widely investigated as one of the key elements to enable high bit-rate signals overcoming electronics limits. So far, pulse compression has often used before data modulation at the transmitter to generate high bit-rate signals. Our work, on the other hand, implements the pulse compression for RZ-DPSK signal for inline applications. A useful inline application of the data pulse compression is to generate an aggregate high-speed data rate based on optical time multiplexing of many channels with lower-speed data rates. The higher

bit-rates of aggregate signals depend on the pulsewidths of lower bit-rate signals. Therefore, the compression of an inline 10 Gb/s RZ-DPSK signal using a distributed Raman amplifier-based compressor (DRA-PC) is done. The RZ-DPSK signal with pulsewidth of 20 ps after 30 km standard single mode fiber (SSMF) transmission is compressed down to in picoseconds duration such as 12, 7.0, and 3.2 ps. The pulse compression of the inline signal is applied in two works. In the first work, a compressed signal with the pulsewidth of 3.2 ps is multiplexed to a 40 Gb/s OTDM signal and then successfully demultiplexed. The second application is wavelength multicasting of the inline compressed RZ-DPSK signal to get multicast signals with short-pulsewidths for increasing the throughput of network and wavelength resource. The DRA-PC compresses the inline RZ-DPSK signal with the obtained pulsewidths of 12, 7.0, and 3.2 ps which then interact with two continuous waves (CWs) in an HNLF-based FWM switch. Thus, the pulsewidths of the multicast signals were compressed down to 12.5, 7.89, and 4.27 ps.

Finally, for networking between OTDM and WDM networks, an OTDM-to-WDM conversion is crucially required. However, it is given that in some cases, different WDM channels are expected to be generated in order to connect to each tributary of OTDM signal. In this work, a 20 Gb/s OTDM RZ-DPSK signal is converted to 4x10 Gb/s WDM RZ channels. One tributary of OTDM signal is converted to 2x10 Gb/s WDM RZ signals at two FWM products.

To my mother, Tran Thi Khanh; my mother-in-law, Nguyen Thi  
Huong; my honest husband, Huynh Hung Nam; and my two lovely  
daughters, Huynh Quynh Anh and Huynh Nguyen Minh Ngoc.



## Acknowledgements

At first, I would like to thank my supervisor, Professor Kishi Naoto, for giving me the opportunity to study at the University of Electro-Communications, Tokyo, Japan as a Ph.D. student, and for always supporting me in doing research and daily life. With his patience, kindness and brilliant intuitions help me to overcome the difficulties, especially in the first year. I am grateful to Professor Matsuura Motoharu, for his support and insight suggestions to highlight the researches. Without their supports, everything would have been much more difficult. I would like to acknowledge the supervisory committee. It will be a pleasure to get their valuable comments on this work. I am sincerely grateful to Professor Oki Eiji, sub-supervisor; Professor Ueno Yoshiyasu, and Professor Nishioka Hajime for taking care of the whole examination of Ph.D. degree.

My deepest thanks go to my mothers, my husband for always taking care my kids and giving me the belief for a better future with their understanding.

I always thank Vietnamese government and Danang University of Science and Technology-The University of Danang who gave me a chance to study abroad. I will always have to thank Japanese government and Japanese people who gave me finance and mental support for the great spending time to study in Japan. Besides the achievement in doing research, I am more mature in deeply thinking in life management. I always remember Professor Kishi Naoto words “Finding good news in bad news and bad news in good news”. It opens my active and careful thoughts in the way to do research and in life events.

Finally, I would like to thank all my friends, Labmates for sharing with a lot of memories for always supporting me when I needed their help and sharing colorful discussions in research as well as life experience.



# Contents

<b>List of Figures</b>	<b>vii</b>
<b>List of Tables</b>	<b>ix</b>
<b>Acronyms</b>	<b>xi</b>
<b>1 Introduction</b>	<b>1</b>
1.1 Fiber-Optic Communication in Telecommunication Network . . .	2
1.2 Motivation and Significant Contributions of Thesis . . . . .	4
1.3 Objectives, and Structure of This Thesis . . . . .	10
<b>2 Chromatic Dispersion and Nonlinearities for Pulse Compression and Wavelength Multicasting Techniques</b>	<b>15</b>
2.1 Chromatic Dispersion . . . . .	16
2.2 Self-Phase Modulation . . . . .	17
2.3 Four-Wave Mixing . . . . .	19
2.3.1 Four-Wave Mixing Scheme Using a Single Pump . . . . .	19
2.3.2 Four-Wave Mixing Scheme Using Multi-Pumps . . . . .	22
2.4 Stimulated Raman Scattering . . . . .	24
2.5 Pulse Compression . . . . .	25
2.6 Summary . . . . .	27
<b>3 All-Optical Waveform Conversion and Waveform Sampling with Multicast Short-Pulsewidth Signals</b>	<b>29</b>

## CONTENTS

---

3.1	All-Optical NRZ-to-RZ Conversion with Multicast Short-Pulsewidth RZ Signals . . . . .	30
3.1.1	Introduction . . . . .	30
3.1.2	The Concept of Proposed Scheme . . . . .	33
3.1.3	Experimental Setup . . . . .	35
3.1.4	Experimental Results and Discussions . . . . .	38
3.2	All-Optical Waveform Sampling using Wavelength Multicasting Technique . . . . .	48
3.2.1	Introduction . . . . .	48
3.2.2	Principle Operation . . . . .	50
3.2.3	Experimental Setup . . . . .	51
3.2.4	Experimental Results and Discussions . . . . .	54
3.3	Summary . . . . .	59
4	<b>Pulse Compression and Wavelength Multicasting of an Inline RZ-DPSK Signal</b>	<b>61</b>
4.1	Pulse Compression of an Inline RZ-DPSK Signal . . . . .	62
4.1.1	Introduction of an Inline RZ-DPSK Signal Compression . .	62
4.1.2	Operation Principle . . . . .	64
4.1.3	Experimental Setup . . . . .	65
4.1.4	Experimental Results and Discussions . . . . .	67
4.2	Application of Pulse Compression of RZ-DPSK Signal . . . . .	72
4.2.1	Inline OTDM Signal Generation . . . . .	72
4.2.1.1	Experimental Setup . . . . .	73
4.2.1.2	Experimental Results and Discussions . . . . .	74
4.2.2	Wavelength Multicasting of an Inline RZ-DPSK Signal with Tunable Short-Pulsewidths . . . . .	76
4.2.2.1	Introduction . . . . .	76
4.2.2.2	Concept of Operation Principle . . . . .	78
4.2.2.3	Experimental Setup . . . . .	80
4.2.2.4	Experimental Results and Discussions . . . . .	81
4.3	Summary . . . . .	88

<b>5</b>	<b>OTDM-to-WDM Conversion of RZ-DPSK Signal with Multicast WDM Signals</b>	<b>89</b>
5.1	Introduction . . . . .	90
5.2	Concept of OTDM-to-WDM Conversion . . . . .	92
5.3	Experimental Setup . . . . .	94
5.4	Experimental Results and Discussions . . . . .	97
5.5	Summary . . . . .	102
<b>6</b>	<b>Conclusion and Future Development</b>	<b>103</b>
	<b>References</b>	<b>107</b>
	<b>Publications</b>	<b>123</b>



# List of Figures

1.1	An example of an architecture of telecommunication network. . .	3
1.2	An example structure of optical networks with multi-functions muti-outputs using optical wavelength multicasting technique as- sisted by pulse compression. . . . .	12
2.1	(a) FWM scheme using one probe (b) FWM scheme using many probes. . . . .	20
2.2	An example of conceptual spectra of FWM scheme using multi- pumps signal for generating many new idlers. . . . .	22
2.3	Schematic of the quantum mechanical process taking place during Raman scattering [30], [31]. . . . .	25
2.4	General scheme of fiber Raman amplifier [30], [31]. . . . .	25
2.5	Scheme of fiber-based compressor used in this thesis. . . . .	26
2.6	Scheme of a distributed Raman amplifier-based compressor used this thesis. . . . .	27
3.1	Operational principle of the scheme of NRZ-to-RZ conversion and wavelength multicasting using RA-MPC with multi-functions: wave- form conversion, wavelength multicasting, and pulsewidth tunability.	33
3.2	Experimental setup of NRZ-to-RZ conversion and wavelength mul- ticasting with tunable short-pulsewidth using RA-MPC. . . . .	36
3.3	Autocorrelation traces of RZ clocks 1, 2, 3 and 4 after compression at the output of RA-MPC at Raman pump power ( $P_r$ ) of 0.82 W	38



## LIST OF FIGURES

---

3.4	FWM spectra at the output of HNLF with different values of Raman pump power ( $P_r$ ) of (a) 0.42 W, (b) 0.62 W, and (c) 0.82 W. . . . .	39
3.5	Eye patterns of all multicast converted RZ signals (a) channel 1, (b) channel 2, (c) channel 3, and (d) channel 4 with the pulsewidth of around 4.68 ps corresponding Raman pump power ( $P_r$ ) of 0.82 W. . . . .	41
3.6	BER curves of converted RZ channels with pulsewidth of around 4.68 ps corresponding to $P_r$ of 0.82 W. . . . .	42
3.7	Autocorrelation traces of different pulsewidths of (a) RZ clock 4 (clk. 4) after compression (before FWM) and (b) channel 4 (ch. 4) after conversion (after FWM) at various values of $P_r$ . . . . .	43
3.8	Eye patterns of converted RZ signal at channel 4 with various pulsewidths (a) 21.03 ps (without compression), (b) 12.17 ps, (c) 7.89 ps and (d) 4.68 ps corresponding to $P_r$ 0.42, 0.62 and 0.82 W, respectively. . . . .	44
3.9	Receiver sensitivities of all multicast RZ signals output compared to the NRZ signal in cases of without compression and with compression at $P_r$ of 0.42, 0.62 and 0.82 W. . . . .	44
3.10	The concept of all-optical waveform sampling using wavelength multicasting technique. . . . .	51
3.11	The concept of all-optical waveform sampling using wavelength multicasting with RA-MPC. . . . .	52
3.12	Experimental setup of all-optical waveform sampling using Raman amplification-based multiwavelength pulse compressor. LD: laser diode, EAM: electro-absorption modulator, PPG: pulse pattern generator, EDFA: erbium-doped fiber amplifier, DPSK: Differential phase shift keying, OBPF: optical band pass filter, WDM: wavelength division multiplexing, DSF: dispersion-shifted fiber, TFRL: tunable fiber Raman laser, VOA: variable optical attenuation . . . . .	53
3.13	Spectra of multiwavelength sampling pulses before and after compression using RA-MPC with the Raman pump power of 0.9 W. . . . .	55

---

## LIST OF FIGURES

3.14	Eye patterns of four multiwavelength sampling pulses compressed by RA-MPC. . . . .	56
3.15	Autocorrelation traces of four multiwavelength sampling pulses compressed by RA-MPC. . . . .	56
3.16	Spectra after HNLF for sampling waveform of NRZ data signal. .	57
3.17	Temporal profiles of four waveforms of sampled outputs in case of NRZ waveform sampling. The inserted envelope is the waveform of NRZ data signal. . . . .	57
3.18	Spectra after HNLF for waveform sampling of RZ data signal. . .	58
3.19	Temporal profiles of four waveforms of sampled outputs in case of RZ waveform sampling. The inserted envelope is the waveform of RZ signal . . . . .	58
4.1	Experimental setup of the inline pulse compression for RZ-DPSK signal. LD: laser diode, EAM: electro-absorption modulator, PPG: pulse pattern generator, EDFA: erbium-doped fiber amplifier, DPSK: Differential phase shift keying, OBPF: optical band pass filter, WDM: wavelength division multiplexing, DSF: dispersion-shifted fiber, TFRL: tunable fiber Raman laser, VOA: variable optical attenuation . . . . .	66
4.2	The spectrum of RZ-DPSK signal at the input of DRA-PC (before compressing) and at the output of DRA-PC (after compressing) with various Raman pump powers ( $P_r$ ). . . . .	67
4.3	Autocorrelation traces of RZ-DPSK signal at the input of DRA-PC (before compressing) and at the output of DRA-PC (after compressing) with different pulsewidths of 12, 7,0 and 3.2 ps corresponding to Raman pump power ( $P_r$ ) of 0.45, 0.64 and 0.80 W, respectively. . . . .	68
4.4	Eye patterns of demodulated RZ-DPSK signal after compressing to 12 ps (a), 7.0 ps (b), and 3.2 ps (c). . . . .	69
4.5	BER curves of RZ-DPSK signal at the input/output of DRA-PC with various pulsewidths of 20, 12, 7,0 and 3.2 ps in comparison with the back-to-back data pulse at the transmitter. . . . .	70

## LIST OF FIGURES

---

4.6	Autocorrelation traces of the compressed RZ-DPSK signal with pulsewidths of 2.53 and 1.83 ps. . . . .	71
4.7	Experimental setup for the multiplexing and demultiplexing of a 40 Gb/s OTDM stream which is based on the RZ-DPSK signal compressed by DRA-PC. . . . .	73
4.8	Spectra at the output of HNLF-based FWM switch for demultiplexing 40 Gb/s OTDM signal. . . . .	74
4.9	Eye patterns of (a) the multiplexed 40 Gb/s OTDM signal, (b) and its demultiplexed 10 Gb/s signal (b) before and (c) after demodulation. . . . .	75
4.10	(a) BER characteristics of inline 10 Gb/s baseband signal and 10 Gb/s signal demultiplexed from 40 Gb/s OTDM signal. (b) Autocorrelation trace of 10 Gb/s RZ-DPSK signal with pulsewidth of 2.95 ps after demultiplexing. . . . .	76
4.11	(a) Operation principle of wavelength multicasting for RZ-DPSK signal with tunable pulsewidth using DRA-PC. (b) Temporal profiles of all signals in the process. (c) Conceptual spectra of wavelength multicasting of RZ-DPSK signal after FWM process. . . .	79
4.12	Experimental setup of wavelength multicasting of RZ-DPSK signal with tunable short-pulsewidth using distributed Raman amplifier-based pulse compressor (DRA-PC). . . . .	81
4.13	Spectra at the output of HNLF corresponding to different values of Raman pump powers ( $P_r$ ) of (a) 0.45, (b) 0.64, and (c) 0.82 W. . . . .	82
4.14	Autocorrelation traces of the RZ-DPSK signal (a) at the input of compressor (before compressing) and multicast signal at channel 4 (ch 4) with pulsewidths of (b) 12.5, (c) 7.89 and (d) 4.27 ps corresponding to Raman pump power ( $P_r$ ) of 0.45, 0.64, and 0.80 W, respectively. . . . .	83
4.15	Eye patterns of the demodulated multicast RZ-DPSK signal at channel 4 (ch 4) with various pulsewidths of 12.5 (a), 7.89 (b) and 4.27 ps (c). . . . .	84

---

## LIST OF FIGURES

4.16	BER measurement of multicast RZ-DPSK signals with the pulsewidth around of 12.5, 7.89, and 4.27 ps at different values of Raman pump power ( $P_r$ ) of (a) 0.45, (b) 0.64 and (c) 0.80 W, respectively.	85
4.17	Receiver sensitivities of all converted RZ-DPSK signals with many pulsewidths corresponding to different values of Raman pump power at $BER = 10^{-9}$ .	86
5.1	(a) Operation principle of the OTDM-to-WDM conversion using wavelength multicasting technique. (b) Conceptual temporal profiles of all signals used in this conversion. (c) Conceptual spectra of all signals in the OTDM-to-WDM conversion.	93
5.2	Experimental setup of OTDM-to-WDM conversion with multicast WDM RZ signals using wavelength multicasting technique.	95
5.3	Autocorrelation trace of 10 Gb/s RZ-DPSK baseband signal	97
5.4	Eye patterns of 10 Gb/s baseband RZ-DPSK signal, 20 Gb/s OTDM RZ-DPSK signal and 2x10 Gb/s compressed WDM RZ clocks.	98
5.5	Autocorrelation traces of RZ clock 1 (clk.1) and clock 2 (clk.2) before and after compression.	99
5.6	Spectra at the output of HNLF after conversion.	99
5.7	Autocorrelation traces of multicast WDM RZ-DPSK after conversion (a) at channel 1, (b) channel 2, (c) channel 3 and (d) channel 4.	100
5.8	Eye patterns of demodulated WDM RZ-DPSK signals after conversion (a) at channel 1, (b) channel 2, (c) channel 3 and (d) channel 4.	101
5.9	BER characteristics of multicast WDM RZ signals compared 10 Gb/s RZ-DPSK baseband signal.	101



# List of Tables

3.1	Characteristics of 17 km dispersion-shifted fiber (DSF). . . . .	37
3.2	Characteristics of 320 m highly nonlinear fiber (HNLF). . . . .	37
5.1	Characteristics of 500 m highly nonlinear fiber (HNLF). . . . .	96



# Acronyms

<b>ASE</b>	amplified spontaneous emission
<b>AWG</b>	arrayed waveguide grating
<b>BER</b>	bit-error-rate
<b>CATV</b>	cable television
<b>CW</b>	continuous wave
<b>DCF</b>	dispersion compensating fiber
<b>DRA</b>	distributed Raman amplifier
<b>DRA-PC</b>	distributed Raman amplifier-based pulse compressor
<b>DPSK</b>	differential phase shift keying
<b>DDF</b>	dispersion decreasing fiber
<b>DL</b>	delay line
<b>DSF</b>	dispersion-shifted fiber
<b>EAM</b>	electro-absorption modulator
<b>EDFA</b>	Erbium-doped fiber amplifier
<b>EOM</b>	electro-optic intensity modulator
<b>FTTX</b>	fiber-to-the-X
<b>FWHM</b>	full width half maximum
<b>FWM</b>	four-wave mixing
<b>GVD</b>	group velocity dispersion
<b>MLL</b>	mode-locked laser



## LIST OF TABLES

---

<b>HDTV</b>	high-definition television
<b>HNLF</b>	highly nonlinear fiber
<b>IFWM</b>	intra-channel FWM
<b>IXPM</b>	intra-channel cross-phase modulation
<b>IP</b>	internet protocol
<b>LD</b>	laser diode
<b>LNМ</b>	LiNbO <sub>3</sub> modulator
<b>NRZ</b>	nonreturn-to-zero
<b>OBPF</b>	optical bandpass filter
<b>OCG</b>	optical comb generator
<b>OSNR</b>	optical signal noise ratio
<b>OOK</b>	on-off-keying
<b>OTDM</b>	optical time division multiplexing
<b>PC</b>	polarization controller
<b>PPG</b>	pulse pattern generator
<b>PRBS</b>	pseudorandom bit sequence
<b>RA-MPC</b>	Raman amplification-based multiwavelength pulse compressor
<b>RZ</b>	return-to-zero
<b>SPM</b>	self-phase modulation
<b>SBS</b>	stimulated Raman scattering
<b>SNR</b>	signal-noise-ratio
<b>SUT</b>	signal under test
<b>TDCM</b>	tunable dispersion-compensating module
<b>TDL</b>	tunable delay line
<b>TFRL</b>	tunable fiber Raman laser
<b>VOA</b>	variable optical attenuator

## LIST OF TABLES

---

<b>XPM</b>	cross-phase modulation
<b>WDM</b>	wavelength division multiplexing
<b>WDM-PTC</b>	WDM power time controller



# Chapter 1

## Introduction

From the beginning of optical communication links in the late 1970s, their growth capacities exponentially enable the unprecedented huge services for the global telecommunication through the internet. To satisfy the continuing demand for high capacity, optical technologies have to master the challenges for increasing speed-rate channels. Multicast is understood that one data signal is converted into many signals with the same data information. Currently, this functionality is realized in internet protocol (IP) digital routers. In future, it will be desirable that all-optical networks may take a lot of advantages by all-optical multicast function. Basically, optical multicast will be required for circuit-switching data at the fixed given wavelength by power splitters. However, two popular solutions to increase the capacity of optical networks by multiplexing signals are wavelength division multiplexing (WDM) and optical time division multiplexing (OTDM). Therefore, it is required that the initial signal is multicast to different wavelengths using wavelength multicasting technique. Moreover, it is also expected that OTDM signals could be multiplexed again by WDM technique in order to improve capacity transmission in optical fiber systems. The bit-rates of OTDM signals depend on the pulsewidths of the signals before multiplexing. In this thesis, all demonstrations use wavelength multicasting technique to generate many multicast signals at different wavelengths to increase wavelengths resource and capacity of the networks. Furthermore, in different scenarios adapting to traffic demand and network conditions, for instance, in order to multiplex these

## 1. INTRODUCTION

---

multicast signals into higher bit-rate OTDM signals, the pulsewidths of these signals should be short and can be changed. The generations of multicast signals with short-pulsewidths also provide the other applications, such as all-optical sampling and OTDM-to-WDM conversion, which will be mentioned in detail in the motivation of the thesis. On top of that, the purpose of the research is the investigation of wavelength multicasting technique in the aforementioned applications with the short-pulsewidths of multicast signals. This chapter introduces the contribution of fiber-optic communication in telecommunication network and emphasizes the motivation

### 1.1 Fiber-Optic Communication in Telecommunication Network

A questionnaire is that how optical fiber communication entrenches in future telecommunication networks by the support for other means of communications. Optical communication strongly supports the modern and vast communications networks, especially the global internet network. Indeed, there would be no global high-speed internet without the optical long-haul backbone. From the first of 2005 to the end of 2020, the digital universe value has been estimated 307-fold growth, up to 40 trillion gigabytes. From 2015 until 2020, it is expected that the digital universe will double every two years [1].

Figure 1.1 illustrates an example of an architecture of telecommunication network. The topology of the lowest layer in access network generally is a tree-like graphic. This layer uses means of transportation such as copper, coaxial, wireless and optical fiber. Nowadays, with the evolution of optical fiber communication, the Fiber-to-the-X (FTTX) where X is home, or building has emerged as a main media of transmission which provides services such as high-definition television (HDTV) by cable television (CATV) or internet protocol television (IPTV) [2–4]. All the access networks from the different end-users such as residential, business, or mobiles are transported over metro networks. The topology of the lowest layer of the metro network could be a mesh-like or a ring-like structure. The metro

## 1.1 Fiber-Optic Communication in Telecommunication Network

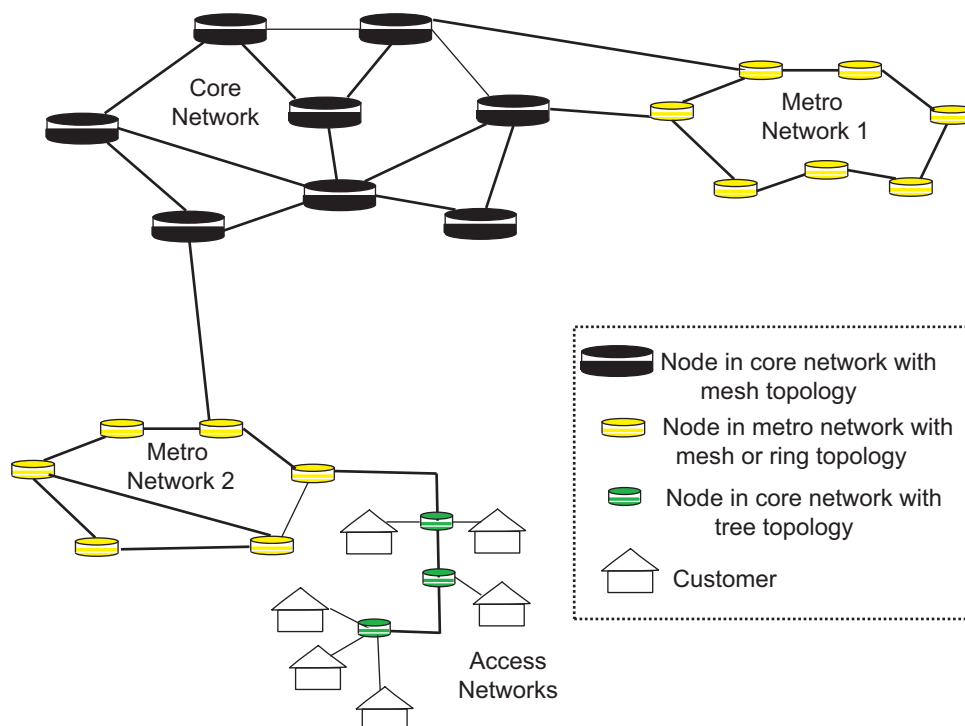


**Figure 1.1:** An example of an architecture of telecommunication network.

networks use time division multiplexing (TDM), and optical multiplexing technologies at the lowest layers. The largest network which connects to many metro networks is the core network. The tendency structure of core network is to have a mesh-like topology at the lowest layer. The reason comes from the fact that the economical connection among many different cities are aggregated by physical diverse routes where a lot of traffic is transported on core network. The core network aims to connect metro networks together through the exchange nodes. However, it is noted that the core networks differ significantly in their structures due to geography areas. For instance, European core networks have smaller distance limitations so that there are different technologies and graphical structures compared to the United States network [5]. The technologies at the lowest layer of core networks seem likely those of metro networks. However, the core network provides services which are different from the metro networks regarding provisioning requirements, quality of service (QoS). Therefore, concerning with

## 1. INTRODUCTION

---

impact to the industrial telecommunications structure, the optical communication systems is the greatest potential means of transmission in huge capacities over long distances such as metro and core networks.

### 1.2 Motivation and Significant Contributions of Thesis

Nowadays, the ever-increasing of high-bandwidth point-to-multipoint demands such as real-time streams high-definition television (HDTV), big-data sharing, and data center migration services have required the need for improving the network throughput and decreasing the blocking probability in optical networks. For instance, in data center, migration operations which transfer a huge amount of client data from one center to others is necessary. Among of a variety of optical signal processing in fiber optical communications, optical wavelength multicasting has been arising such a promising technique to copy data information of initial signal to many signals at different wavelengths, leading the increase of wavelength network resources. Thanks to wavelength multicasting technique, the wavelength throughput of network could increase efficiently and flexibly, therefore, the capacity of optical networks also could increase. However, it is considered that the increased capacities of optical networks depend on the number of multicast signals. If the pulsewidths of multicast RZ signals are short, the higher bit-rate signals could be composed from the lower bit-rate multicast RZ signals by using optical time multiplexing technique, which is a next potential stage after wavelength multicasting process. Therefore, in this thesis, the effort aims to obtain multicast RZ signals with short-pulsewidths which are on the order of some picoseconds with the assistance of pulse compression. Arguably, the most valuable up-to-date application of short-width optical pulses has been considered in ultra-high-bit-rate optical telecommunications systems. This thesis aims to develop mainly some key functions for monitoring signal, increasing network capacities and improving the flexibility and efficiency of WDM and OTDM networks using wavelength multicasting technique. The overview of the proposed functions taking into account the limitation of different past works are described as follows.

- **The first demonstration is waveform conversion and wavelength multicasting with multicast tunable short-pulsewidth signals.**

It is well-known that nonreturn-to-zero (NRZ) and return-to-zero (RZ) are two widely waveforms used in WDM and OTDM networks, respectively. The NRZ-to-RZ format conversion would be one of the main processes to implement all-optical networking for interfaces between WDM and OTDM networks. The first demonstration is the NRZ-to-RZ conversion to obtain multicast short-pulsewidth RZ signals with the assistance of and wavelength multicasting and pulse compression techniques. This work aims to increase efficiently the wavelength resources in WDM and OTDM networks and in the networking between them thanks to the multicast short-pulsewidth RZ signals. It is desirable to generate higher bit-rate signals based these RZ signals by optical time multiplexing. The bit-rate of multiplexed OTDM signals depends on the pulsewidth of the lower bit-rate RZ signals, therefore, it is required that the pulsewidth should be tunable to provide the flexibility of the bit-rate of multiplexed signals. As the aforementioned reasons, NRZ-to-RZ conversion and wavelength multicasting with multicast tunable short-pulsewidth RZ signals are realized. Different approaches have been demonstrated to achieve NRZ-to-RZ on-off keying (OOK) and wavelength multicasting with the consideration for pulsewidth tunability of the converted RZ signals [6], [7]. In detail, Refs. [6] and [7] have reported 4x10 Gb/s wavelength multicasting and NRZ-to-RZ with the tunable pulsewidth range from 17.9 to 22.2 ps and from 33 ps to 67 ps, respectively. However, it is importantly noted that the point-to-multipoint structure should be able to adapt flexibly to the aggregate channels from different lower rates channels during transmissions to different destinations depending on traffic demand through the networks. For instance, with the obtained pulsewidths in Refs. [6] and [7], it is challenging for multiplexing these signals into higher bit-rate OTDM signals to increase the speed of multicast signals after NRZ-to-RZ conversion and wavelength multicasting, such as 40 Gb/s. Therefore, the schemes in Refs. [6] and [7] are not able to convert NRZ signal to multicast short-pulsewidth RZ signals which are crucial for the



## 1. INTRODUCTION

---

pulsewidth requirement of OTDM streams considered as a potential application after waveform conversion and wavelength multicasting. It is, therefore, necessary that the process of waveform conversion is implemented simultaneously with the replica of information of input signal to different signals with short-pulsewidths. The waveform conversion and wavelength multicasting with tunable short-pulsewidth using a Raman amplification-based multiwavelength pulse compressor (RA-MPC) is investigated. An NRZ data signal is multicast to four RZ data signals in a continuously wide range from 12.17 to 4.68 ps. The short-pulsewidths are required for the generations of many aggregate higher bit-rate signals from lower bit-rate multicast signals based on optical time multiplexing technique.

- **The second demonstration is all-optical waveform sampling in real-time.**

Nowadays, high-bandwidth signals in communications are most widely monitored by all-optical sampling techniques which are novel to perform time-resolved measurements of optical signals at such high bit-rate signals whose bandwidth is not able to be reached by conventional photo-detectors attached before electronic sampling processor. In addition, the signals could always be analyzed off-line by capturing their samples and processing later called capture-and-process-later techniques. However, these off-line techniques are not able to catch up instantaneous amplitude changes of such high-bandwidth signals. Therefore, an effort to characterize such signals is all-optical real-time waveform sampling which has emerged as powerful tools for many applications such as monitoring signals, especially OOK signals in this thesis, with aggregate rates that are desirable higher than practical electronic processing rates. Some all-optical waveform sampling schemes have been demonstrated using various effects in an electro-optic intensity modulator (EOM) [8] or highly nonlinear fiber (HNLF) switch [9]. Meanwhile, some methods which copy sample signal (input signal) into many replicas using wavelength multicasting technique before sampling process

[10] instead of using several sampling HNLF-switches [11] have been proposed. Nevertheless, those sampling pulses in Refs. [8] and [9] are difficult to use for sampling high-bandwidth signals so as to precisely capture waveform of signals due to their long-pulsewidths which are not on the order of a few picoseconds. Indeed, for sampling waveform of high-bandwidth signals such as military radar, it is desirable to use sampling short-pulses in order that the waveform does not change significantly through the sampling time. Therefore, the use of multiwavelength sampling clocks with short-pulsewidths which is less than 3 ps brings in the advantage of the proposed scheme compared to the previous works [8], [9]. The other benefit is the use of only one gate for sampling instead of more than one gate in Refs. [10] and [11]. In the proposed setup, four 10 Gb/s sampled signals with short-pulsewidths which are on the order of picoseconds are obtained after multicasting and sampling simultaneously, leading a sampling rate of 40 GSample/s.

- **The third implementation is pulse compression and wavelength multicasting of an inline RZ-differential phase shift keying (DPSK).**

Moving to phase-modulated data signals, particularly RZ-DPSK signal, it is attractive to give attention owing to robust tolerance to the effects of some fiber nonlinearities, and the support to high spectral efficiency. The other obvious benefit of DPSK signal compared OOK signal is the 3 dB-lower optical signal-to-noise ratio (OSNR) required to reach a given bit-error-rate (BER) associated with a balanced receiver. The balanced receiver aside, the similarity equipment between the transmissions of DPSK and conventional OOK signals bring in the feasibility of the commercial DPSK system deploy without major overhauls of existing fiber infrastructure and manufacturing base. In addition, for increasing the bit-rate of signals, the investigation of all-optical pulse compression has been popularly studied as one of the key elements to enable the high bit-rate signals overcoming electronics limitations. So far, the optical pulse compression has often used before data modulation at the transmitter to generate high bit-rate signals

## 1. INTRODUCTION

---

due to its simplicity. Indeed, this process has the benefit that the modulated data signal with short-pulsewidth will be always obtained if the pulse compression is successful. On the other hand, if the pulse compression is used for the modulated data signal, it is necessary to consider the possibility of data signal compression because of its dependence on the characteristics of data signals. At intermediate nodes, it is necessary to compress the data signal for inline applications such as the generation of the higher bit-rate signal from aggregating lower bit-rate signals based on optical time multiplexing technique. Therefore, for inline applications, the pulse compression of the phase-modulated data signal has brought in a desirable solution which generates an aggregate high-speed signal based on many lower-speed signals in order to efficiently facilitate routing and to optimize adaptive links with different capacities. The required pulsewidths of lower-speed-rate signals depend on the bit-rate of the aggregate signals. For example, the 10 Gb/s signal with the pulsewidth of 10 ps could be multiplexed into a 40 Gb/s OTDM signal. The compression of the inline RZ-DPSK signal is attractive owing to the aforementioned reasons for increasing network capacities. The pulse compression of an OOK signal and multiwavelength OOK signals has been also demonstrated [12], [13]. Different from the compression of OOK signals, a concern in pulse compression-induced phase noises would degrade the phase information of signal. Main reasons might be residual phase noise due to self-phase modulation (SPM) or the accumulation of amplified spontaneous emission (ASE) noise through the compression process. Therefore, an investigation of the possibility of the soliton pulse compressors, particularly using DRA, for an inline RZ-DPSK signals is attractive. In this work, after 30 km standard single mode fiber (SSMF) transmission, the RZ-DPSK signal with the pulsewidth of 20 ps is compressed down to various pulsewidths of 12, 7.0, and 3.2 ps with error-free operations. A 40 Gb/s OTDM signal is aggregated from 10 Gb/s RZ-DPSK signal with the pulsewidth of 3.2 ps and then is successfully demultiplexed.

Furthermore, this compression is the first stage for wavelength multicasting of the inline compressed RZ-DPSK signal. Many bandwidth-intensity

services in the metro and access networks such as internet protocol television (IPTV), video distribution, and tele-conferencing need multicasting process for broadcasting. The purpose of wavelength multicasting of an RZ-DPSK signal with short-pulsewidth is to aggregate each multicast signal at lower speed-rate to higher speed-rate signals for supporting the point-to-multipoint structure or the routing in wavelength-routed networks. The wavelength multicasting of RZ-DPSK signal has been experimentally demonstrated in nonlinear devices in a lot of works [14]–[16]. However, the tunable short-pulsewidth multicast RZ-DPSK signals has not been demonstrated so far. The demand of tunable short-pulsewidth signals for generating higher bit-rate signals is crucial to flexibly increase the overall capacity of optical networks. For instance, the pulsewidths of 10 and 5 ps is required for the aggregate OTDM signals with the bit-rates of 40 and 80 Gb/s, respectively. Thus, the purpose of the work is to generate the multicast RZ-DPSK signals with short-pulsewidths from an inline input RZ-DPSK signals with long-pulsewidth. The pulsewidths of the multicast signals were compressed in the range of 12.5 and 4.27 ps after wavelength multicasting process assisted by pulse compression of RZ-DPSK signal.

- **The final work in this thesis is OTDM-to-WDM conversion with multicast WDM RZ-DPSK signals.**

Two widely multiplexing ways to increase the network capacity are OTDM and WDM techniques. However, in wavelength routed-networks, different wavelengths are expected to be available in order to connect all the tributaries of OTDM stream. Therefore, it is beneficial to convert a single-wavelength high-rate channel to different lower-rate channels using wavelength multicasting technique in order to obtain multicast WDM signals providing the wavelength flexibility in routing and wavelength assignment. In conventional OTDM-to-WDM conversions, only one WDM channel is converted from one tributary of OTDM signal [17]–[21]. Therefore, it is still challenging for the previous reports concerning the number of WDM RZ outputs. For example, the setups in Refs. [17]–[21] are not

## 1. INTRODUCTION

---

able to allow a double number of WDM-RZ channels compared to that of tributaries of OTDM signal. The other concern is that in these schemes [17]–[20], the phase-preserving is difficult to be obtained, thus, it is not able to operate for phase-modulated signals. Hence, in this thesis, a realization of OTDM-to-WDM conversion using wavelength multicasting technique to obtain at the same time 4x10 Gb/s WDM RZ channels corresponding to 2 tributaries of 20 Gb/s OTDM signal. This OTDM-to-WDM conversion has the advantage of improving the flexibility of wavelength selection and modulation format transparency. Error-free operations are achieved for 4x10 Gb/s WDM channels with power penalties within 2.5 dB compared to the 10 Gb/s baseband signal and small received power variations within 0.5 dB among WDM RZ channels at BER of  $10^{-9}$ .

Optical wavelength multicasting technique used in this thesis requires nonlinear interaction of four-wave mixing (FWM) in a nonlinear medium. It is normally obtained with the utilization of nonlinear optical materials in which HNLF is one of promising tools with femtosecond-scale response for the efficient optical signal processing. Therefore, wavelength multicasting technique uses FWM process in an HNLF is one of great solutions either to enhance the previous schemes or to bring in new achievements which are experimentally demonstrated in this thesis.

Through all the thesis, optical wavelength multicasting technique is used for the demonstrations of many important all-optical functions such as NRZ-to-RZ conversion with tunable short-pulsewidth multicast signals, all-optical waveform sampling in real-time, pulse compression and wavelength multicasting of an in-line RZ-DPSK signal, and OTDM-to-OTDM conversion. The throughput and capacity of networks are able to be increased owing to WDM multicast signals with short-pulsewidths.

### 1.3 Objectives, and Structure of This Thesis

From observations on the challenges in the previous demonstrations and in the trend of telecommunication networks in general and optical communication systems, in particular, the objectives of this thesis are to obtain optical wavelength

multicast signals with short-pulsewidths in order to increase wavelength resource and capacity in WDM and OTDM networks using wavelength multicasting technique. A variety of applications in WDM and OTDM networks using wavelength multicasting technique is shown in Fig. 1.2. As seen in Fig. 2, it also partly shows the significant contributions and the transparency connection among the applications demonstrated using wavelength multicasting technique through the thesis.

Aside from chapter 1 which is a brief overview of the application of optical wavelength multicasting technique on some key functions for efficient optical systems, chapter 2 gives a brief basic theory of nonlinearities on fiber for wavelength multicasting and pulse compression. The first part of chapter 3 demonstrates waveform conversion with multicast output signals using wavelength multicasting and pulse compression techniques. Different materials, nonlinear processes, number and type of pumps could be exploited for wavelength multicasting in previous works [6], [7]. However, offering the tunability with the pulsewidths which are on the order of a few picoseconds is still a technical challenge in these demonstrations. A one-to-four wavelength multicasting with NRZ-to-RZ waveform conversion with pulsewidth tunability in a wide range from 12.17 to 4.68 ps is experimentally demonstrated in this chapter. This multi-functions features are highly desirable at link and network levels such as optical network elements and access points. The last part of chapter 3 realizes all-optical waveform sampling in real-time. The key different feature of this proposed scheme is on the use of multiwavelength sampling clocks with short-pulsewidths of around 2.5 ps which are required for precisely capturing waveform of high-bandwidth signals.

The pulse compression and wavelength multicasting of an inline RZ-DPSK signal are addressed in chapter 4. Firstly, an pulse compression using adiabatic soliton pulse compressor based on a distributed Raman amplifier (DRA) for an inline RZ-DPSK signal is presented. This proposed scheme gives a potential solution for inline pulse compression, leading to a generation of several higher bit-rate OTDM signals. The demand of short-pulsewidth signals for high bit-rate signals is crucial to increase overall capacity of optical networks. However, the tunable picosecond-pulsewidth for the multicast RZ-DPSK signals has not been demonstrated so far. The 4x10 Gb/s multicast RZ-DPSK signals with tunable

## 1. INTRODUCTION

---

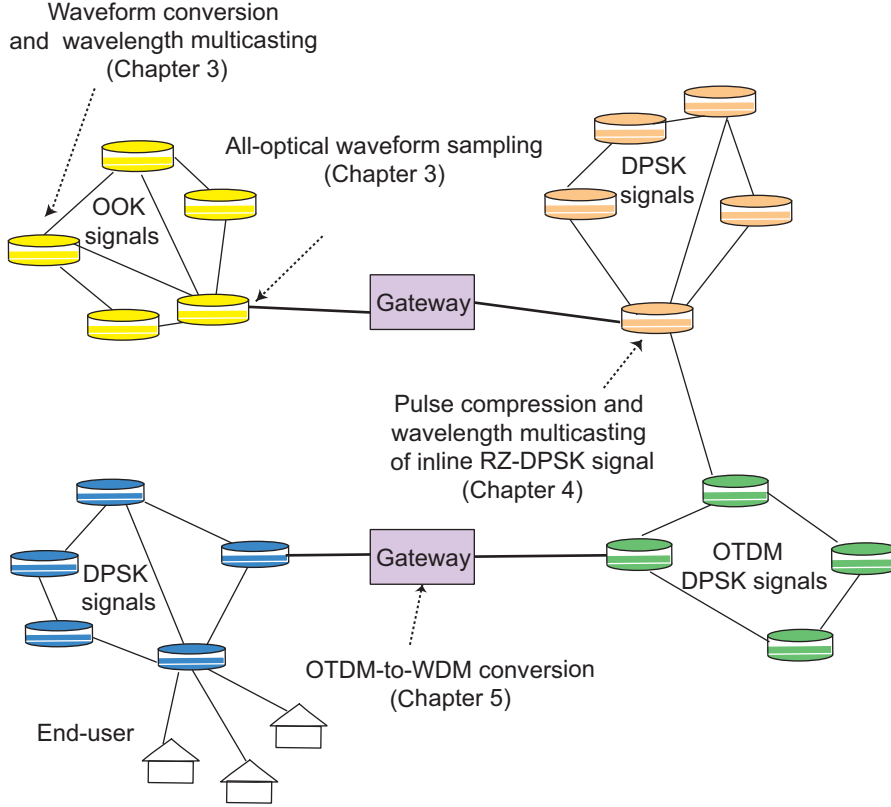


**Figure 1.2:** An example structure of optical networks with multi-functions multi-outputs using optical wavelength multicasting technique assisted by pulse compression.

pulsewidths using a DRA-based compressor (DRA-PC) and an HNLF are demonstrated. The pulsewidths of multicast signals are compressed down to around 12.5 and 4.27 ps after wavelength multicasting process. Thus, this work gives a potential solution for the generation of several higher bit-rate OTDM signals with different wavelengths from the short-pulsewidth multicast RZ-DPSK signals.

Chapter 5 realizes a OTDM-to-WDM conversion of RZ-DPSK signal with multicast WDM RZ signals using wavelength multicasting technique. Each 10 Gb/s tributary of the input 20 Gb/s OTDM signal is converted to 2x10 Gb/s WDM RZ signals at two FWM products, leading 4x10 Gb/s WDM signals at

four FWM products for two tributaries of 20 Gb/s OTDM signal. This proposed scheme improves the network capacity and the flexibility of wavelength assignment.

Finally, chapter 6 gives conclusions on the achieved results of all demonstrations in this thesis. Some future works are also considered.





## Chapter 2

# Chromatic Dispersion and Nonlinearities for Pulse Compression and Wavelength Multicasting Techniques

At such high optical intensities, the refraction index of fiber is affected by the existence of optical signals through the optical Kerr effect [22]. Then, signal-induced refractive index variations translate into the phase shift of optical signals. This phase shift, in conjunction with fiber dispersion, results in nonlinearities which affect signal impairments, limiting the capacity and reach of fiber-optic transmission systems. However, the optical nonlinearities turn out to be useful and attracted many realizations of ultra-fast optical signal processing functions, especially self-phase modulation (SPM), four-wave mixing (FWM). Furthermore, stimulated Raman scattering is also applied in Raman amplification used for pulse compression demonstrations in this thesis.

## 2.1 Chromatic Dispersion

Chromatic dispersion results from the differences of frequencies traveling along an optical fiber at different speeds. The different frequencies reach the end of the fiber at different times, causing the spread of light pulse. This phenomenon happens because the propagation constant  $\beta$  depends on the optical angular frequency  $\omega$  and the refractive index at frequency  $\omega$  ( $n(\omega)$ ), therefore, different spectral components disperse through propagation and desynchronized at the end of fiber [22]. Mathematically, the effects of fiber dispersion are obtained by expanding  $\beta$  in a Taylor series about the center frequency  $\omega_0$  of the pulse.

$$\beta(\omega) = n(\omega) \frac{\omega}{c} = \beta_0 + \beta_1 (\omega - \omega_0) + \frac{1}{2} \beta_2 (\omega - \omega_0)^2 + \dots, \quad (2.1)$$

where

$$\beta_m = \left( \frac{d^m \beta}{d\omega^m} \right)_{\omega=\omega_0} \quad (m = 0, 1, 2, \dots). \quad (2.2)$$

- The zero-order term  $\beta_0$  describes a common phase shift.
- The first-order term  $\beta_1$  is the inverse of group velocity of the pulse,  $v_g$ .

$$\beta_1 = \frac{1}{v_g} = \frac{n_g}{c} = \frac{1}{c} \left( n + \omega \frac{dn}{d\omega} \right), \quad (2.3)$$

where  $n_g$ ,  $v_g$ , and  $c$  are the group index, the group velocity, and the light velocity, respectively.

- The second-order term  $\beta_2$  is the derivative of  $\beta_1$  with respect to frequency.

$$\beta_2 = \frac{1}{c} \left( 2 \frac{dn}{d\omega} + \omega \frac{d^2 n}{d\omega^2} \right) = -\frac{D\lambda^2}{2\pi c}, \quad (2.4)$$

where  $D$  is the dispersion fiber parameter. Other speaking,  $\beta_2$  is the derivative of the inverse of the group velocity with respect to frequency, and specifies the variation in group velocity for different frequency components of the pulse, leading to pulse broadening due to different frequency components traveling with different velocities. This phenomenon is known as the group

velocity dispersion (GVD), and  $\beta_2$  is generally referred to as GVD parameter. The most notable characteristic is that the wavelength  $\lambda$  at which the value of  $\beta_2$  is equal to zero, is referred to as the zero-dispersion wavelength.  $\beta_2$  is related to the dispersion parameter,  $D$  as follows

$$D = \frac{d\beta_1}{d\lambda} = -\frac{2\pi c}{\lambda^2} \beta_2 \quad (2.5)$$

The unit of  $D$  is expressed in ps/km/nm. The dispersion can be divided into two terms, the material and waveguide dispersion. The material dispersion happens because the fact that the refractive index of the optical fiber depends on the frequency of optical signal. Meanwhile, the effect of the waveguide dispersion to  $D$  is that the value of  $D$  depends on fiber-design parameters. Therefore, dispersion-shifted fibers (DSF) [23] have been found for applications in optical communication systems.

- The third-order term (higher-order dispersion)  $\beta_3$  is the derivative of  $\beta_2$  with respect to frequency as follows

$$\beta_3 = \frac{d\beta_2}{d\omega} \quad (2.6)$$

$\beta_3$  is related to the dispersion slope  $S$  as following description:

$$S = \frac{dD}{d\lambda} = \frac{4\pi c}{\lambda^3} \beta_2 + \left(\frac{2\pi c}{\lambda^2}\right)^2 \beta_3 \quad (2.7)$$

At the zero-dispersion wavelength,  $\beta_2$  is equal to zero and  $S$  is proportional to  $\beta_3$ .

## 2.2 Self-Phase Modulation

A pulse of light, when traveling in a nonlinear medium, induces a varying refractive index of the medium due to the dependence of refractive index on the intensity of pulse light responsible for the optical Kerr effect. This variation in refractive index produces a phase shift that is proportional to the intensity of pulse, giving rise to the chirping of the pulse because the different components of

## 2. CHROMATIC DISPERSION AND NONLINEARITIES FOR PULSE COMPRESSION AND WAVELENGTH MULTICASTING TECHNIQUES

---

the pulse undergo different phase shifts. This phase shift makes self-phase modulation (SPM) arise. SPM strongly affects the signal quality of systems using the high transmitted powers because the chirping effect is proportional to the power of transmitted signal. To understand the effects of SPM, a normalized amplitude  $U$  is related to the slowly varying amplitude of the pulse envelope  $A$  defined as following [22]

$$A(z, \tau) = \sqrt{P_0} \exp(-\alpha z/2) U(z, \tau), \quad (2.8)$$

where  $\tau$  is a normalized time scale measured by the ratio of the time  $T$  which is measured in the frame of reference moving with pulse at the group velocity  $v_g$  and the initial pulsewidth  $T_0$ .

$$\tau = \frac{T}{T_0} = \frac{t - z/v_g}{T_0} \quad (2.9)$$

$P_0$  is the peak power of the incident pulse and  $\alpha$  represents fiber loss.  $P_0$  is related to the nonlinear length  $L_{NL}$  which is defined by

$$L_{NL} = \frac{1}{\gamma P_0}, \quad (2.10)$$

where  $\gamma$  is the nonlinear coefficient of fiber. Concerning in the normalized amplitude  $U(z, T)$  defined by Eq. (2.8), the propagation equation could be described by ignoring chromatic dispersion

$$\frac{\partial U}{\partial z} = \frac{j}{L_{NL}} \exp(-\alpha z) |U|^2 U \quad (2.11)$$

The solution of this equation is governed by

$$U(z, T) = U(0, T) \exp[j\phi_{NL}(z, T)], \quad (2.12)$$

where  $U(0, T)$  is the field amplitude at  $z = 0$  and

$$\phi_{NL}(z, T) = |U(0, T)|^2 \frac{L_{eff}}{L_{NL}}, \quad (2.13)$$

where the effective length  $L_{eff}$  is given by

$$L_{eff} = [1 - \exp(-\alpha z)]/\alpha \quad (2.14)$$

Equation (2.12) indicates that SPM gives rise to an intensity-dependent phase shift, but the pulse shape is remained.  $L_{eff}$  is smaller than the propagated distance  $z$  due to fiber loss. From Eqs. (2.10), (2.13), and (2.14), it is seen that the nonlinear phase shift  $\phi_{NL}$  is proportional to the fiber length, signal power and the nonlinear coefficient. SPM-induced spectral broadening is the consequence of the time dependence of  $\phi_{NL}$ . The difference in the frequency domain is given by

$$\partial\omega(T) = -\frac{\partial\phi_{NL}}{\partial T} = -\frac{\partial}{\partial T}(|U(0, T)|^2) \frac{L_{eff}}{L_{NL}} \quad (2.15)$$

In case of the incident signal is a super-Gaussian pulse with the incident field  $U(0, T)$ , SPM-induced chirp is

$$\partial\omega(T) = \frac{2m}{T_0} \frac{L_{eff}}{L_{NL}} \left[\frac{T}{T_0}\right]^{2m-1} \exp\left[-\left(\frac{T}{T_0}\right)^{2m}\right] \quad (2.16)$$

where  $m=1$  for a Gaussian pulse. For the larger values of  $m$ , the incident pulse becomes nearly rectangular and its leading and trailing edges have a steeper slope.

## 2.3 Four-Wave Mixing

In general, four-wave mixing (FWM) occurs when the lights of two or more different frequencies are launched into a optical fiber [24], [25]. In this thesis, wavelength multicasting technique uses FWM process in a highly nonlinear fiber (HNLF) which is a widely way to generate multiple copies. Depending on different applications, the number of pump and probe signals is different from the schemes. Two distinct kinds of FWM process which use single pump and multi-pumps signals for the wavelength multicasting of input data signal are presented.

### 2.3.1 Four-Wave Mixing Scheme Using a Single Pump

Figures 2.1(a) and (b) illustrate the conceptual spectra of FWM scheme in case of using only one pump. The number of the probe employed in this case could be one or more than one as shown in Figs. 2.1(a) and (b), respectively. In

## 2. CHROMATIC DISPERSION AND NONLINEARITIES FOR PULSE COMPRESSION AND WAVELENGTH MULTICASTING TECHNIQUES

---

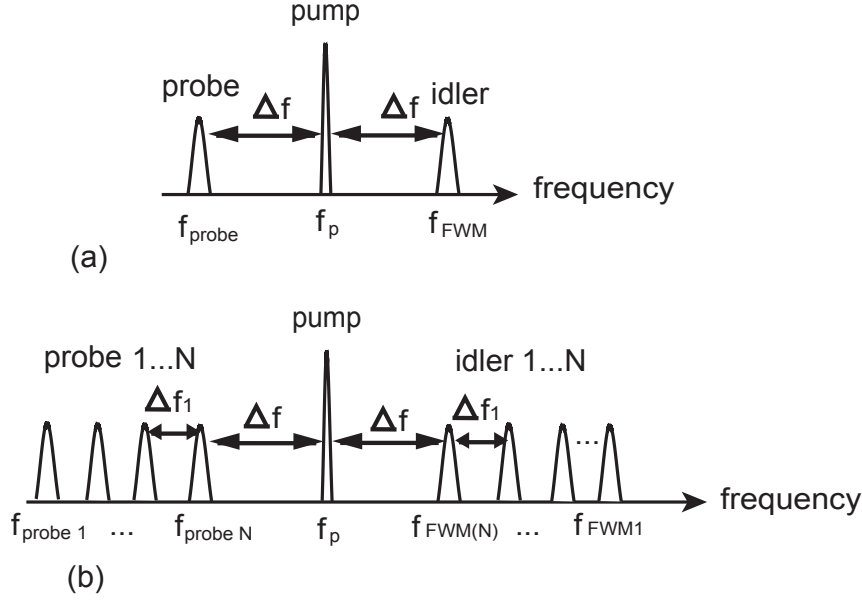


**Figure 2.1:** (a) FWM scheme using one probe  
(b) FWM scheme using many probes.

Fig. 2.1 (a), the power from a high-intensity pump is transferred to a probe, while simultaneously generating a new FWM product (idler) located at frequency described as follows [24]

$$f_{FWM} = 2f_p - f_{probe} = f_p + \Delta f \quad (2.17)$$

where  $\Delta f$  is the frequency separation between the pump and probe ( $\Delta f = f_p - f_{probe}$ ). The electric field of the FWM idler is expressed as follows [24]

$$E_{FWM}(t) \propto E_{pump}^2(t)E_{probe}^*(t), \quad (2.18)$$

where  $E_{pump}(t)$ , and  $E_{probe}(t)$  are the electric fields of the pump and probe, respectively; \* denotes the complex conjugate of the electric field. The power of generated FWM idler ( $P_{FWM}$ ) is generally calculated by the following expression [26]–[28]

$$P_{FWM}(L) = \eta\gamma^2 P_{pump}^2 P_{probe} \exp(-\alpha L) \left[ \frac{(1 - \exp(-\alpha L))^2}{\alpha^2} \right], \quad (2.19)$$

where  $\eta$ ,  $\gamma$ , and  $\alpha$  are the efficiency, the nonlinear coefficient of the fiber, and the attenuation coefficient of the fiber, respectively;  $P_{pump}$  is the power of the pump and  $P_{probe}$  is the probe power. The efficiency  $\eta$  which depends on the phase mismatch is expressed: [26]–[28]

$$\eta = \frac{\alpha^2}{\alpha^2 + \Delta\beta^2} \left( 1 + \frac{4 \exp(-\alpha L) \sin^2(\Delta\beta L/2)}{(1 - \exp(-\alpha L))^2} \right) \quad (2.20)$$

$\Delta\beta$ , so-called phase mismatch due to dispersion, is the differences of the propagation constants of the different signals. When the wavelengths of pump and probe are near the zero-dispersion wavelength of fiber and the effect of cross-phase modulation (XPM) and the four-order dispersion is ignored,  $\Delta\beta$  is given as follows

$$\Delta\beta = \frac{2\lambda_p^4 \pi}{c^2} \frac{dD}{d\lambda} (f_p - f_{probe})^2 (f_p - f_0), \quad (2.21)$$

where  $\lambda_0 (= c/f_0)$ , and  $\lambda_p$  is the zero-dispersion wavelength and the wavelength of the pump, respectively;  $c$  is the vacuum light speed;  $dD/d\lambda$  is the dispersion slope. The conversion efficiency is defined as the ratio of the power of FWM idler ( $P_{FWM}(L)$ ) and the power of the probe ( $P_{probe}$ ) [25]. From Eq. (2.19), the conversion efficiency is given by:

$$\frac{P_{FWM}(L)}{P_{probe}} = \eta \gamma^2 P_{pump}^2 \exp(-\alpha L) \left[ \frac{(1 - \exp(-\alpha L))^2}{\alpha^2} \right] \quad (2.22)$$

This conversion efficiency depends on the power of the pump, the fiber length, the fiber nonlinear coefficient and the phase mismatch which is due to the dispersion. To obtain high conversion efficiency, it is required that wavelength of the pump coincides with the zero-dispersion wavelength of fiber.

In order to obtain  $N$  idlers, the required number of probe signals must be the same as the number of idlers as shown in Fig. 2.1(b). Many probes with frequency spacing between adjacent probes  $\Delta f_1$  interact with the pump to generate many new idlers at the new frequencies described as follows:

$$f_{FWM(N)} = 2f_p - f_{probeN}, \quad (2.23)$$



## 2. CHROMATIC DISPERSION AND NONLINEARITIES FOR PULSE COMPRESSION AND WAVELENGTH MULTICASTING TECHNIQUES

---

where  $f_p$  is the frequency of the pump and  $f_{probeN}$  is the frequency of probe  $N$ .  $N$  is the number of probes. The electric field of the idler  $N$  is governed by following relation [24]

$$E_{FWM(N)}(t) \propto E_{pump}^2(t)E_{probeN}^*(t), \quad (2.24)$$

where  $E_{pump}(t)$ , and  $E_{probeN}(t)$  are the electric fields of the pump and probe  $N$ , respectively;  $*$  denotes the complex conjugate of the electric field. In application of FWM process for wavelength multicasting demonstrated in chapter 3, the data signal are set as the pump and the multiwavelength return-to-zero (RZ) clocks is set as many probes. Therefore, the input data signal is multicast to many RZ idlers with different wavelengths.

### 2.3.2 Four-Wave Mixing Scheme Using Multi-Pumps

An example of conceptual spectra of FWM scheme using multi-pumps is shown in Fig. 2.2.

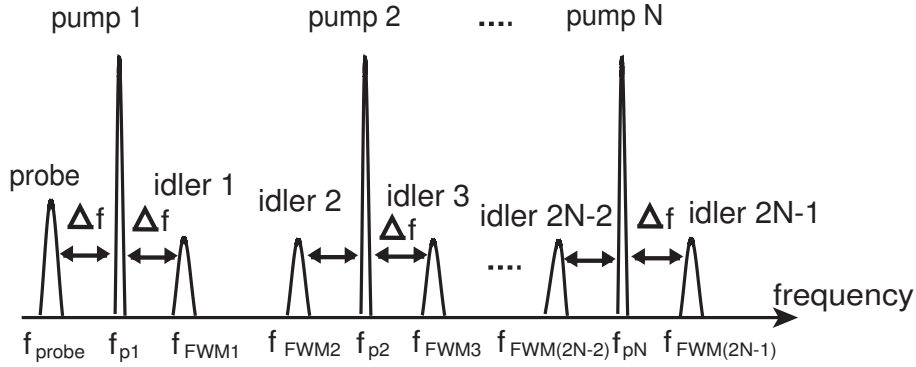


**Figure 2.2:** An example of conceptual spectra of FWM scheme using multi-pumps signal for generating many new idlers.

When the multiple pumps at the frequencies  $f_{p1}, \dots, \text{and } f_{pN}$  and the probe signal at the frequency  $f_{probe}$  interact together over FWM process, the FWM idlers are generated at frequencies described as follows [24]

$$f_{FWM1} = 2f_{p1} - f_{probe} = f_{p1} + \Delta f \quad (2.25)$$

For  $N \geq 2$

$$f_{FWM(2N-2)} = f_{pN} - f_{p1} + f_{probe} = f_{pN} - \Delta f \quad (2.26)$$

$$f_{FWM(2N-1)} = f_{pN} + f_{p1} - f_{probe} = f_{pN} + \Delta f, \quad (2.27)$$

where  $\Delta f$  is the frequency separation between the pump 1 and probe signal ( $\Delta f = f_{p1} - f_{probe}$ );  $N$  is the number of pumps. The electric field of each idler is governed as following [24]

$$E_{FWM1}(t) \propto E_{pump1}^2(t) E_{probe}^*(t) \quad (2.28)$$

$$E_{FWM(2N-2)}(t) \propto E_{pump1}^*(t) E_{probe}(t) E_{pumpN}(t) \quad (2.29)$$

$$E_{FWM(2N-1)}(t) \propto E_{pump1}(t) E_{probe}^*(t) E_{pumpN}(t), \quad (2.30)$$

where  $E_{pump1}(t)$ ,  $E_{pumpN}(t)$  and  $E_{probe}(t)$  are the electric field of the pump 1, pump  $N$  and probe, respectively;  $*$  denotes the complex conjugate of the electric field. The power of the outermost generated FWM idler at channel  $2N-1$  is given as follows [26]–[28]

$$P_{FWM(2N-1)}(L) = 4\eta\gamma^2 P_{probe} P_{pump1} P_{pumpN} \exp(-\alpha L) \left[ \frac{(1 - \exp(-\alpha L))^2}{\alpha^2} \right], \quad (2.31)$$

where  $P_{probe}$ ,  $P_{pump1}$ , and  $P_{pumpN}$  are the powers of probe, pump 1, and pump  $N$ , respectively. The remained parameters are defined in section 2.3.1 with the exception of the phase mismatch. It is assumed that when the effect of cross-phase modulation (XPM) and self-phase modulation (SPM) and the four-order dispersion can be neglected, the phase mismatch which is the difference of the propagation constants of the FWM idler at channel  $2N-1$ , probe, pump 1 and pump  $N$  in FWM process is expressed as follows for the outermost channel  $2N-1$  [26], [27]

$$\Delta\beta = \beta_{FWM(2N-1)} + \beta_{probe} - \beta_{pump1} - \beta_{pumpN} \quad (2.32)$$

$$= \frac{2\lambda^2\pi}{c} (f_{pN} - f_{probe})(f_{p1} - f_{probe}) \left[ D(\lambda) + \frac{\lambda^2}{2c} \frac{dD}{d\lambda} [(f_{pN} - f_{probe}) + (f_{p1} - f_{probe})] \right], \quad (2.33)$$

where  $\beta$  indicates the propagation constant,  $\lambda$  is the wavelength. In the demonstration of wavelength multicasting in chapter 4, the input data signal is set as a

## 2. CHROMATIC DISPERSION AND NONLINEARITIES FOR PULSE COMPRESSION AND WAVELENGTH MULTICASTING TECHNIQUES

---

pump, meanwhile, the multiwavelength continuous waves (CWs) are set as many probes. Therefore, the input data signal is multicast at many idlers. In addition, in chapter 5, the FWM scheme using multiple pumps is also used for OTDM-to-WDM conversion. However, the pump which is the nearest to the OTDM signal is a CW and other pumps must be RZ clocks in order to sample with all tributaries of the OTDM signal for obtaining multicast WDM RZ signals.

### 2.4 Stimulated Raman Scattering

A brief introduction to stimulated Raman scattering (SRS) and its application in Raman amplification is presented. SRS is an important nonlinear process that can make optical fibers become broadband Raman amplifiers and tunable Raman lasers. Raman amplifiers use SRS of silica glass fiber, which is an inelastic scattering of a photon with a molecule. Basically, in Raman scattering, if a sufficiently powerful optical wave (the pump) is launched into the fiber, a new field (the Stokes wave) is generated by stimulated scattering at the expense of the pump power. In WDM systems, multiwavelength channels are launched into a fiber, the SRS causes power to be transferred from the channels with higher frequency to the channels with lower frequency. Therefore, it can also severely affect the performance of multichannel lightwave systems [22], [29]. The scattering process could be illustrated with regard to quantum mechanics as shown in Fig. 2.3. A pump photon  $\nu_p$  belonging to the ground state of molecule excites a molecule up to a virtual level which means that this level could not exist in a certain time. The molecule quickly decays to a lower energy level leading a emitted signal photon  $\nu_s$  in the process. The stimulated emission is possible even from the virtual upper state to the first molecule vibration state. Hence, the stimulated emission occurs when an incident optical signal is with frequency equal to that of the Stokes wave. The frequency difference between the signal photon and the pump ( $\nu_p - \nu_s$ ) is named the Stokes shift. In standard transmission fibers with a Ge-doped core, the peak of this frequency shift is about 13.2 THz. Figure 2.4 shows an general scheme of Raman amplifier. The signal propagates from the input to the output of the amplifier. The pump which travels in the same or opposite direction as the signal is called the co-pump or counter pump,

respectively. This setup is named a distributed Raman amplifier (DRA) as the fiber being pumped is the actual transmission span that links two points. DRA is used in the setups presented in chapters 3 and 4 for pulse compression.

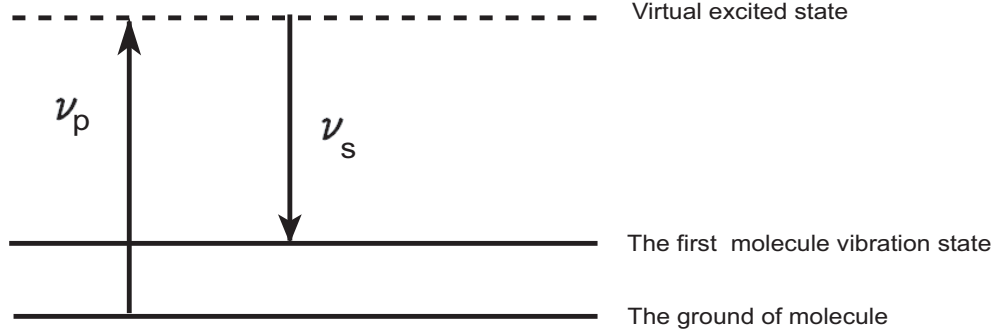


**Figure 2.3:** Schematic of the quantum mechanical process taking place during Raman scattering [30], [31].

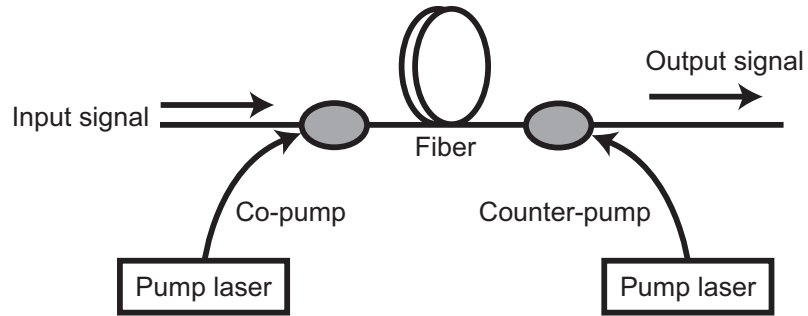


**Figure 2.4:** General scheme of fiber Raman amplifier [30], [31].

## 2.5 Pulse Compression

One of the important applications of nonlinear effects is pulse compression by an interplay between nonlinear and dispersive effects occurring simultaneously in optical fiber. The principle is that the pulse compression occurs when the initial chirped pulse propagates over an anomalous dispersion regime of an optical fiber. Practically, to efficiently compress the pulsewidth of signal, an HNLF followed

## 2. CHROMATIC DISPERSION AND NONLINEARITIES FOR PULSE COMPRESSION AND WAVELENGTH MULTICASTING TECHNIQUES

---

by a single mode fiber (SMF) is often used [32]. Nonlinear fibers have been used in recent years for pulse compression because of their unusual dispersive and nonlinear characteristics [33]-[35]. As a result, the pulses could be chirped through SPM by a large amount. In SPM-induced chirp pulse, the high frequency (blue-shifted) components occur near the trailing edge of pulse whereas the low-frequency components (red-shifted) occur near the leading edge. If the leading edge of pulse is delayed by just the right amount so that the trailing edge catches up with the leading edge during passage of the pulse through SMF, thus the pulse is compressed [22]. In chapter 5, the fiber-compressor with a setup shown in Fig. 2.5 is used to compress the multiwavelength RZ clocks.

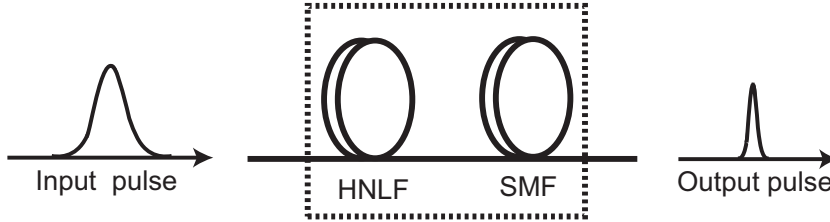


**Figure 2.5:** Scheme of fiber-based compressor used in this thesis.

The other compressor based on a DRA uses adiabatic soliton pulse compression technique. This compressor with a setup shown in Fig. 2.6 is used to compress the multiwavelength RZ clocks and RZ data signal in chapters 3 and 4, respectively. It consists of a 17 km dispersion-shifted fiber (DSF) and a wavelength tunable fiber Raman laser (TFRL). The Raman pump generated by a TFRL is injected into DSF in a counter-pump through a WDM coupler. The wavelength of TFRL could be tuned in the range between 1425 and 1495 nm with the maximum output power of 2.4 W. By the interplay between SPM and GVD, the input optical pulse could be compressed after propagating through an anomalous-dispersion regime of DSF. If a hyperbolic-secant pulse whose full width half maximum  $\tau_{\text{FWHM}}$  and the peak power  $P_1$  which are satisfied Eq.(2.34), is launched into an ideal lossless fiber, the pulse will be undistorted without changing in shape [22]

$$P_1 = \frac{3.11 |\beta_2|}{\gamma \tau_{\text{FWHM}}^2}, \quad (2.34)$$

where  $\beta_2$  and  $\gamma$  are the group velocity dispersion and the nonlinear coefficient of fiber, respectively. However, there is no lossless optical fiber in practice. Thus, an increase in pulsewidth as it is commonly observed in fiber transmissions. Therefore, in order to compress the optical pulses, it is required to increase the soliton peak power using a distributed fiber amplifier such as DRA. From Eq. (2.34), the relationship between the pulsewidth  $\tau_{\text{FWHM}}$  of the pulse and the peak power of the fundamental soliton pulse  $P_1$  is as follows

$$\tau_{\text{FWHM}} \propto \sqrt{\frac{1}{P_1}} \quad (2.35)$$

From Eq. (2.35), it could be seen that the pulsewidth  $\tau_{\text{FWHM}}$  of the soliton pulse is inversely proportional to the square-root of the peak power of the optical pulse  $P_1$ . Therefore, the pulsewidth of pulse could be compressed if increasing its peak power since the soliton condition is kept during the amplification.

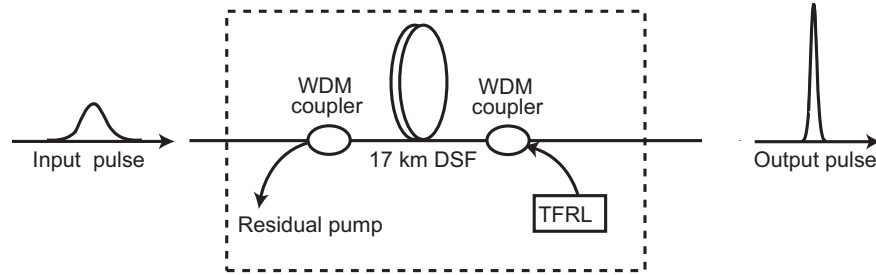


**Figure 2.6:** Scheme of a distributed Raman amplifier-based compressor used this thesis.

## 2.6 Summary

In this chapter, chromatic dispersion and optical nonlinearities including SPM, FWM, and SRS are briefly reviewed as useful effects for the applications of optical wavelength multicasting and pulse compression techniques. The improved features of optical signal processing in this thesis is the use of wavelength multicasting and pulse compression techniques to generate multicast short-pulsewidth signals, leading multiwavelength channels at the outputs. The demonstrations

## **2. CHROMATIC DISPERSION AND NONLINEARITIES FOR PULSE COMPRESSION AND WAVELENGTH MULTICASTING TECHNIQUES**

---

of waveform conversion with wavelength multicasting, all-optical waveform sampling in real-time, pulse compression and wavelength multicasting of an inline RZ-DPSK signal, and OTDM-to-WDM conversion with multicast WDM RZ-DPSK signals are experimentally realized.

## Chapter 3

# All-Optical Waveform Conversion and Waveform Sampling with Multicast Short-Pulsewidth Signals

In this chapter, two experimental demonstrations including all-optical nonreturn-to-zero (NRZ)-to-return-to-zero (RZ) conversion with multicast RZ signals and all-optical waveform sampling with multicast sampled signals using wavelength multicasting technique are presented. The first experiment is NRZ-to-RZ conversion and wavelength multicasting with tunable short-pulsewidths. The clear eyes pattern, spectra, bit-error-rate (BER) and autocorrelation traces of pulsewidths of multicast signals indicate the successful conversion. These functions could apply in optical network elements which could be realized waveform conversion and wavelength multicasting simultaneously in all-optical manners in order to increase wavelength resources and capacity of network. The second implementation is all-optical waveform sampling in real-time based on wavelength multicasting technique. By this way, the input signal under test (SUT) is multicast into many sampled signals with different wavelengths corresponding to different time



### **3. ALL-OPTICAL WAVEFORM CONVERSION AND WAVEFORM SAMPLING WITH MULTICAST SHORT-PULSEWIDTH SIGNALS**

---

points of SUT in the same frame. The power of each multicast sampled signal at four-wave mixing (FWM) product is proportional to that of SUT at the time overlapping with the sampling pulse. Therefore, the waveform of SUT could be captured in real-time.

Both these demonstrations operations are related to multiwavelength pulses compression and wavelength multicasting techniques. The multiwavelength RZ pulses are compressed by a Raman amplification-based multiwavelength pulse compressor (RA-MPC). Then these pulses interact with the input signal which need to process (waveform converting or sampling) using FWM effect in wavelength multicasting technique through a highly nonlinear fiber (HNLF)-based on FWM switch. The advantages of the proposed schemes comes from the facts that the multicast RZ signals with short-pulsewidths which are on the order of a few picoseconds are achieved. In the first demonstration, with the short-pulsewidths multicast 10 Gb/s RZ signals, a next stage after the conversion could be considered for composing higher bit-rate streams from these lower bit-rate multicast 10 Gb/s signals by using optical time multiplexing technique. In the second demonstration, by sampling the SUT using wavelength multicasting technique, the waveform of SUT could be reconstructed more precisely in real-time. The key issue in the proposed scheme is the use of the multiwavelength sampling clocks with short-pulsewidths compressed by RA-MPC. The short-width sampling pulse could sample the SUT in the sampling time in which the waveform of SUT does not change significantly in that time.

## **3.1 All-Optical NRZ-to-RZ Conversion with Multicast Short-Pulsewidth RZ Signals**

### **3.1.1 Introduction**

All-optical signal processing which implements multiple functionalities at the same time such as waveform conversions, wavelength multicasting and pulsewidth adjustment has been beneficially emerged for future all-optical networks applications [6], [7], [36], [37]. It is well-known that nonreturn-to-zero (NRZ) and

### 3.1 All-Optical NRZ-to-RZ Conversion with Multicast Short-Pulsewidth RZ Signals

---

return-to-zero (RZ) are two widely waveforms used in wavelength division multiplexing (WDM) and optical time division multiplexing (OTDM) networks, respectively. Therefore, NRZ-to-RZ format conversion would be one of the main processes to implement all-optical networking for interfaces between WDM and OTDM networks. Moreover, with the ever-growth of high-bandwidth point-to-multipoint applications such as high-definition television (HDTV) as well as data storage area networks (big-data sharing, and data center migration), wavelength multicasting has emerged recently to improve network capacity by increasing the wavelength resource [38], [39]. Hence, demonstrations of all-optical NRZ-to-RZ waveform conversion with multiwavelength channels has been done in a lot of works [40]–[47]. If the pulsewidth of each 10 Gb/s multicast RZ signal is on the order of a few picoseconds, the higher bit-rate OTDM streams could compose from the lower bit-rate 10 Gb/s RZ signal by using optical time multiplexing technique, which is a potential next stage after this conversion. The advantage of this conversion comes from the aforementioned facts. Therefore, the effort aims to obtain the multicast RZ signals with short-pulsewidth through waveform conversion and wavelength multicasting with an assistance of pulse compression. A combination of these multiple functions are particularly desirable to efficiently improve the wavelength resource of network as well as the multiplexing of higher bit-rate OTDM signals from lower bit-rate RZ signals.

The well-established methods for all-optical waveform conversion and wavelength multicasting with tunable pulsewidth using different nonlinear media such as nonlinear fiber or semiconductor optical amplifier (SOA) have been demonstrated [6], [7]. Refs. [6] and [7] have realized one-to-four 10 Gb/s NRZ-to-RZ waveform conversion and wavelength multicasting with different long-pulsewidths. The range are from 17.9 to 22.2 ps in Ref. [6] and from 33 to 67 ps in Ref. [7]. However, obtaining tunable pulsewidth at picosecond duration is still technical challenging in the demonstrations of Refs. [6] and [7] since the high-speed signals at symbol-rate over 100 Gbaud require the short-pulsewidth which are on the order of some picoseconds [48], [49]. In Ref. [6], the pulsewidth tunability of the pulse is based on the changes of the radio frequency (RF) powers which applied for phase modulator to generate multiwavelength RZ clocks with the range from 19 dBm (corresponding to multicast RZ signals with pulsewidth of 22.2 ps) to 25

### 3. ALL-OPTICAL WAVEFORM CONVERSION AND WAVEFORM SAMPLING WITH MULTICAST SHORT-PULSEWIDTH SIGNALS

---

dBm (corresponding to multicast RZ signals with pulsewidth of 17.9 ps). From these values, it is clearly seen that, the higher power of RF signal caused the pulsewidth be smaller. However, it is difficult to obtain the shorter pulsewidth for this scheme due to the maximum limited power applied for that modulator. In Ref. [7], the pulsewidth tunability of the pulse is based on the adjustment of the orientation of the polarizer. The polarizer is set in order to achieve the multicast RZ-OOK signal with the shortest pulsewidth of 33 ps. Therefore, the pulse compression of multicast signals with short-pulsewidths has not been demonstrated so far. To obtain multicast RZ signals with short-pulsewidths, the need of the multiwavelength RZ clocks with short-pulsewidth are considered. One of popular devices, mode-locked laser (MLL), is used to generate short-width RZ pulses [50], [51]. However, the use of MLL is restricted in terms of pulsewidth flexibility. Recently, RA-MPC has emerged powerfully to generate the high-quality RZ clocks with tunable short-pulsewidths which are a few picoseconds [19], [52], [53]. Therefore, the key issue of the proposed idea is the use of the multiwavelength RZ clocks with short-pulsewidths compressed by Raman amplification multiwavelength pulse compressor (RA-MPC) to achieve the multicast RZ signals with tunable short-pulsewidths.

In this chapter, a realization of simultaneous one-to-four multicast with NRZ-to-RZ waveform conversion with tunable pulsewidth in a range from 12.17 to 4.68 ps using RA-MPC is experimentally done. The RA-MPC is employed to generate four synchronous 10 GHz WDM RZ pulses with the pulsewidths compressed down to 3.50 ps. The 4x10 Gb/s compressed pulses and an input 10 Gb/s NRZ signal interact together through four-wave mixing (FWM) effect in a highly nonlinear fiber (HNLF). Since the FWM products have the data of input signal and waveforms of the compressed RZ clocks, the multicast signals with short-pulsewidth are achieved. Error-free operations of four multicast RZ signals are obtained with negative power penalties within 1 dB compared with the back-to-back NRZ signal and small received power variation among four multicast RZ signals at bit-error-rate (BER) of  $10^{-9}$ . Besides, NRZ-to-RZ conversion and wavelength multicasting without pulse compression are also realized in order to compare to the quality of the converted compressed RZ data signals using RA-MPC. The results show

### 3.1 All-Optical NRZ-to-RZ Conversion with Multicast Short-Pulsewidth RZ Signals

that the receiver sensitivities of the converted RZ data signals with compression are better than those of the converted RZ data signals without compression.

#### 3.1.2 The Concept of Proposed Scheme

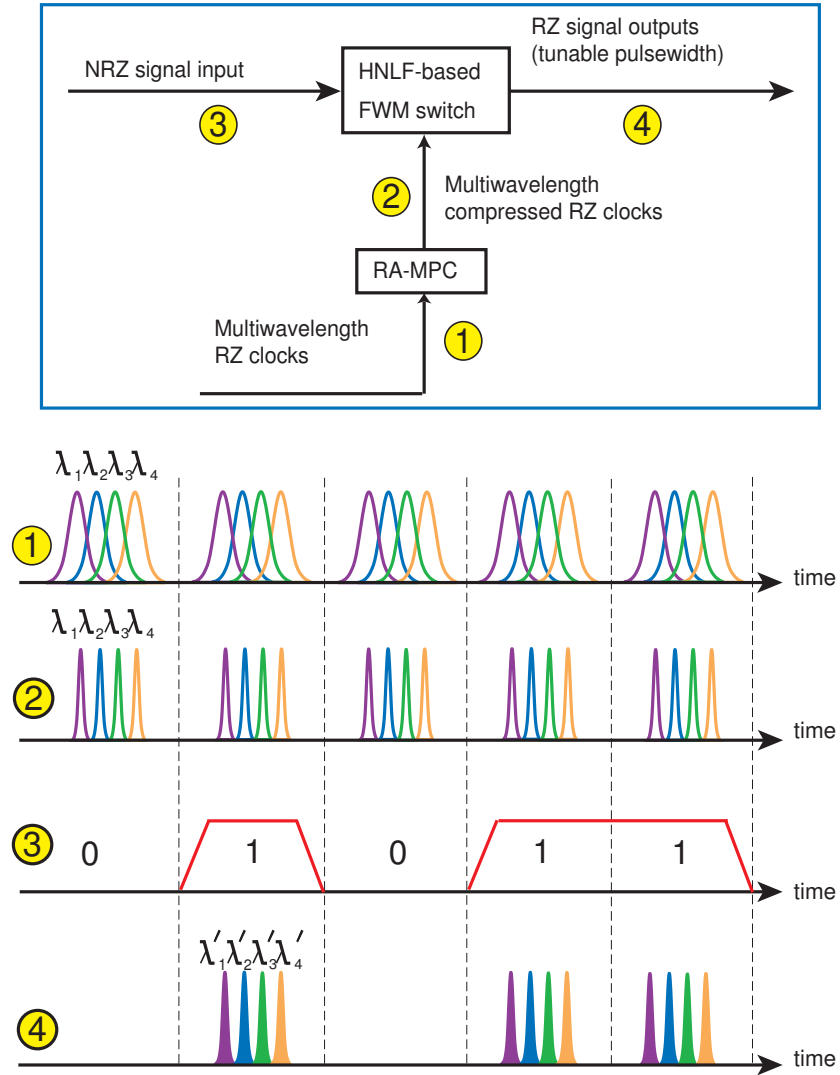


**Figure 3.1:** Operational principle of the scheme of NRZ-to-RZ conversion and wavelength multicasting using RA-MPC with multi-functions: waveform conversion, wavelength multicasting, and pulsewidth tunability.

### 3. ALL-OPTICAL WAVEFORM CONVERSION AND WAVEFORM SAMPLING WITH MULTICAST SHORT-PULSEWIDTH SIGNALS

---

Figure 3.1 illustrates the conceptual demonstration of waveform conversion and wavelength multicasting with tunable short-pulsewidth. The scheme consists of a multiwavelength pulse compressor, named RA-MPC and a HNLF-based FWM switch. The notable feature of this scheme compared to the previous setups is the achievement of getting multiwavelength RZ clocks with a wide short-pulsewidth tuning range by RA-MPC. Firstly, RA-MPC, based on adiabatic soliton compression technique, inherits high power amplification of a distributed Raman amplifier (DRA) for the multiwavelength RZ clocks. The multiwavelength RZ clocks, fundamental soliton pulses, are adiabatically amplified by DRA in an anomalous dispersion fiber. Each fundamental soliton of  $\text{sech}^2$  pulse has a peak power described as following [22], [54]

$$P_1 = \frac{3.11 |\beta_2|}{\gamma \tau_{\text{FWHM}}^2} \quad (3.1)$$

where  $P_1[\text{W}]$  is the peak power of fundamental soliton pulse;  $\tau_{\text{FWHM}}[\text{ps}]$  is the full width half maximum of pulse used as the pulsewidth of pulse in practice;  $\beta_2[\text{ps}^2/\text{km}]$  is the group velocity dispersion and  $\gamma[\text{W}^{-1}\text{km}^{-1}]$  is the nonlinear coefficient of fiber. Referring from Eq. (3.1), the pulsewidth  $\tau_{\text{FWHM}}$  of the pulse is related to the peak power of the fundamental soliton pulse  $P_1$  described as following.

$$\tau_{\text{FWHM}} \propto \sqrt{\frac{1}{P_1}} \quad (3.2)$$

From Eq. (3.2), it could be referred that the peak power of the optical pulse,  $P_1$  is inversely proportional to the square-root of the pulsewidth  $\tau_{\text{FWHM}}$  of soliton pulse. Therefore, an increase in the peak of the RZ clock pulse by increasing Raman pump power could make its pulsewidth be compressed since the soliton condition is preserved during amplification process. By controlling Raman pump power of DRA, the pulsewidth management of the input RZ clock source could be obtained.

The multiwavelength pulses source is a time interleaved source to avoid crosstalk such as FWM phenomena probably occurring during compression process through RA-MPC. A 15 ps time spacing between adjacent compressed pulses is set to simultaneously optimize the overlap of the multiwavelength RZ clocks and NRZ

### 3.1 All-Optical NRZ-to-RZ Conversion with Multicast Short-Pulsewidth RZ Signals

---

signal at the flat top of NRZ waveform in FWM process. In the HNLF-based FWM switch, the RZ clocks with pulsewidth tunability generated from RA-MPC nonlinearly interact with the input NRZ data signal over FWM process. The input NRZ signal is converted into many multicast RZ signals at four FWM idlers at different wavelengths. When the NRZ data signal and RZ clock are injected into a fiber with length  $L$ , a new FWM idler is generated owing to FWM process. The power of generated FWM idler  $P_{FWM}$  is generally calculated by the following expression [28]

$$P_{FWM}(L) = \eta\gamma^2 P_{NRZ}^2 P_{clk} \exp(-\alpha L) \left[ \frac{(1 - \exp(-\alpha L))^2}{\alpha^2} \right], \quad (3.3)$$

where  $\eta$ ,  $\gamma$ , and  $\alpha$  are the efficiency, the nonlinear coefficient of the fiber, and the attenuation coefficient of the fiber, respectively;  $P_{NRZ}$  is the power of NRZ signal set as a pump and  $P_{clk}$  is the power of RZ clock set as a probe signal. It could be seen from Eq. (3.3) that FWM products have data of the input NRZ signal and follow waveforms of the compressed clocks through FWM process. The pulsewidths of multicast RZ signals at FWM idlers are on the order of some picoseconds since these pulsewidths inherit the pulsewidths of RZ clocks sources. By compressing the clocks sources with various pulsewidths using RA-MPC before interacting with the NRZ signal in HNLF-based FWM switch, the converted RZ signals with tunable pulsewidth could be achieved.

#### 3.1.3 Experimental Setup

Figure 3.2 illustrates the experimental setup of NRZ-to-RZ conversion and wavelength multicasting with tunable pulsewidth of multicast RZ signals. From four laser diodes (LDs) and an electro-absorption modulator (EAM), the 4x10 GHz WDM-RZ clocks at wavelengths of 1538.19 ( $\lambda_1$ ), 1541.35 ( $\lambda_2$ ), 1544.53 ( $\lambda_3$ ), and 1547.72 nm ( $\lambda_4$ ) are modulated. Four RZ clocks, which are amplified by an erbium-doped fiber amplifier (EDFA), are put in front of the input of a tunable dispersion compensating module (TDCM) to compensate EAM-induced frequency chirping. Powers and time spacing of the WDM clock pulses are individually adjusted by a WDM power and time controller (WDM-PTC) to guarantee the fundamental soliton powers of the clock pulses and interleaved time among

### 3. ALL-OPTICAL WAVEFORM CONVERSION AND WAVEFORM SAMPLING WITH MULTICAST SHORT-PULSEWIDTH SIGNALS

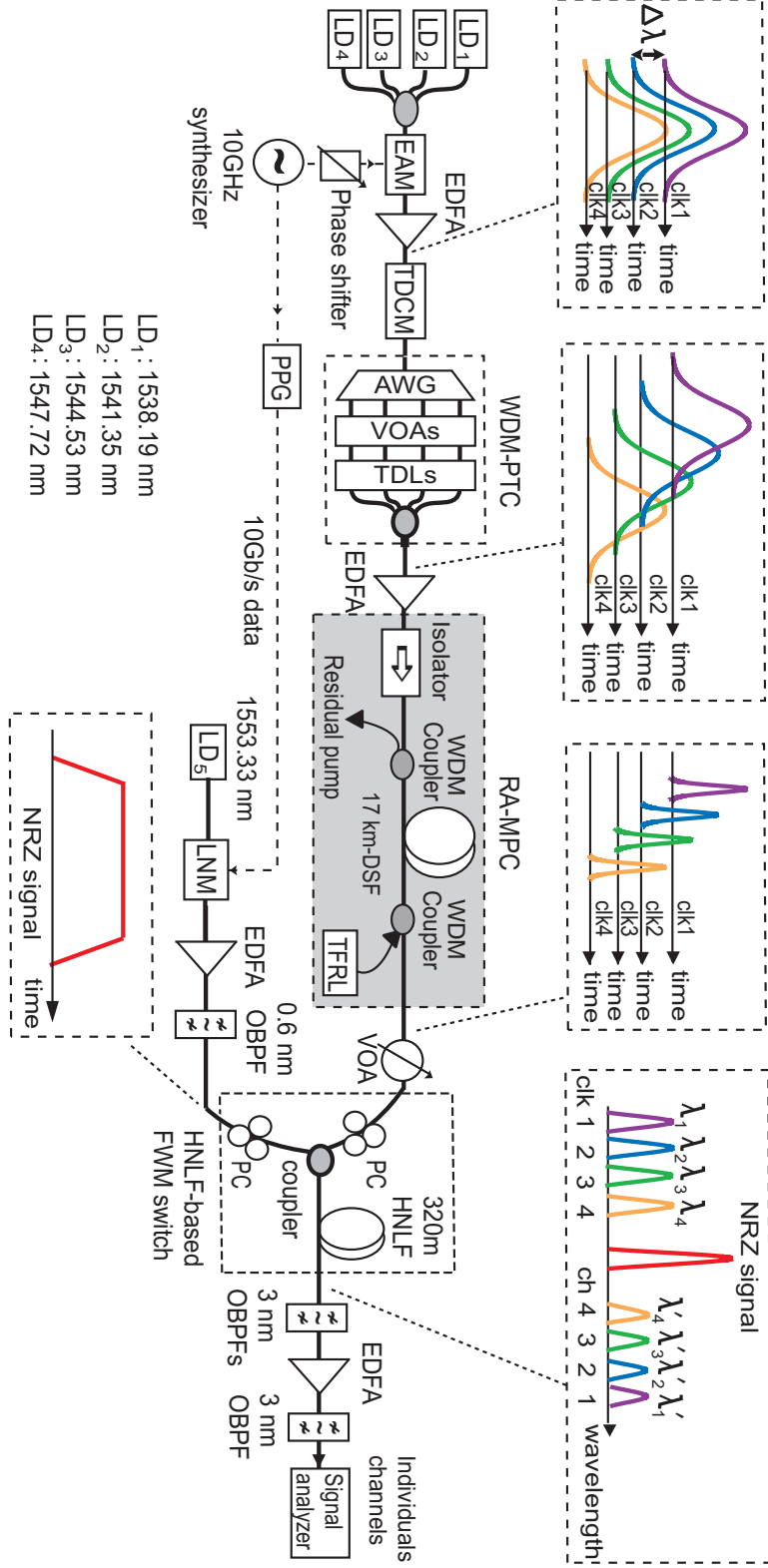


**Figure 3.2:** Experimental setup of NRZ-to-RZ conversion and wavelength multicasting with tunable short-pulsewidth using RA-MPC.

### 3.1 All-Optical NRZ-to-RZ Conversion with Multicast Short-Pulsewidth RZ Signals

---

them. The WDM-PTC includes an arrayed waveguide grating (AWG), variable optical attenuators (VOAs), tunable delay lines (TDLs), and a coupler. After WDM-PTC, to ensure the fundamental soliton power, an EDFA amplifies powers of RZ clocks which then are injected into RA-MPC. The RA-MPC based adiabatic soliton compression technique compresses multiwavelength RZ clocks. The setup of RA-MPC includes a 17 km dispersion-shifted fiber (DSF) with a counter-propagation tunable fiber Raman laser (TFRL) operating at 1454 nm and two WDM couplers. The Raman pump wavelength is set at the value of 1454 nm to optimize the quality of compression performance. Table 3.1 lists the parameters of DSF. A phase shifter is used for controlling time delay of the multiwavelength RZ clocks in order to get optimized overlap of the multiwavelength RZ clocks and the NRZ signal in FWM process.

**Table 3.1:** Characteristics of 17 km dispersion-shifted fiber (DSF).

Parameter	Value	Unit
Length	17	km
Attenuation	0.197	dB/km
Dispersion at 1552 nm	3.8	ps/nm/km
Dispersion slope at 1552 nm	0.059	ps/nm <sup>2</sup> /km

**Table 3.2:** Characteristics of 320 m highly nonlinear fiber (HNLF).

Parameter	Value	Unit
Length	320	m
Attenuation	0.82	dB/km
Dispersion at 1550 nm	-0.06	ps/nm/km
Dispersion slope at 1550 nm	0.023	ps/nm <sup>2</sup> /km
Nonlinear coefficient ( $\gamma$ )	28	W <sup>-1</sup> · km <sup>-1</sup>
Effective core area of fiber ( $A_{\text{eff}}$ )	9	$\mu\text{m}^2$



### 3. ALL-OPTICAL WAVEFORM CONVERSION AND WAVEFORM SAMPLING WITH MULTICAST SHORT-PULSEWIDTH SIGNALS

---

An NRZ data signal at the wavelength of 1553.33 nm is modulated by a LiNbO<sub>3</sub> modulator (LNM) driven by an electrical data from a pulse pattern generator (PPG). After LNM, the NRZ signal is amplified by an EDFA and filtered by a 0.6 nm optical band pass filter (OBPF). The powers and polarization of the NRZ signal and compressed multiwavelength RZ clocks are optimized to obtain good output waveforms and the largest conversion efficiency by a set of an EDFA, VOA and two polarization controllers (PCs). The NRZ signal, which is set as a pump in FWM-based HNLF switch, has parameters as described in Table 3.2. At the output of HNLF, three 0.3 nm OBPFs and an EDFA were used for individually selecting each multicast channel under investigation. These multicast RZ signals are analyzed to obtain BER measurements as well as spectra, waveforms, and eye patterns.

#### 3.1.4 Experimental Results and Discussions

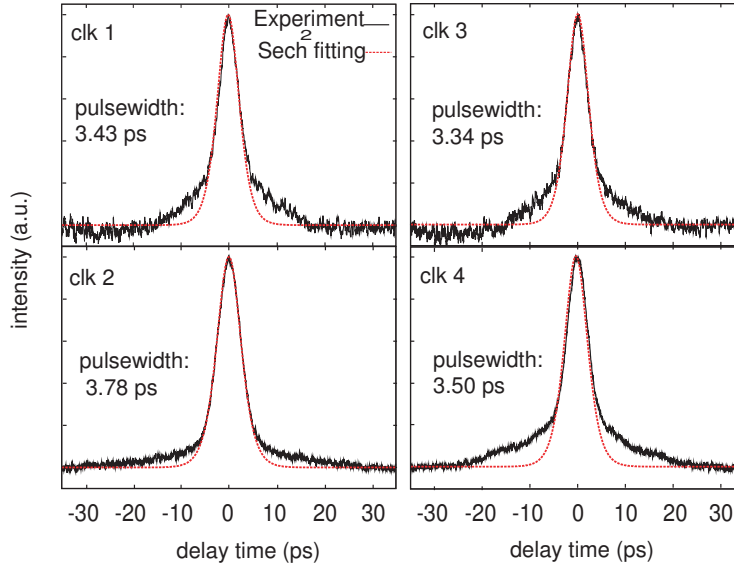


**Figure 3.3:** Autocorrelation traces of RZ clocks 1, 2, 3 and 4 after compression at the output of RA-MPC at Raman pump power ( $P_r$ ) of 0.82 W

### 3.1 All-Optical NRZ-to-RZ Conversion with Multicast Short-Pulsewidth RZ Signals

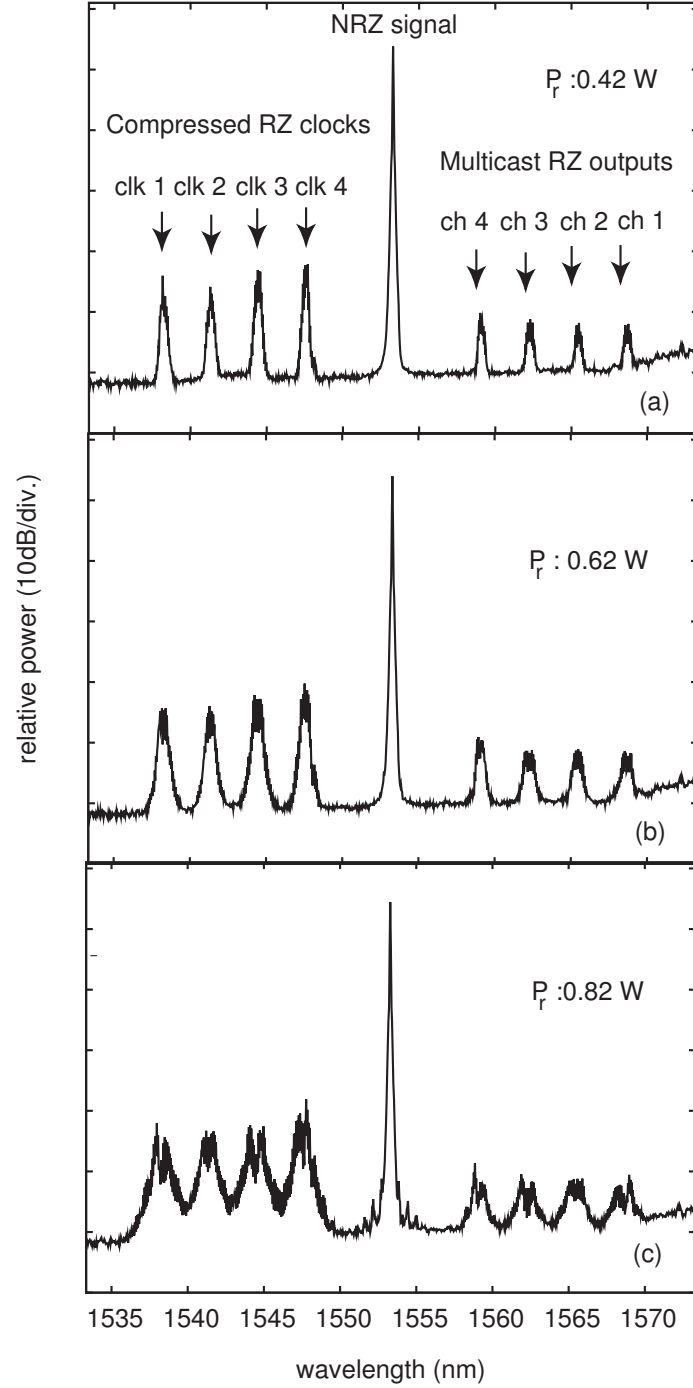


**Figure 3.4:** FWM spectra at the output of HNLF with different values of Raman pump power ( $P_r$ ) of (a) 0.42 W, (b) 0.62 W, and (c) 0.82 W.

### 3. ALL-OPTICAL WAVEFORM CONVERSION AND WAVEFORM SAMPLING WITH MULTICAST SHORT-PULSEWIDTH SIGNALS

---

In this experiment, the compression of multiwavelength RZ clocks was based on adiabatic soliton compression in DRA. Since the energy of RZ pulses was increased by increasing Raman pump power ( $P_r$ ) of DRA, the soliton pulses were compressed. The multiwavelength RZ clocks are required as fundamental soliton pulses for this compression technique. The peak power of each RZ pulse depended on pulsewidths and their relation was expressed by Eqs. (3.1) and (3.2). The pulsewidths of four RZ clocks were compressed to around 11.33, 6.45 and 3.5 ps corresponding to Raman pump power ( $P_r$ ) of 0.42, 0.62 and 0.82 W, respectively. Figure 3.3 shows autocorrelation traces of four RZ clocks after compressing at the output of RA-MPC as  $P_r$  was 0.82 W. The RZ clocks 1, 2, 3 and 4 (clks. 1, 2, 3, and 4) at the wavelengths of 1538.19, 1541.35, 1544.53, and 1547.72 nm with their pulsewidths of around 20.0 ps were compressed down to 3.43, 3.78, 3.34, and 3.50 ps, respectively. When the pulse is compressed, the spectrum is broadening. To avoid the crosstalk from the neighboring channels induced by the spectrum overlapping, the frequency spacing is not smaller than the bandwidth of each channel. The frequency spacing between the adjacent pulses is set to 400 GHz. The four multiwavelength RZ pulses are compressed to around 3.5 ps with the bandwidth of each compressed RZ pulse of around 120 GHz. It is obviously seen that these compressed RZ clocks pulses had high quality since their waveforms were well-matched to  $\text{sech}^2$  fitting. These compressed RZ clocks and the 10 Gb/s NRZ data signal interacted together through FWM effect in HNLF. The time spacing between neighboring compressed RZ clocks were set to 15 ps to ensure that all these clocks were sampled at the flat-top of the waveform of NRZ signal in FWM process.

Figure 3.4(a), (b) and (c) show the spectra at the output of HNLF corresponding to Raman pump powers ( $P_r$ ) of 0.42, 0.62 and 0.82 W, respectively. It is seen that each RZ clock and each multicast RZ signal had the notches at their central regions. The reason comes from the fact. Originating from multiwavelength RZ clocks compressed by RA-MPC, spectra of these pulses have the notches located at their spectral center. The probable concern would be the residual frequency chirp near the leading and trailing pulse edges. After FWM process, the spectra of multicast channels also have the notches as seen from Fig. 3.4. In this FWM process, the NRZ signal was set as a pump and all multiwavelength compressed

### 3.1 All-Optical NRZ-to-RZ Conversion with Multicast Short-Pulsewidth RZ Signals

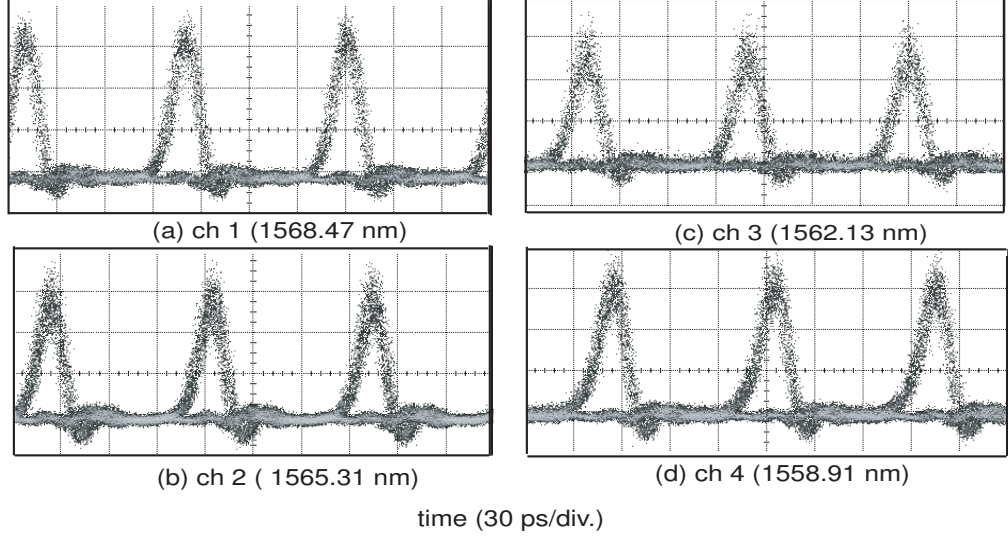


**Figure 3.5:** Eye patterns of all multicast converted RZ signals (a) channel 1, (b) channel 2, (c) channel 3, and (d) channel 4 with the pulsewidth of around 4.68 ps corresponding Raman pump power ( $P_r$ ) of 0.82 W.

RZ clocks were sampled at the flat-top of NRZ signal, therefore, the spectra of multicast signals were inversion compared to those of the multiwavelength RZ clocks with respect to the frequency of NRZ data pump, quite likely a mirror reflection. Channels 1, 2, 3 and 4 (chs. 1, 2, 3, and 4) were simultaneously generated at the wavelengths of 1568.47 ( $\lambda'_1$ ), 1565.31 ( $\lambda'_2$ ), 1562.13 ( $\lambda'_3$ ), and 1558.94 nm ( $\lambda'_4$ ), respectively. Each multicast channel was individually selected for eye patterns, pulsewidths and BER measurements.

Figure 3.5(a), (b), (c), and (d) show eye patterns of four multicast RZ signals located at the wavelengths of 1568.47, 1565.31, 1562.13, and 1558.94 nm, respectively. When  $P_r$  was set at 0.82 W, the pulsewidth of all multicast signals is around 4.68 ps. To investigate the performance of waveform conversion and multicasting process, BER characteristics of all signals were performed as a function of the received power as plotted in Fig. 3.6. Error-free operations were obtained with small received power variation of around 0.5 dB at BER of  $10^{-9}$  among multicast signals. Negative power penalties within 1 dB were achieved

### 3. ALL-OPTICAL WAVEFORM CONVERSION AND WAVEFORM SAMPLING WITH MULTICAST SHORT-PULSEWIDTH SIGNALS

with respect to the back-to-back NRZ input signal. The obtained results are well reasonable in comparison with the results in Refs. [42], [55]–[58] in which receiver sensitivities of RZ signals could be improved by several dB compared with those of NRZ signals. It was found that these receiver sensitivity enhancements are around from 2 to 3 dB in theoretical and experimental demonstrations [55], 3 dB in experimental work [56], up to 3.2 dB in theoretical simulations [57], [58], and 1.5 dB in experimental work [42]. The reasons result from the fact as following. At the same average optical power at the receiver, RZ signal has a higher peak power in comparison with that of NRZ one. Since received electrical power is proportional to the square of incident optical power, the electrical power of RZ pulse is higher than that of a NRZ one [42]. Therefore, in a comparison to NRZ pulse, RZ pulse has a signal-to-noise ratio (SNR) gain leading a receiver sensitivity improvement [57].

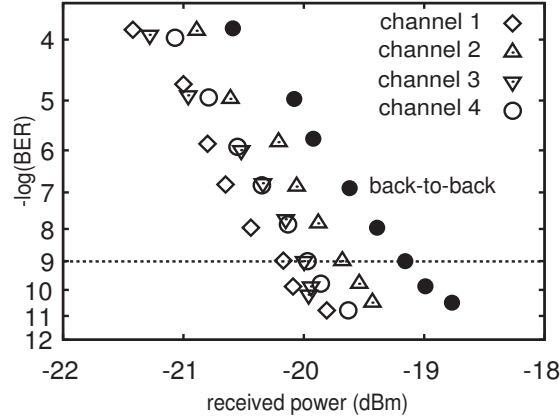


**Figure 3.6:** BER curves of converted RZ channels with pulsewidth of around 4.68 ps corresponding to  $P_r$  of 0.82 W.

Autocorrelation traces of clock 4 (clk. 4) after compression at the output of RA-MPC and channel 4 (ch. 4) after FWM at the output of HNLF at various values of  $P_r$  are shown in Figs. 3.7(a) and (b). Increasing  $P_r$  causes pulsewidths of the WDM clock pulses decrease, therefore, the pulsewidth of multicast RZ signals were smaller. For example, the pulse at channel 4 was compressed to 12.17, 7.89, and 4.68 ps as  $P_r$  was set to 0.42, 0.62, and 0.82 W, respectively. The multicast

### 3.1 All-Optical NRZ-to-RZ Conversion with Multicast Short-Pulsewidth RZ Signals

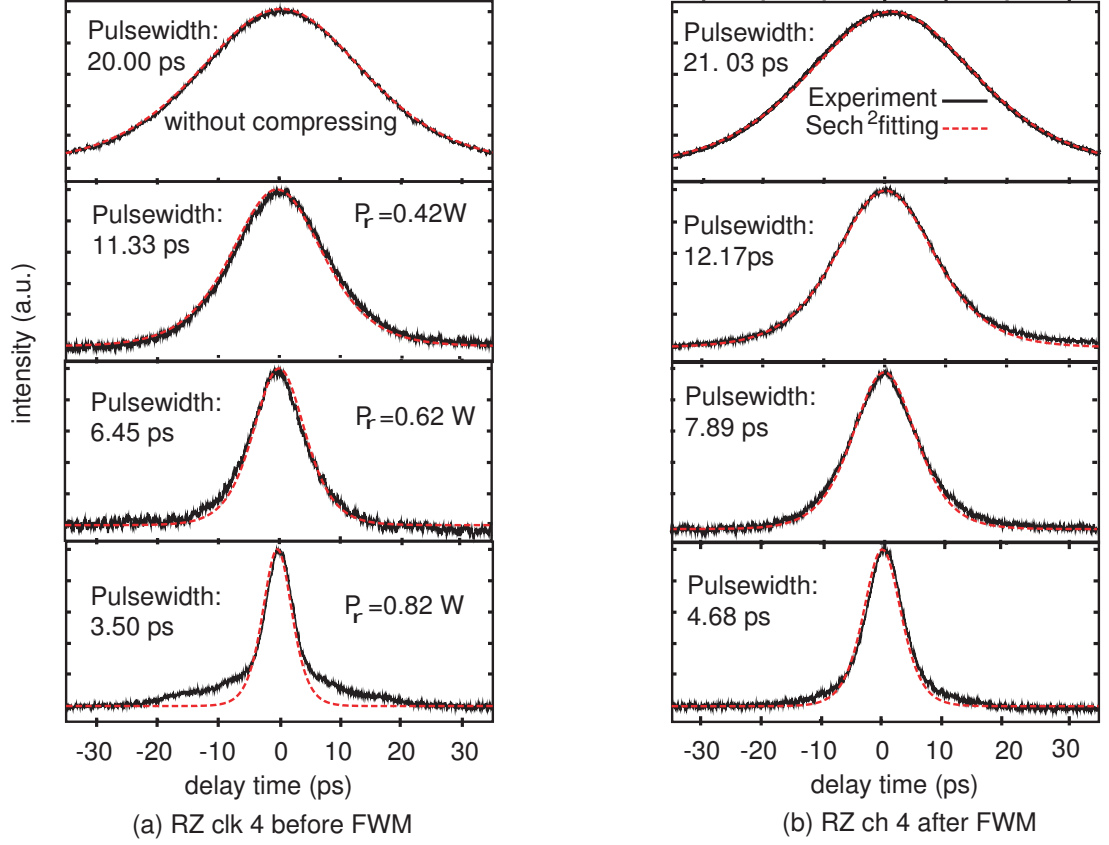


**Figure 3.7:** Autocorrelation traces of different pulsewidths of (a) RZ clock 4 (clk. 4) after compression (before FWM) and (b) channel 4 (ch. 4) after conversion (after FWM) at various values of  $P_r$ .

signals had the pulsewidth decreased from 21.03 ps (without pulse compression) to 12.17, 7.89, and 4.68 ps (after compression). The waveforms as plotted in solid lines were well-matched to  $\text{sech}^2$  fitting as plotted in dash lines. The similar features were also obtained for the remain channels with different pulsewidths. Figure 3.8 shows eye patterns of converted signal at channel 4 in cases without compression (in Fig. 8(a)), and with compression at  $P_r$  of 0.42 W, 0.62 W, and 0.82 W (in Fig. 3.8(b), (c), and (d)), respectively. Eye patterns of these RZ signals were almost invariant due to limitation bandwidth of 30 GHz bandwidth sampling oscilloscope. To simultaneously observe all receiver sensitivities at

### 3. ALL-OPTICAL WAVEFORM CONVERSION AND WAVEFORM SAMPLING WITH MULTICAST SHORT-PULSEWIDTH SIGNALS

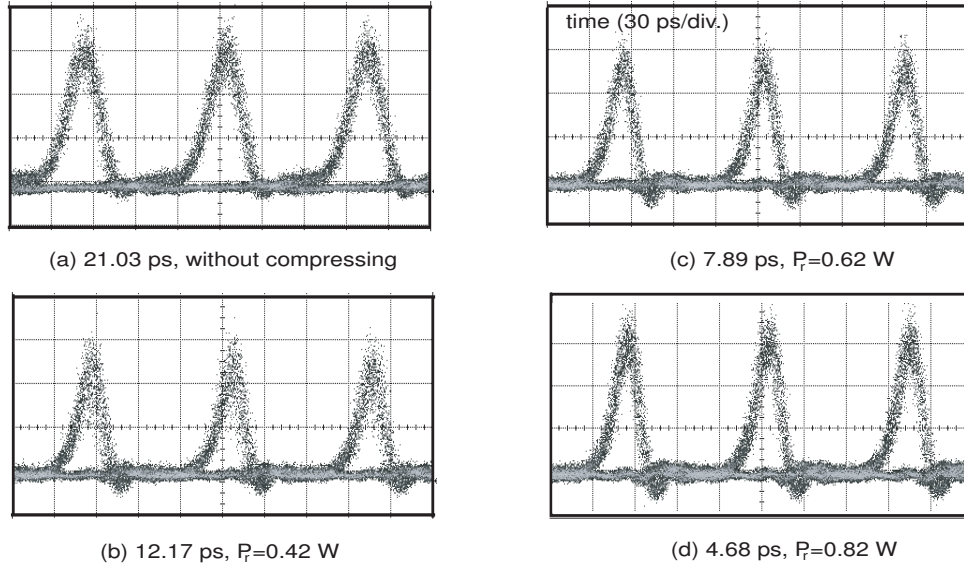


**Figure 3.8:** Eye patterns of converted RZ signal at channel 4 with various pulsewidths (a) 21.03 ps (without compression), (b) 12.17 ps, (c) 7.89 ps and (d) 4.68 ps corresponding to  $P_r$  0.42, 0.62 and 0.82 W, respectively.

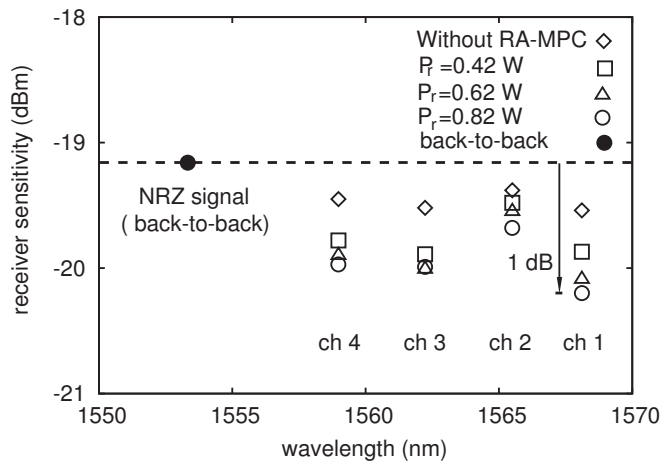


**Figure 3.9:** Receiver sensitivities of all multicast RZ signals output compared to the NRZ signal in cases of without compression and with compression at  $P_r$  of 0.42, 0.62 and 0.82 W.

### 3.1 All-Optical NRZ-to-RZ Conversion with Multicast Short-Pulsewidth RZ Signals

---

BER of  $10^{-9}$  of the converted signals, their receiver sensitivity was also measured at different values of pulsewidths by changing Raman pump power. The NRZ-to-RZ conversion and wavelength multicasting are also implemented without using RA-MPC in order to compare with a case of using RA-MPC. The sensitivities of the back-to-back NRZ and all RZ outputs signals at four values of pulsewidths (21.03, 12.17, 7.89, and 4.68 ps) are illustrated in Fig. 3.9. The small differences in the sensitivities of four converted RZ signals were obtained. The sensitivity of NRZ signal was 1 dB larger than the best sensitivity of RZ signal at channel 1 as Raman pump power was set to 0.82 W. The resulted sensitivities indicated that the receiver sensitivities of RZ data signals with short-pulsewidths using RA-MPC are better in comparison to the case of without using of RA-MPC. It could be referred from Refs. [55], [57], and [58] that the receiver sensitivity would be enhanced for the shorter RZ pulse compared to longer one, even if the used receiver bandwidth is only 0.7 times data rate. The BER measurement system of this experiment in the thesis employs an optical receiver that has a receiver bandwidth of around 8 GHz. The pulsewidth of all converted RZ signals was tunable from around 21.03 to 12.17, 7.89, 4.68 ps leading to negative power penalties compared to the back-to-back NRZ signal. The receiver sensitivity of the shorter pulsewidth of the multicast signal was smaller compared with that of the longer one. The receiver sensitivity improvement of the shorter pulsewidth signals were consistent with the previous works [42], [55], [57], [58], and have also been discussed in the last part for Fig. 3.6. However, it could be observed that there was a small gap in the amount of receiver sensitivity enhancement when the pulsewidth was compressed to 4.68 ps in comparison with longer pulsewidths of signals. Main concerns would be that the bandwidth of signal with such as a short-pulsewidth duration is excessively larger than the receiver bandwidth, causing less impact of pulsewidth on receiver sensitivity. This dependence of pulsewidth on receiver sensitivity has been analyzed in details in Ref. [58]. From Figs. 3.6 and 3.9, it is clearly seen that power penalties at BER= $10^{-9}$  of channels 1 and 2 were the best and worst, respectively compared to those of the remained multicast signals (channels 3 and 4). Meanwhile, power penalty of channel 3 was just a very little better than that of channel 4. The reason would be that the location of channel 1 was furthest compared to those of the others so that crosstalk induced by the



### 3. ALL-OPTICAL WAVEFORM CONVERSION AND WAVEFORM SAMPLING WITH MULTICAST SHORT-PULSEWIDTH SIGNALS

---

neighboring channels did not affect channel 1 strongly. The maximum 0.35 dB difference in amount of power penalty of channel 2 compared to channels 3 and 4 would be due to the imperfect tuning filter when selecting the individual channel 2 under investigation.

In this scheme, the frequency of NRZ signal nearly coincides with the zero-dispersion wavelength frequency in order to satisfy the phase-matching condition. Even though the conversion efficiency dependency of spacing between wavelength of the pump (input data signal) and the zero-dispersion wavelength of the fiber has not been investigated, it is expected that the wavelength of the pump could set around the zero wavelength dispersion to obtained a desired FWM efficiency by adjusting the power of the pump [28]. In this work, when tuning the wavelength of RZ clock 1 which was further from the wavelength of pump at the wavelength of 1528.77 nm or 1567.95 nm, the significant conversion efficiency also could be obtained. Therefore, the tunable wavelength of multicast signals could be achieved. In our scheme, the time spacing between two adjacent pulses is set to 15 ps so that the RZ clocks can avoid crosstalk such as FWM phenomena probably occurring during compression process through RA-MPC and the RZ clocks can sample the 10 Gb/s NRZ signal over its flat-top. The 4x10 GHz multiwavelength RZ clocks with frequency spacing of 400 GHz (3.2 nm) between adjacent channels occupy the overall frequency range within the gain bandwidth of RA-MPC which was 12 nm (1.5 THz). The maximum number of multicast channels depends on the conversion bandwidth, bandwidth of signals, and time spacing of the multiwavelength pulse generated from RA-MPC, the gain bandwidth of RA-MPC for NRZ-to-RZ format conversion using in our scheme. Therefore, the obtained maximum number of multicast channels is four channels in this work. However, the expected maximum number of multicast signals is eight channels when the frequency spacing and time spacing are set as the values of 200 GHz and 10 ps, respectively. The gain bandwidth could be improved if using the multiwavelength pumps for Raman amplification. Hence, the maximum number of channels depends on the conversion bandwidth in FWM process. The frequency and time channel spacing determine the packing density of the multiwavelength pulses which is related to the bit-rate and the spectral efficiency.

### 3.1 All-Optical NRZ-to-RZ Conversion with Multicast Short-Pulsewidth RZ Signals

---

The spectral efficiency of each 10 Gb/s multicast signal is only 0.025 b/s/Hz. However, the pulsewidth of each multicast signal is on the order of some picoseconds so that the multicast signals could be multiplexed to higher bit-rate OTDM signals. Therefore, the spectral efficiency could be improved. For example, the spectral efficiency of 80 Gb/s OTDM signal with the frequency spacing of 400 GHz is 0.2 b/s/Hz. The spectral efficiency could be increased if the frequency spacing is reduced to the value of 200 GHz.

If a lot of multicast channels are required such as 100 multicast channels with frequency spacing between adjacent channels of 400 GHz, the total required spacing is over 39.6 THz. Therefore, it is obvious that our scheme could not satisfy for this requirement. In Ref. [59], the wavelength conversion using FWM with the frequency range from the pump and the probe of around 41 THz is achieved in a dispersion-engineered highly nonlinear fiber. Therefore, it is expected that this setup could be considered for the requirement of 100 multicast channels. However, it is challenging for the demonstration of wavelength multicasting with a large number of channels due to the available equipment and the complexity of the unwanted nonlinearities such as self-phase modulation (SPM) and cross-phase modulation (XPM) in conversion process. So far, 40-fold multicasting of 40 Gb/s NRZ signal with frequency spacing of 100 GHz has been achieved [60].

In practice, optical wavelength multicasting has not been used. The multicast is only implemented in internet protocol (IP) digital router. The evolution is toward WDM wavelength multicasting with different wavelengths for all-optical networks in future. The required number of multicasting wavelengths depends on the scale of networks and the demand from clients. In our scheme, the 4x10 Gb/s multicast RZ-OOK signals are obtained with the shortest pulsewidth which is less than 5 ps. Therefore, it is desirable that these multicast signals could be multiplexed into the higher bit-rate OTDM signals up to 80 Gb/s if the high bit-rate signals are required. The potential total capacity provided by this scheme is 4x80 Gb/s.

## 3.2 All-Optical Waveform Sampling using Wavelength Multicasting Technique

### 3.2.1 Introduction

Thanks to the advantages of recent technologies in high-speed backbone data networks, the growing trend of bandwidth demanding applications such as data and video sharing, cloud computing, radar systems and data collection systems have brought in a need for higher capacities in signal transmission and monitoring signal [24], [61]. Nowadays, the high-speed signals in communication are most widely monitored by all-optical sampling technique which is novel to display time-resolved measurements of such high-speed optical signal whose bandwidth is not able to be reached by conventional photo-detectors attached in electronic sampling processor [61]. In all-optical sampling techniques, optical signal is sampled in optical domain by an optical sampling gate and the sampled signals are converted into electrical signals and then are processed. By this way, it reduces the requirement of high-bandwidth of electronic devices for detecting process because the bandwidth of the measurement instrument limitation is only due to the optical sampling gate. This is the advantages of optical sampling method compared to conventional electronics sampling [62]. These signals could always be analyzed off-line by capturing their samples and then processing.

After early work [63] using optical sampling in a  $\text{LiIO}_3$  crystal, the recent works have demonstrated the usefulness of all-optical sampling with verified high refresh rate eye-diagram analysis of data at several hundreds Gb/s using FWM [64], [65] or all-optical sampling with resolving the temporal shape of data pulses [66], [67]. However, it is challenging that these methods are not compatible with instantaneous amplitude changes of signals as well as capturing the details and singular manners such as transient events which need real-time processing. The basic idea in real-time waveform sampling is that how to capture the sampled points so that the sampling rate is larger two times the highest frequency content of the signal. For instance, the capture of a waveform of a 10 Gb/s NRZ signal requires a sampling rate of around 30 GSamples/s [68]. Therefore, an effort to

### 3.2 All-Optical Waveform Sampling using Wavelength Multicasting Technique

---

characterize signals for real-time applications such as signal recognition by monitoring waveform signal is all-optical waveform sampling which has emerged as a powerful tool. All-optical real-time waveform sampling has been demonstrated by using various effects in an electro-optic intensity modulator (EOM) [8] or HNLF switches [9]–[11]. In the demonstration in Ref. [10], waveform sampling is realized by multicasting the input signal before sampling process using a sampling pulse source from a high-repetition-rate MLL. This approach need to use two nonlinear processes which are multicasting and sampling, thus, there might be complex in setup and operation. The other demonstrations in Refs. [8], and [9] use the multiwavelength sampling pulses instead of a sampling pulse in Ref. [10]. Nevertheless, those sampling pulses are difficult to use for sampling high-speed signals so as to precisely capture waveforms due to their long-pulsewidths. Indeed, for sampling waveform of high-bandwidth signals such as military radar, it is desirable to use sampling short pulses in order that the waveform does not change significantly over the sampling time. The generation of optical signal with short-pulsewidth has been emerged as an active area of research for several decades, and the existence of such pulses has brought a variety of applications to sampling pulse source. For real-time waveform sampling of the high-speed high-bandwidth signal, a high-repetition-rate of sampling pulse sources beyond 10 GHz maybe is required. For that requirement, the proposed scheme in this chapter has overcome the difficulty of Refs. [8], and [9] by generating the 4x10 GHz multiwavelength sampling clocks sources with pulsewidths which are less than 3.0 ps. These sampling pulses sources employ four continuous waves (CWs) from four laser diodes (LDs) followed by a high-bandwidth electro-absorption modulator (EAM) controlled by a 10 GHz radio frequency (RF) signal in order to generate pulses with widths of 20 ps. Furthermore, to reach the requirement for the sampling short pulse source, the generated pulses are compressed by using RA-MPC. The pulsewidths of the multiwavelength sampling pulses sources were compressed down to some picoseconds, via adiabatic fundamental soliton compression. The distinguished feature of the proposed scheme in this work is the use of the 4x10 GHz multiwavelength sampling clocks compressed by RA-MPC with pulsewidths of less than 3.0 ps. The RA-MPC operation is based on adiabatic soliton compression which takes advantage of high power amplification

### 3. ALL-OPTICAL WAVEFORM CONVERSION AND WAVEFORM SAMPLING WITH MULTICAST SHORT-PULSEWIDTH SIGNALS

---

for high-quality WDM-RZ sampling compressed clocks. The proposed idea is to use several sampling clocks with short pulsewidth compressed by RA-MPC to get simultaneous multiple sampled signals by using wavelength multicasting technique. Hence, a high sampling-rate in a single optical sampling gate is achieved corresponding to the number of wavelengths of the sampling pulses.

In this demonstration, a realization of all-optical waveform sampling of arbitrary signal called signal under test (SUT) using wavelength multicasting technique to get simultaneously many multicast sampled signals is focused. Four synchronous 10 GHz WDM pulses are compressed by RA-MPC with the pulsewidth which are less than 3 ps. These four compressed pulses interact with the input SUT over FWM effect in an HNLF. It results in four sampled signals based on wavelength multicasting conversion. The power of each sampled signal is proportional to that of the SUT at the time overlap with the sampling pulse and the waveform of sampled signal inherit that of the sampling compressed pulse. Therefore, four 10 Gb/s sampled signals with short-pulsewidth at picosecond range are obtained, leading a sampling rate of 40 GSample/s. The sampled data is acquired by the 30 GHz sampling oscilloscope and then is processed. The reconstructed waveforms are well-matched with the SUT waveforms.

#### 3.2.2 Principle Operation

The concept of all-optical waveform sampling using multiwavelength sampling clocks is shown in Fig. 3.10. In the optical sampling system using wavelength multicasting technique, the optical signal under test (SUT) is multicast and sampled simultaneously in optical domain by using multiwavelength sampling clocks through an optical sampling gate such as an HNLF-based FWM switch. The SUT is sampled at many points decided by multiwavelength sampling pulses in the same frame where transient changes of STU occur, leading real-time process. After WDM-filter, the multicast sampled signals are obtained and then are sent to photodiodes (PDs) for converting to electrical signals. These electric signals are processed by processor to reconstruct the waveform of SUT.

In this demonstration, before sampling process, the multiwavelength sampling pulses are compressed by RA-MPC. The detailed concept of all-optical wave-

### 3.2 All-Optical Waveform Sampling using Wavelength Multicasting Technique

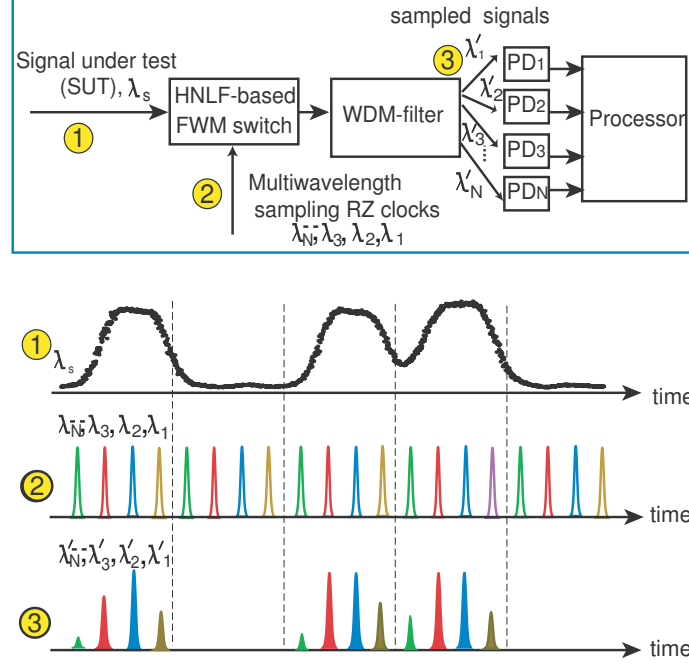


**Figure 3.10:** The concept of all-optical waveform sampling using wavelength multicasting technique.

form sampling using multiwavelength sampling clocks compressed by RA-MPC is shown in Fig. 3.11. Firstly, delay block controls the delay of WDM-RZ clocks to synchronize with the target of sampling-rate. After the delay block, the WDM RZ pulses are simultaneously compressed down to some picoseconds by RA-MPC. The SUT and sampling compressed clocks are injected into a sampling gate. After the sampling gate, the data information of input signal is copied to the FWM sampled products after wavelength multicasting conversion. The power of each sampled signal is proportional to that of the SUT at sampling point. WDM filter is used to get the sampled signals which then are processed. Hence, all-optical waveform sampling of the SUT is achieved.

#### 3.2.3 Experimental Setup

The experimental setup of all-optical waveform sampling is shown in Fig. 3.12. Four 10 GHz WDM-RZ clocks at the wavelengths of 1538.19 ( $\lambda_1$ ), 1541.35 ( $\lambda_2$ ),

### 3. ALL-OPTICAL WAVEFORM CONVERSION AND WAVEFORM SAMPLING WITH MULTICAST SHORT-PULSEWIDTH SIGNALS

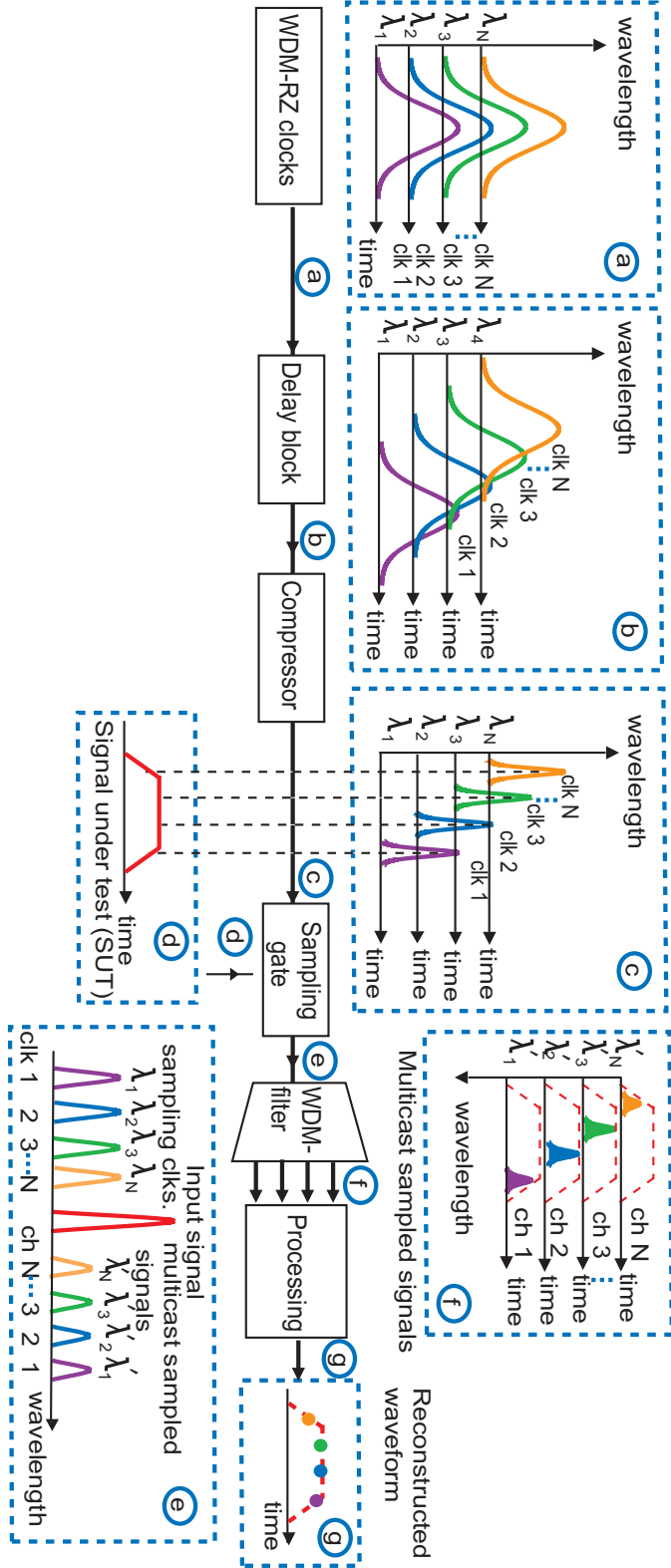


Figure 3.11: The concept of all-optical waveform sampling using wavelength multicasting with RA-MPC.





### 3. ALL-OPTICAL WAVEFORM CONVERSION AND WAVEFORM SAMPLING WITH MULTICAST SHORT-PULSEWIDTH SIGNALS

---

1544.53 ( $\lambda_3$ ), and 1547.72 nm ( $\lambda_4$ ) which are  $\text{sech}^2$ -shaped pulses with pulsewidth of around 20 ps are modulated from four laser diodes (LDs) by an electroabsorption modulator (EAM). The powers of four RZ clocks are then boosted with an erbium-doped fiber amplifier (EDFA). A tunable dispersion compensating module (TDCM) is used to compensate frequency-chirping induced by EAM. The powers of the WDM-RZ clocks and time spacing among them are controlled individually by a WDM power and time controller (WDM-PTC) to ensure the equal power and time-interleaved among the clock pulse trains. The WDM-PTC includes of an arrayed waveguide grating (AWG), variable optical attenuators (VOAs) in series with tunable delay lines (TDLs), and a coupler. To ensure the fundamental soliton condition in the compression process, an EDFA is used to amplify the WDM-RZ clocks which are then injected into the input of RA-MPC. The Raman pump wavelength is set at 1454 nm for the pulse compression to optimize high-quality compression performance. An input SUT at the wavelength of 1553 nm is generated from signal generator and is then boosted by an EDFA and filtered by a 0.6 nm optical band pass filter (OBPF). The use of an EDFA and a VOA is to optimize FWM efficiency by adjusting powers of the SUT and the sampling WDM-RZ clocks, respectively. Meanwhile, the polarization of both the clocks and SUT are monitored by two polarization controllers (PCs) to maximize interaction among the signals. A phase shifter controls the time delay of the RZ clocks for obtaining the overlap among the RZ clocks and the STU at the sampling time in FWM process. The SUT is set as a pump for FWM process in HNLF, which has the parameters as shown in Table 3. 2. After the sampling process, the multicast sampled RZ signals are filtered and amplified individually by OBPFs and an EDFA, respectively. Each generated sampled signal is then separated from the other signals to be processed by a 30 GHz electronic sampling oscilloscope. The sampled signals are off-line processed to combine the temporal profile to capture the waveform of SUT.

#### 3.2.4 Experimental Results and Discussions

In the experiment, the sampling RZ clocks were compressed by RA-MPC owing to the adiabatic soliton compression. Fundamental soliton pulses are required for

### 3.2 All-Optical Waveform Sampling using Wavelength Multicasting Technique

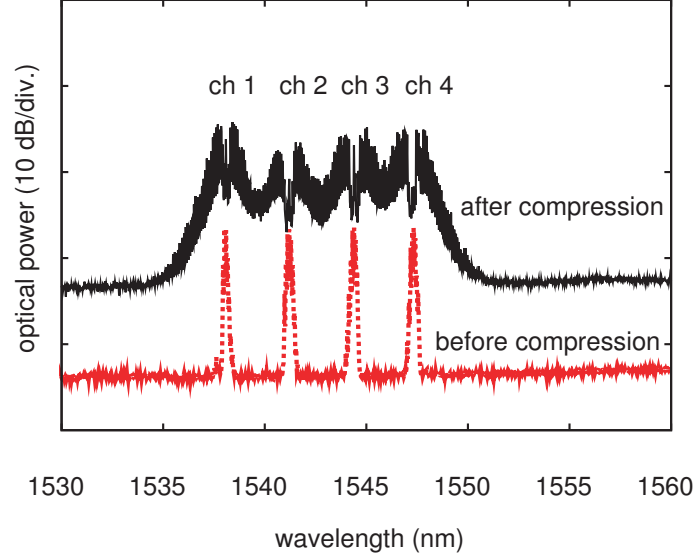


**Figure 3.13:** Spectra of multiwavelength sampling pulses before and after compression using RA-MPC with the Raman pump power of 0.9 W.

this compression technique. The dependence of pulsewidth of the RZ clocks on its peak power was described in Eqs. (3.1) and (3.2). The spectra of the multiwavelength sampling compressed clocks before and after compression are shown in Fig. 3.13. Their spectra became broader when pulsewidths were compressed. The reason is that the increase of Raman pump power made the peak power of sampling clock increase, leading its pulsewidth compression owing to adiabatic soliton compression in the DRA. Clocks (clks.) 1, 2, 3 and 4 with pulsewidths of around 20 ps are successfully compressed to 2.62, 2.96, 2.70, and 2.82 ps, respectively when the Raman pump power was set to 0.9 W. Autocorrelation traces and eye patterns of four sampling compressed and their autocorrelation traces are illustrated in Figs. 3.14 and 3.15, respectively. The spacing time between two adjacent sampling clocks is to 25 ps. It is obviously seen that the spectra and waveforms of sampling compressed clocks are well-fit to  $\text{sech}^2$  function.

Firstly, a demonstration of all-optical waveform sampling of NRZ signal is presented. Figure 3.16 shows the spectra at the output of the HNLF after sampling process based on wavelength multicasting technique. Channels 1, 2, 3 and 4 at the wavelengths of 1567.81 ( $\lambda'_1$ ), 1564.65 ( $\lambda'_2$ ), 1564.65 ( $\lambda'_3$ ), and 1558.25

### 3. ALL-OPTICAL WAVEFORM CONVERSION AND WAVEFORM SAMPLING WITH MULTICAST SHORT-PULSEWIDTH SIGNALS

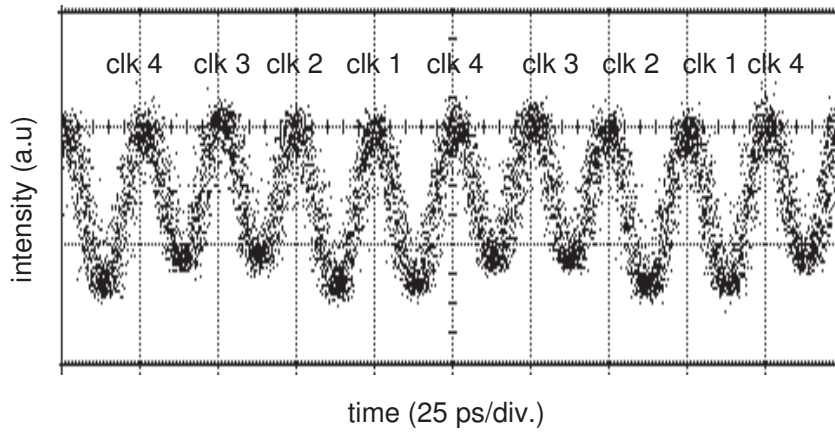


**Figure 3.14:** Eye patterns of four multiwavelength sampling pulses compressed by RA-MPC.

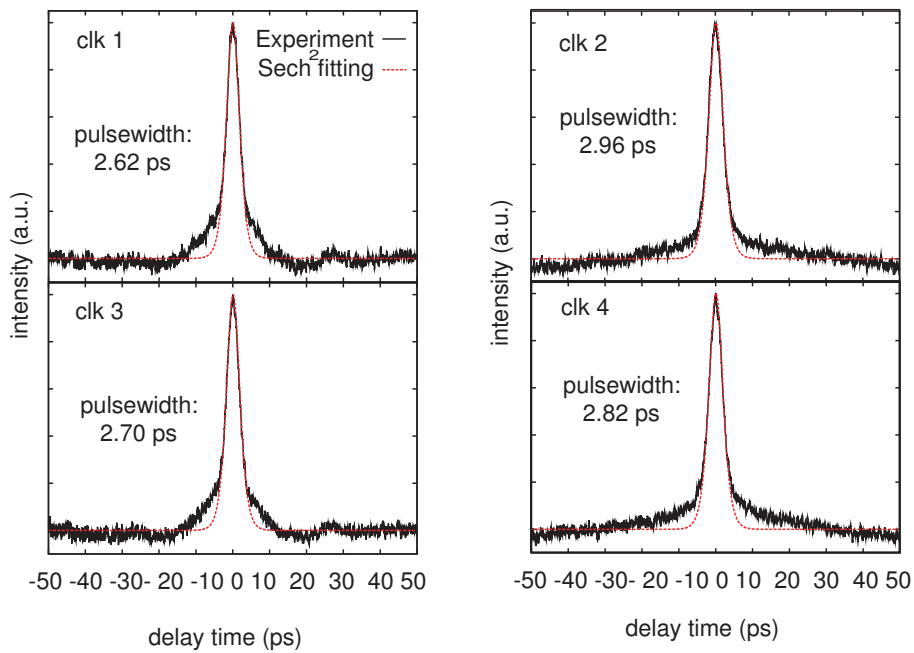


**Figure 3.15:** Autocorrelation traces of four multiwavelength sampling pulses compressed by RA-MPC.

nm ( $\lambda'_4$ ) were simultaneously generated. To enable simultaneous observation of

### 3.2 All-Optical Waveform Sampling using Wavelength Multicasting Technique

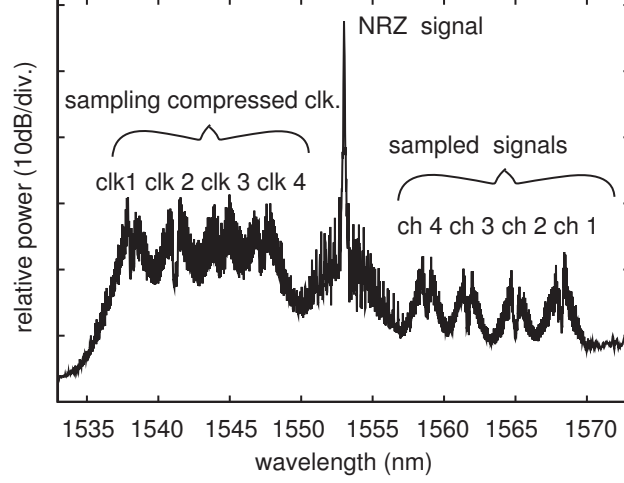


**Figure 3.16:** Spectra after HNLF for sampling waveform of NRZ data signal.

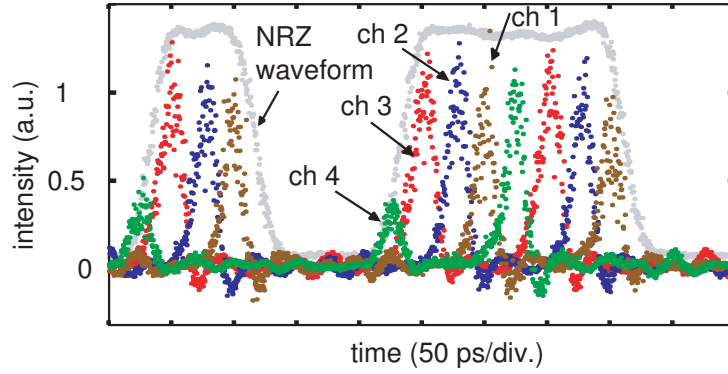


**Figure 3.17:** Temporal profiles of four waveforms of sampled outputs in case of NRZ waveform sampling. The inserted envelope is the waveform of NRZ data signal.

the waveforms of the four sampled data signals for the reconstruction of input waveform, an off-line process was implemented by combining the waveforms of 4x10 Gb/s FWM outputs to capture the waveform of SUT. The data information was copied to the four FWM sampled products. The power of optical sampled signal was proportional to that of the data signal at the sampling time. Hence, a 40 GSample/s all-optical waveform sampling was achieved. Due to the lack of

### 3. ALL-OPTICAL WAVEFORM CONVERSION AND WAVEFORM SAMPLING WITH MULTICAST SHORT-PULSEWIDTH SIGNALS

OBPFs, each sampled signal was filtered individually. The temporal profiles of four sampled signals were processed off-line as shown in Fig. 3.17. The combined temporal profiles of four multicast signals resulted an envelope which was well-matched with the waveform of NRZ signal. It is evidently indicated that the waveform of NRZ signal was successfully reconstructed.

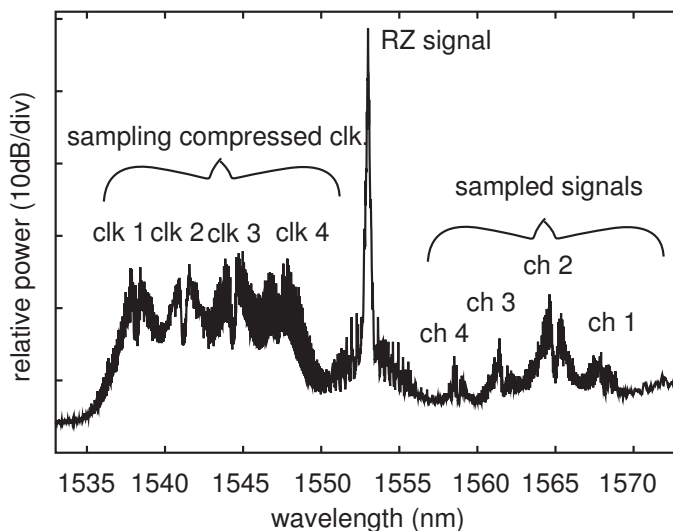


**Figure 3.18:** Spectra after HNLF for waveform sampling of RZ data signal.

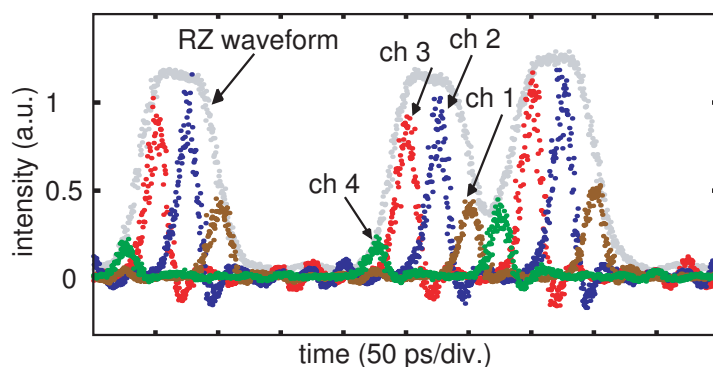


**Figure 3.19:** Temporal profiles of four waveforms of sampled outputs in case of RZ waveform sampling. The inserted envelope is the waveform of RZ signal

An all-optical waveform sampling for an RZ signal was also demonstrated. The spectra of sampled signals at the output of HNLF using wavelength multicasting process based FWM effect are shown in Fig. 3.18. Similarly, four multicast channels 1, 2, 3 and 4 (chs. 1, 2, 3, and 4) at the wavelengths of 1567.81 ( $\lambda'_1$ ), 1564.65 ( $\lambda'_2$ ), 1564.65 ( $\lambda'_3$ ), and 1558.25 nm ( $\lambda'_4$ ) were simultaneously generated. The power of each multicast signal was proportional to that of the SUT at the sampling time, leading a 40 GSample/s all-optical waveform sampling. An off-line process by combining the waveforms of four FWM outputs was done. Temporal profiles of four multicast sampled signals shown as in Fig. 3.19 illustrated the reconstructed waveform are well-fit to the original waveform of the RZ data signal.

A 40 GSample/s FWM-based all-optical waveform sampling of NRZ and RZ data signals was successfully implemented. The multiwavelength sampling pulses were compressed owing to soliton adiabatic compression in RA-MPC with the pulsewidths which were less than 3 ps. The reconstructed waveforms were matched well with input waveforms of the SUT. The number of sampled signal determine the sampling-rate. Therefore, this proposed scheme is potential for higher sampling-rate due to the flexible number of sampling clocks compressed by RA-MPC if using the multiwavelength pumps for Raman amplification to increase the gain bandwidth or reducing the frequency spacing between adjacent pulses of 200 GHz. If the frequency spacing is 200 GHz and time spacing is 12.5 ps, the maximum number of the sampling pulses is eight channels within the gain bandwidth of Raman amplification. Therefore, the sampling rate of 80 GSample/s could be obtained. The sampling-rate depends on the number of multiwavelength pulses. And the issues such as the number of multiwavelength pulses, wavelength detuning have been discussed in the multiwavelength pulses sources in the first demonstration in section 3.1.4.

### 3.3 Summary

In conclusion, the first demonstration is 4x10 Gb/s pulsewidth-tunable NRZ-to-RZ and wavelength multicasting using RA-MPC with a wide pulsewidth tuning range from around 4.68 to 12.17 ps by changing Raman pump power of 0.82 and 0.42 W, respectively. Error-free operations are reached for all multicast signals

### 3. ALL-OPTICAL WAVEFORM CONVERSION AND WAVEFORM SAMPLING WITH MULTICAST SHORT-PULSEWIDTH SIGNALS

---

with negative power penalties in comparison with the error-free operation of NRZ signal and small gap among converted RZ signals at BER of  $10^{-9}$ . The waveform and wavelength multicasting conversions without using RA-MPC have also been realized. In comparison with the converted RZ signals without compression, the receiver sensitivities of the compressed RZ signals with pulse compression (using RA-MPC) were enhanced. This scheme is able to increase more RZ output channels owing to the ability for increasing more multiwavelength RZ clocks compressed by RA-MPC if using multi-pumps for Raman amplification.

A technique using wavelength multicasting for all-optical waveform sampling of signals, particularly NRZ-OOK and RZ-OOK signals, is experimentally demonstrated. The sampling clocks source compressed by RA-MPC interact with the sample signal, forming multiple sampled signals. The number of sampled outputs could be easily increased by using more sampling clocks respected to the sampling-rate. The most notable part of the proposed scheme is the use of multiwavelength sampling pulse with short-widths compressed by RA-MPC and wavelength multicasting to sample signal. The RA-MPC could compress the sampling clocks with the pulsewidths which are on the order of a few picoseconds with almost same high-quality for all clocks. This sampler could capture the waveform of arbitrary amplitude-modulated signals in real-time, thus, it is useful for real-time applications.

## Chapter 4

# Pulse Compression and Wavelength Multicasting of an Inline RZ-DPSK Signal

The phase-modulated signals, particularly differential phase-shift-keying (DPSK) signal, attract much attention owing to robust tolerance to the effects of some fiber nonlinearities, and support high spectral efficiency. The obvious improvement of DPSK signal compared to on-off-keying (OOK) signal is the 3 dB-lower optical signal-to-noise ratio (OSNR) required to reach a given bit-error-rate (BER) associated with a balanced receiver which is the benefit of DPSK signal. This chapter demonstrates pulse compression of an inline 10 Gb/s return-to-zero (RZ)-DPSK signal through a distributed Raman amplifier-based pulse compressor (DRA-PC) and wavelength multicasting of this inline RZ-DPSK signal in a highly nonlinear fiber (HNLF)-based four-wave mixing (FWM) switch. Firstly, RZ-DPSK signal is transmitted over 30 km standard single mode fiber (SSMF) and then compressed by DRA-PC. The first application of the inline pulse compression is the generation of a higher bit-rate 40 Gb/s optical time division multiplexing (OTDM) stream multiplexed from lower bit-rate 10 Gb/s compressed RZ signal. The other application after pulse compression is the wavelength multicasting of the compressed RZ-DPSK signal using FWM process with multiple pumps. The obtained results



#### **4. PULSE COMPRESSION AND WAVELENGTH MULTICASTING OF AN INLINE RZ-DPSK SIGNAL**

---

show good performances in compression and wavelength multicasting concerning in good bit-error-rate (BER) operations and high-quality of compressed signals with short-pulsewidths.

### **4.1 Pulse Compression of an Inline RZ-DPSK Signal**

#### **4.1.1 Introduction of an Inline RZ-DPSK Signal Compression**

All-optical signal compression has been intensively used as one of the main elements to enable ultra-high-speed signals which overcome electronic limitations [69], [70]. The high-quality pulses with short-widths which are on the order of some picoseconds are generated by using the soliton compression which is based on the two key techniques. The first is the gradually decreasing of the value of dispersion along fiber by a dispersion-decreasing fiber (DDF) [71], [72], a step-like dispersion profiled fiber (SDPF) [73] and a comb-like dispersion profiled fiber (CPF) [74]. The second is that the peak power of soliton pulse is increased during pulse propagation in an anomalous dispersion fiber by an erbium-doped fiber amplifier (EDFA) [75] and a distributed Raman amplifier (DRA) [76]. The width of compressed signal in picosecond duration could be obtained by tuning the gain of optical amplifier. The DRA-based pulse compressor (DRA-PC) has a benefit over the others due to the high power at the output because the pulse is amplified during compression process. It is clearly shown that this compressor has been a powerful device to compress many pulses with different wavelength simultaneously [13], [52]. This compressor plays an important function in the multiplexing exchange between wavelength division multiplexing (WDM) and optical time division multiplexing (OTDM) [19], [53] as well as in the combination of waveform conversion and wavelength multicasting with pulsewidth tunability [77]. This technique enables the pulse compression with the width which are some of picoseconds with wide tuning range by controlling Raman pump power of DRA.

Recently, DPSK signals are widely attractive for high-bit-rate optical fiber communication systems owing to their larger robustness to fiber nonlinearities and their better receiver sensitivity compared with OOK signals [78]–[81]. To deal with the current trend to more advanced modulation format for the optimization of higher spectral efficiency [82], [83], it is attractive to detect the ability of pulse compression for phase-modulated signals which have not been realized in the past works. Different from the OOK signals compression [12], [13], the phase information of the phase-modulated signals could be degraded due to phase noises induced during the compression. Main reasons might be due to the residual phase noise caused by imperfect dechirping of self-phase modulation (SPM) over fiber dispersion, and the conversion of amplitude noise to phase noise by the fluctuation of gain [84], [85]. In practice, the optical signal is mostly compressed before data signal modulation at the transmitter to obtain the high-speed signals, leading the limitation in which the data signal could not be compressed for inline applications on the transmission. This process has the benefit that the pulse compression does not depend on the signal formats (amplitude and/or phase). On the other hand, if the pulse compression is used for the modulated data signal, it is necessary to consider the possibility or performance of data signal compression because of its dependence on the characteristics of data signals. Thus, it is attractive to demonstrate the pulse compression for the phase-modulated signals, particularly for RZ-DPSK signals using DRA-PC. Moreover, this work demonstrates the pulse compression for the phase-modulated signal, specifically for an inline RZ-DPSK data signal for inline applications. For example, the RZ-DPSK signal is transmitted from the source to the other nodes on the network for different services. The most important achievement in this work is the use of the pulse compressor for the inline RZ-DPSK signal which makes the pulsewidth of the RZ-DPSK signal being compressed down to a few of picoseconds at arbitrary location along the transmission. With short-pulsewidth, this compressed data pulse could be aggregated into higher speed-data-rate from lower speed-data-rate of signals using optical time multiplexing technique. In this chapter, a lower data-rate of 10 Gb/s RZ-DPSK signal with pulsewidth of about 20 ps was compressed down to 3.2 ps and then was aggregated into a 40 Gb/s optical time division multiplexing (OTDM) signal. However, the pulse compression after the data modulation

#### 4. PULSE COMPRESSION AND WAVELENGTH MULTICASTING OF AN INLINE RZ-DPSK SIGNAL

---

would be a challenge because noises directly affect the features of the modulated data signal. Therefore, this is the first effort to directly compress the pulse of RZ-DPSK signal for the useful above applications.

In this chapter, the pulse compression for an inline 10 Gb/s RZ-DPSK signal using DRA-PC is realized. The RZ-DPSK signal with pulsewidth of 20 ps transmitted over 30 km SSMF and then compressed down to a few of picoseconds by controlling Raman pump power of DRA. At bit-error-rate (BER) of  $10^{-9}$ , error-free operations at pulsewidths of 12, 7.0, and 3.2 ps are achieved with low power penalties within 2.3 dB compared to the back-to-back signal at the transmitter. To clearly investigate the quality of the compressed RZ-DPSK signal in inline applications, the 10 Gb/s signal compressed with pulsewidth of 3.2 ps is multiplexed to generate a 40 Gb/s OTDM signal. This OTDM signal is then demultiplexed to 10 Gb/s DPSK signal by using an optical gate based on four-wave-mixing (FWM) in a highly nonlinear fiber (HNLF). A 1.2 dB-power penalty of demultiplexed signal compared to the 10 Gb/s baseband signal is obtained.

##### 4.1.2 Operation Principle

The notable feature of this scheme in comparison with the past works is on the utilization of DRA-PC to compress RZ-DPSK signal. The RZ-DPSK signal is required as a fundamental soliton pulse adiabatically amplified in an anomalous dispersion fiber using DRA. The energy of the pulse is increased by the amplification in the DRA, thus, the soliton pulse based on adiabatic soliton compression technique is obtained. The fundamental soliton pulse has a peak power governed by the expression [86]

$$\tau_{\text{FWHM}}\sqrt{P_1} = 2.9\lambda^{3/2}\sqrt{|D| A_{\text{eff}}} \quad (4.1)$$

where  $\tau_{\text{FWHM}}$ [ps],  $P_1$ [mW],  $\lambda$  [ $\mu\text{m}$ ],  $D$ [ps/nm/km], and  $A_{\text{eff}}$  [ $\mu\text{m}^2$ ] are the full width at half maximum of pulse referred as the pulsewidth of pulse in practice, the peak power of fundamental soliton pulse, wavelength of pulse signal, dispersion coefficient, and effective core area of fiber, respectively. From Eq. (4.1), the

pulsewidth,  $\tau_{\text{FWHM}}$  is related to the peak power of the fundamental soliton pulse  $P_1$  as follows.

$$\tau_{\text{FWHM}} \propto \sqrt{\frac{1}{P_1}} \quad (4.2)$$

Equation (4.2) indicates that the pulsewidth,  $\tau_{\text{FWHM}}$  of soliton pulse is inversely proportional to the square-root of the peak power of the optical pulse,  $P_1$ . Therefore, the RZ-DPSK signal is compressed when increasing its peak power by Raman pump power because the soliton condition is kept during the amplification. By changing Raman pump power, the pulsewidth of RZ-DPSK signal is tuned at the output of DRA-PC.

#### 4.1.3 Experimental Setup

The experimental setup of the pulse compression of the inline RZ-DPSK signal operated by adiabatic pulse compression in DRA is illustrated in Fig. 4.1. An electro-absorption modulator (EAM) controlled by a 10 GHz synthesizer modulates a 10 GHz pulse from a laser diode (LD) at the wavelength of 1560.61 nm for generating an RZ clock. This RZ clock is boosted by an erbium-doped fiber amplifier (EDFA) assisted by a 0.6 nm optical band pass filter (OBPF). An RZ-DPSK signal with pulsewidth of 20 ps is generated by a DPSK modulator driven by 10 Gb/s data with pseudorandom sequence of  $2^{31}-1$  bits from a pulse pattern generator (PPG) synchronized with a 10 GHz synthesizer. This RZ-DPSK signal is amplified and filtered by an EDFA and a 0.6 nm OBPF, respectively. After being transmitted over 30 km SSMF, the dispersion of RZ-DPSK signal is compensated by a tunable dispersion-compensating module (TDCM). The setup of DRA-PC is described as in Section 3.1.3. A tunable fiber Raman laser (TFRL) operates at 1462 nm to optimize the power amplification. The parameters of DSF are shown as in Table 3.1. After compression, the compressed RZ-DPSK signal with various pulsewidths is analyzed to take the spectra, waveforms, eye patterns, and BER measurements.

#### 4. PULSE COMPRESSION AND WAVELENGTH MULTICASTING OF AN INLINE RZ-DPSK SIGNAL

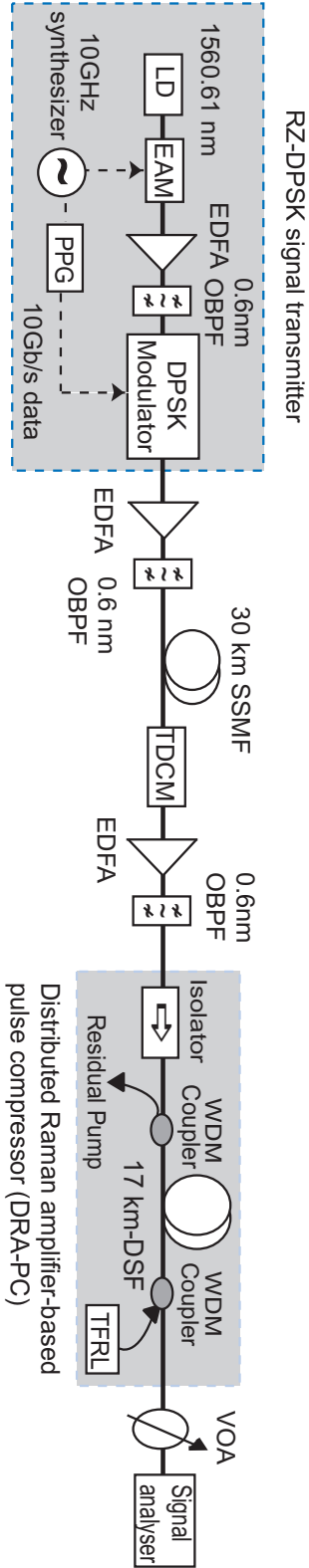


**Figure 4.1:** Experimental setup of the inline pulse compression for RZ-DPSK signal.

LD: laser diode, EAM: electro-absorption modulator, PPG: pulse pattern generator, EDFA: erbium-doped fiber amplifier, DPSK: Differential phase shift keying, OBPf: optical band pass filter, WDM: wavelength division multiplexing, DSF: dispersion-shifted fiber, TFRF: tunable fiber Raman laser, VOA: variable optical attenuation

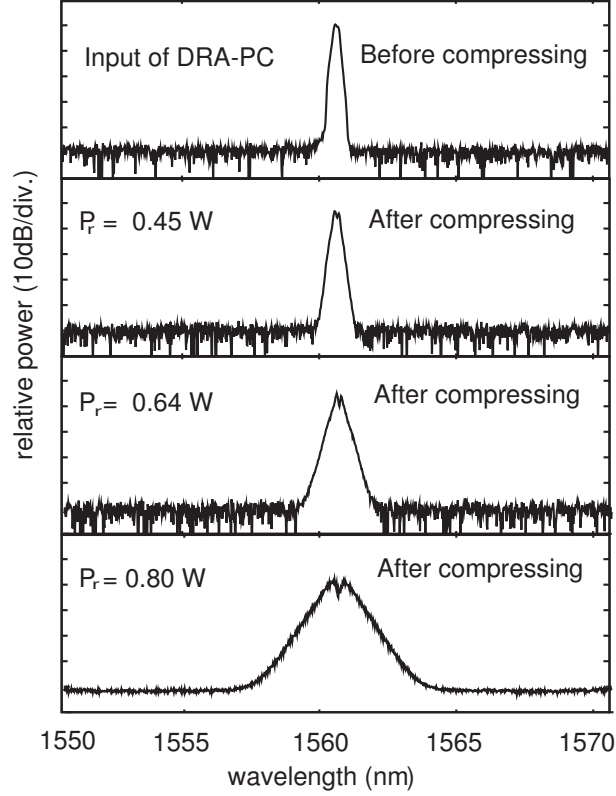


**Figure 4.2:** The spectrum of RZ-DPSK signal at the input of DRA-PC (before compressing) and at the output of DRA-PC (after compressing) with various Raman pump powers ( $P_r$ ).

#### 4.1.4 Experimental Results and Discussions

In the experiment, after being transmitted over 30 km SSMF and being compensated dispersion which was induced through the transmission, the RZ-DPSK signal was put at the input of DRA-PC. The RZ-DPSK signal was compressed due to adiabatic soliton compression in DRA. It is required that this pulse is a fundamental soliton pulse for this compression technique. The dependence between the pulsewidth of the RZ-DPSK signal and its peak power is described in Eqs. (4.1) and (4.2). Figures 4.2 and 4.3 perform the spectra and the autocorrelation traces of RZ-DPSK signal at the input of the compressor (before compression) and at the output of compressor (after compression) with various

#### 4. PULSE COMPRESSION AND WAVELENGTH MULTICASTING OF AN INLINE RZ-DPSK SIGNAL

---

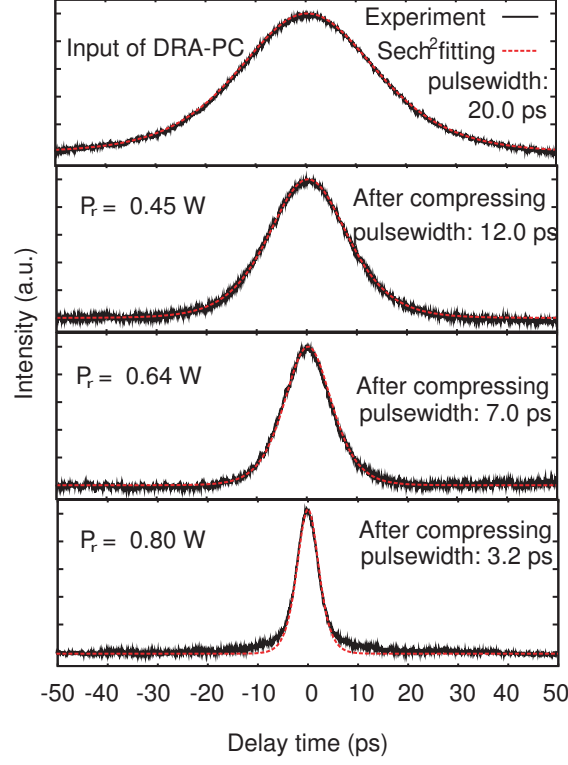


**Figure 4.3:** Autocorrelation traces of RZ-DPSK signal at the input of DRA-PC (before compressing) and at the output of DRA-PC (after compressing) with different pulsewidths of 12, 7.0 and 3.2 ps corresponding to Raman pump power ( $P_r$ ) of 0.45, 0.64 and 0.80 W, respectively.

pulsewidths corresponding to different values of Raman pump power ( $P_r$ ). The RZ-DPSK signal with pulsewidth of 20 ps was compressed down to 12, 7.0 and 3.2 ps corresponding to the values of  $P_r$  of 0.45, 0.64, and 0.80 W, respectively. As increasing  $P_r$ , the spectra of compressed signals were broader, while their pulsewidths became smaller. The increase of  $P_r$  caused the pulsewidth of RZ-DPSK signal output decrease due to adiabatic soliton compression in DRA. It is obviously seen that the RZ-DPSK signals compressed by DRA-PC were the high-quality pulses since their waveforms of pulses were well-matched with  $\text{sech}^2$  fitting with small pedestals. Therefore, the compressed pulses would be suitable for the high-speed signals for inline applications. In comparison to another

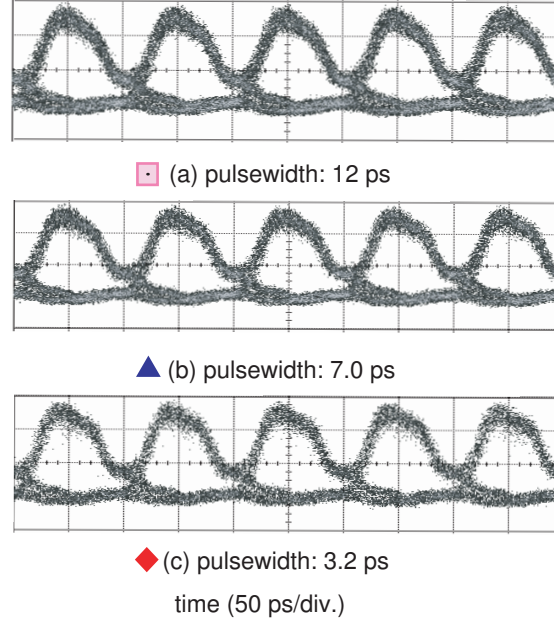


**Figure 4.4:** Eye patterns of demodulated RZ-DPSK signal after compressing to 12 ps (a), 7.0 ps (b), and 3.2 ps (c).

method that needed an additional scheme to suppress pedestal [72], this technique did not require any assistances of signal regenerator to reduce pedestal. Figures 4.4(a), (b), and (c) perform eye patterns of the compressed RZ-DPSK signal with different pulsewidths of 12, 7.0, and 3.2 ps, respectively which were taken by an 30 GHz bandwidth electronics sampling oscilloscope. Although the oscilloscope had a bandwidth limitation respected to the broaden spectra of the signal after compression, the opened-eye patterns imply that the influence of such patterns effect on the phase shift during the compression process would be negligible. The reason is probable that such effect is difficult to be observed due to robust tolerance to the phase noises of the RZ-DPSK signal.

There is considerable concern that phase noises induced during the pulse compression process would cause degradation in receiver sensitivity of the RZ-DPSK signal after compression, BER characteristics of the RZ-DPSK signals with many pulsewidths were measured as a function of received power. Moreover, an effort to find a quantitative experimental receiver sensitivity improvement or degrada-



#### 4. PULSE COMPRESSION AND WAVELENGTH MULTICASTING OF AN INLINE RZ-DPSK SIGNAL

---

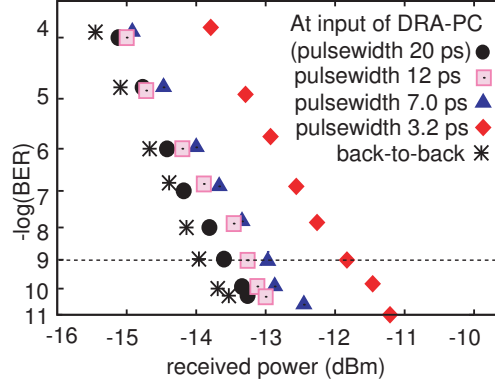


**Figure 4.5:** BER curves of RZ-DPSK signal at the input/output of DRA-PC with various pulsewidths of 20, 12, 7.0 and 3.2 ps in comparison with the back-to-back data pulse at the transmitter.

tion of the shorter width of RZ pulse compared with the longer width of RZ pulse after compression. There was a receiver sensitivity degradation for the shorter pulsewidth of the compressed RZ data signal compared to and the longer pulsewidth of the compressed RZ signal. The primary concern is due to the Raman noise [12]. The BER curves of RZ-DPSK signals at the transmitter (back-to-back), at the input of the DRA-PC (after 30 km SSMF transmission with dispersion compensating), and at the output of the RA-PC (after compressing) with the pulsewidths of 12, 7.0, and 3.2 ps are performed in Fig. 4.5. Power penalties which were less than 2.3 dB were observed in comparison with the back-to-back data signal. The powers of compressed signals with various pulsewidths varied the amounts within 1.5 dB. The shorter pulsewidths of the compressed signal caused its receiver sensitivity be larger. The main reason is probably due to amplified spontaneous emission (ASE) noise of the Raman amplifier. Similar results were also achieved in demonstrations for the RZ-OOK signal compression (at the transmitters) [12], [13] in which a signal and many signals with multiwavelength were compressed, respectively. The waveforms were well-matched fitted to  $\text{sech}^2$  function and good BER operation of the compressed RZ-DPSK signals evidently indicated that the phase-preserving was kept during the compression process. For further performance evaluation of the compressor to shorter pulsewidths, Raman

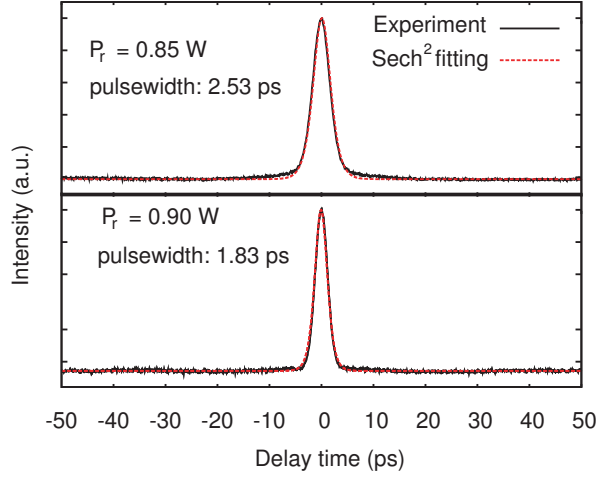


**Figure 4.6:** Autocorrelation traces of the compressed RZ-DPSK signal with pulsewidths of 2.53 and 1.83 ps.

pump power is continued increasing. Autocorrelation traces of the RZ-DPSK signal with pulsewidth of 2.53 and 1.83 ps corresponding to  $P_r$  of 0.85 W and 0.9 W, respectively are shown in Fig. 4.6. The high-quality compressed RZ-DPSK signal were also obtained with the pulsewidth of 2.53 ps and 1.83 ps. However, a stable BER measurement was very hard to be achieved because the 1-bit delay interferometer employed in the DPSK experimental demodulator was not able to support the demodulation of RZ-DPSK signals with such pulsewidths.

In addition, the soliton stability under various variable conditions was discussed. To obtain fundamental soliton pulse compression, the relation between the peak power and pulsewidth of initial signal (input signal at the input of DRA-PC) were described in Eq. (4.1). The interesting feature is that even if the values of the peak power and pulsewidth of initial signal is fluctuated around those of fundamental soliton pulse described in Eq. (4.1), the pulse compression was able also to be achieved. The reason comes from the fact that the fundamental soliton might form for the variation values of power and pulsewidth of the initial pulse but does not hinder soliton formation [22]. Hence, the compression of RZ-DPSK signal with the duty cycles of 33%, 50%, and 66% could also be reached with performances which were different regardless of pedestals and compression factors.

#### 4. PULSE COMPRESSION AND WAVELENGTH MULTICASTING OF AN INLINE RZ-DPSK SIGNAL

---

In case of this work, the residual dispersion, resulted from dispersion compensation after transmission, could affect the shape and width of the initial signal. If the shape of the signal at the input of compressor does not follow  $\text{sech}^2$  fitting, the pulse compression could be got with different performance in comparison with the case of fundamental soliton signal compression [22].

Moving to the compression of the nPSK signal, due to the multi-level of phase modulated in nPSK formats, there is still a challenge because of nonlinear interaction between neighboring pulses. For the phase-modulated signal used in the optical fiber communication systems, nonlinear interaction between the neighboring pulses in a single channel such as intra-channel four-wave mixing (IFWM) and intra-channel cross-phase modulation (IXPM) are one of the primary limitation factors for transmission of high-speed signals [87]–[92]. The pulse compression would be possible for the nPSK signals and OOK signals. It might be impossible for multi-level signals like quadrature amplitude modulation (QAM), pulse amplitude modulation (PAM) signals due to the multi-level amplitude of such signals.

## 4.2 Application of Pulse Compression of RZ-DPSK Signal

### 4.2.1 Inline OTDM Signal Generation

In practice, the optical signal is mostly compressed before data signal modulation at the transmitter to obtain the short-pulsewidth required in high-speed signals, leading the limitation in which the data signal could not compressed for inline applications on transmission. Here, an OTDM signal is composed based on an inline 10 Gb/s compressed RZ-DPSK signal by a multiplexer. Indeed, after compression, the inline RZ-DPSK signal with the pulsewidth of 3.2 ps is multiplexed into a 40 Gb/s OTDM signal. This OTDM stream is then demultiplexed to 10 Gb/s RZ-DPSK baseband signals by using four-wave-mixing (FWM) in a highly nonlinear fiber (HNLF). A 1.2 dB-power penalty of the demultiplexed 10 Gb/s signal with respect to the 10 Gb/s baseband signal compressed by DRA-PC is

obtained.

### 4.2.1.1 Experimental Setup

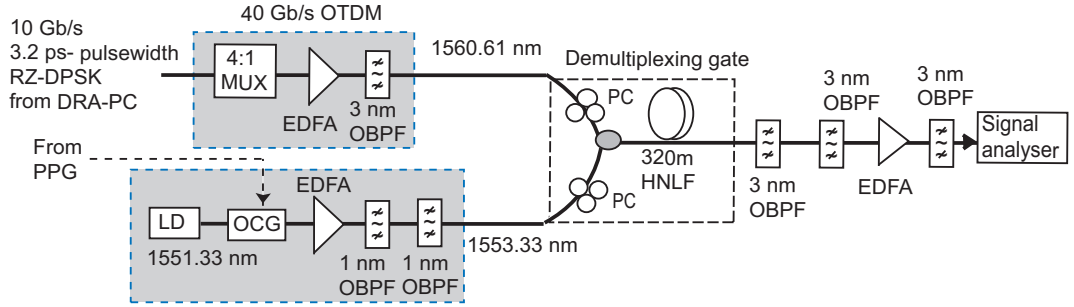


**Figure 4.7:** Experimental setup for the multiplexing and demultiplexing of a 40 Gb/s OTDM stream which is based on the RZ-DPSK signal compressed by DRA-PC.

From Fig. 4.7, this OTDM signal is demultiplexed by using an HNLf-based FWM switch. The power of OTDM signal is increased and filtered by an EDFA and a 3 nm OBPF, respectively before demultiplexing. For the generation of a pulsewidth-short RZ clock used as a pump for the demultiplexing the OTDM stream in HNLf-based FWM switch, an optical comb generator (OCG) is employed. An LD generates a continuous wave at the wavelength of 1551.33 nm. This signal is modulated by OCG driven by 10 GHz clock from the PPG. An EDFA compensates OCG insertion loss. Two 1.0 nm OBPFs are used to engineer the OCG spectrum for filtering a 10 GHz RZ clock with the pulsewidth of 3.5 ps. This RZ clock and the OTDM signal are set as a pump and a probe, respectively for FWM process in the HNLf. Polarization controllers (PCs) are used to optimize polarization state of both clock and data signal. The parameters of the HNLf are described in Table 3. 2. After FWM process, the demultiplexed signal is filtered and boosted by 3 nm OBPFs and an EDFA, respectively for analyzing its waveforms, eye patterns, and BER measurement.

#### 4. PULSE COMPRESSION AND WAVELENGTH MULTICASTING OF AN INLINE RZ-DPSK SIGNAL

---

##### 4.2.1.2 Experimental Results and Discussions

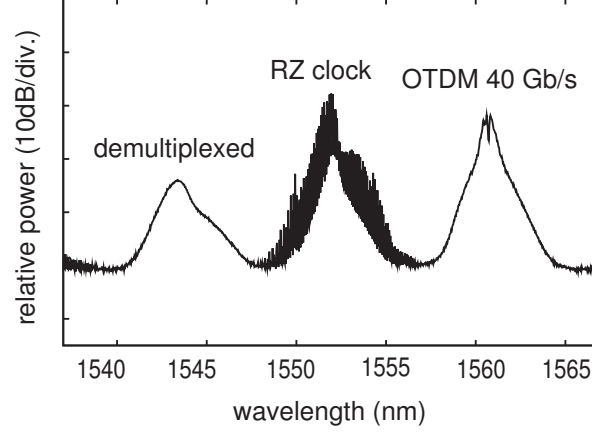
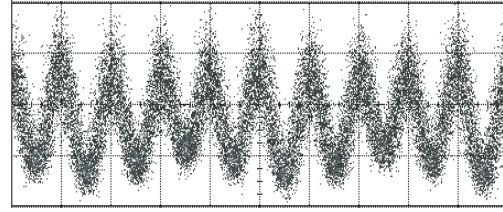


**Figure 4.8:** Spectra at the output of HNLf-based FWM switch for demultiplexing 40 Gb/s OTDM signal.

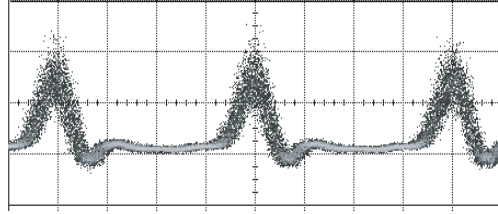
Figure 4.8 shows the spectra of 40 Gb/s OTDM signal demultiplexed by HNLf-based FWM switch. Eye patterns of the multiplexed OTDM stream and the demultiplexed 10 Gb/s RZ-DPSK signal before and after signal demodulation are shown in Figs. 4.9(a), (b) and (c), respectively. The BER characteristics of 10 Gb/s RZ-DPSK signal after demultiplexing and the inline 10 Gb/s base-band RZ-DPSK signal compressed by DRA-PC with pulsewidth of 3.2 ps were performed in Fig. 4.10(a). The demultiplexed signal with pulsewidth of 2.95 ps is well-match with  $\text{sech}^2$  fitting with very low pedestal. The demultiplexed signal with pulsewidth of 2.95 was obtained due to pulse compression after this FWM conversion. The pulsewidth of the FWM signal became shorter than that of RZ clock (3.5 ps) and the OTDM signal (3.2 ps). It comes from the facts that the FWM signal intensity is proportional to the product of the square of the clock ( pump) intensity and the intensity of the OTDM signal (probe). The pedestal existed in the OTDM signal due to the compression as seen in Fig. 4.10(b) was also suppressed due to this relation intensity. A low power penalty within 2 dB was due to noise probably originating from the EDFA and DRA-PC. The small power penalty and clear opening eye patterns of the demultiplexed

## 4.2 Application of Pulse Compression of RZ-DPSK Signal

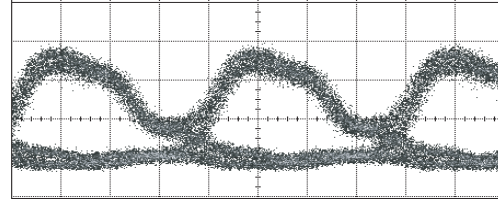
RZ-DPSK signal show that this proposed compressor could bring in a new compression technique for RZ-DPSK signal using DRA-PC. Thanks to this ability of this compressor for inline applications, the aggregate OTDM signal based on the 10 Gb/s compressed RZ-DPSK signal could be generated at the intermediate node where higher bit-rate signals are needed. It is notable to know that this compressor could compress the inline RZ-DPSK signal with tunable pulsewidth by controlling Raman pump power, thus, it is flexible for the use of generating different aggregate higher bit-rate OTDM signals.



(a) multiplexed 40 Gb/s OTDM signal



(b) demultiplexed RZ-DPSK before demodulation



(c) demultiplexed RZ-DPSK after demodulation

time (25ps/div.)

**Figure 4.9:** Eye patterns of (a) the multiplexed 40 Gb/s OTDM signal, (b) and its demultiplexed 10 Gb/s signal (b) before and (c) after demodulation.

#### 4. PULSE COMPRESSION AND WAVELENGTH MULTICASTING OF AN INLINE RZ-DPSK SIGNAL

---

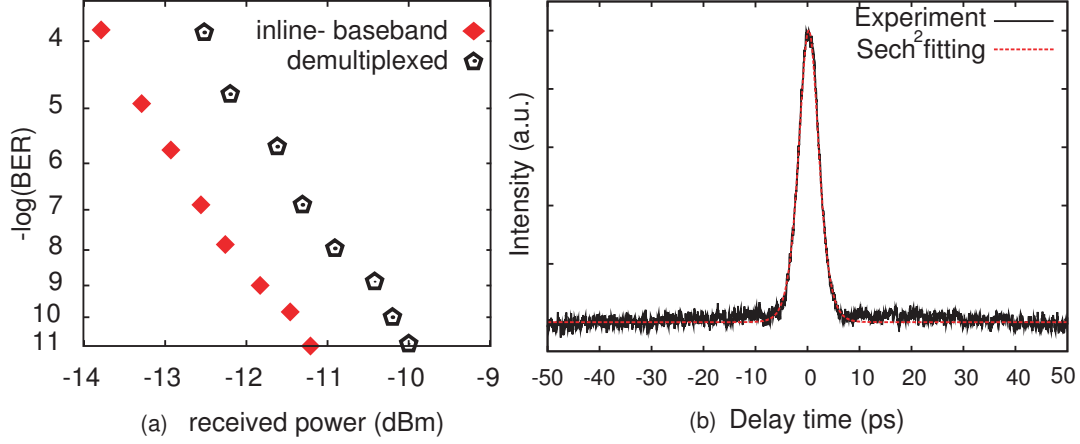


**Figure 4.10:** (a) BER characteristics of inline 10 Gb/s baseband signal and 10 Gb/s signal demultiplexed from 40 Gb/s OTDM signal. (b) Autocorrelation trace of 10 Gb/s RZ-DPSK signal with pulsewidth of 2.95 ps after demultiplexing.

### 4.2.2 Wavelength Multicasting of an Inline RZ-DPSK Signal with Tunable Short-Pulsewidths

#### 4.2.2.1 Introduction

All-optical wavelength multicasting technique, which performs routed-data from single point to multi-points in optical domain, efficiently supports the application of high bandwidth services. These services are such as internet protocol television (IPTV), video-on-demand, teleconferencing and multimedia broadcasting thanks to the ability to enable the rapid resolution of output-port conflict, the failure of lightpath, and carrier-reuse [93]–[99]. So far, multicast signals using wavelength technique has been experimentally demonstrated in nonlinear devices [14]–[16], [100]–[105]. However, these demonstrations focus on the achievement of converted signal in terms of bit-error-rate (BER), optical signal noise ratio (OSNR), or conversion efficiency without the considerations of pulsewidth management. As the applications mentioned through the thesis for multicast signals with tunable short-pulsewidths, a consideration of multicast signals with short-

## 4.2 Application of Pulse Compression of RZ-DPSK Signal

---

pulsewidth tunability is particularly desirable to provide flexibility for the optimization of utilized capacity of different destination links and wavelength resource of the network using pulse compression. The demand of short-pulsewidth signals for the high bit-rate signals is crucial to increase the overall capacity of optical networks. In the wavelength multicasting of an inline RZ-DPSK signal, the multicasting process is implemented at an arbitrary intermedia node where wavelength multicasting is needed after transmission. This inline signal is multicast to different wavelengths with short-pulsewidths thanks to the pulse compression before multicasting process. The multicast signals with short-pulsewidths could be multiplexed to the higher bit-rate OTDM signals to optimize capacity on different destinations. Without the assistance of pulse compression of an inline signal, it is challenging for the previous demonstrations when inline processing is needed. Depending on the requirement of traffic demand and the available condition of network, the inline process is considered. For example, an intermediate node receives the incident data signal and multicasts this signal based on the demand. The important fact is that the pulsewidth multicast RZ-DPSK signals could be compressed at an intermediate node. This feature provides the flexibility in aggregating higher bit-rate channels from lower bit-rate channel by optical time multiplexing technique during transmissions to different destinations through networks. In Ref. [106], the wavelength multicasting of RZ-OOK signal with tunable short-pulsewidths has been realized. However, in that scheme, the RZ-OOK signal is set as a pump in FWM process. Thus, the converted signals are located near the OOK signal, leading no phase-preserving at the converted signals. So that, the scheme in Ref. [106] could not use for the wavelength multicasting of the phase-modulated signals.

Conventionally, mode-locked lasers (MLLs) are used to generate short-pulsewidth clocks which then are launched to DPSK modulators to generate RZ-DPSK signals [107], [108]. However, the use of MLLs is limited at the transmitters and is restricted regarding the pulsewidth flexibility. It is necessary to combine signal compression and wavelength multicasting for generating many multicast signals with the pulsewidth which is on the order of some picoseconds for application in WDM and OTDM networks to increase network capacity. Hence, the other



#### 4. PULSE COMPRESSION AND WAVELENGTH MULTICASTING OF AN INLINE RZ-DPSK SIGNAL

---

application of RZ-DPSK signal compression is the use of DRA-PC for wavelength multicasting to create many multicast RZ-DPSK signals with tunable short-pulsewidths. The short-pulsewidths give rise to the ability of the generation of the aggregate higher bit-rate signals by optical time multiplexing of lower bit-rate signals from multicast signals. However, the maximum bit-rate OTDM signal depends on the pulsewidth of multicast signals. Therefore, the pulsewidth tunability of this proposed scheme improves the flexible management of bit-rate of aggregate signals adapted to optimize utilized capacity on different destinations.

An inline 4x10 Gb/s tunable short-pulsewidth RZ-DPSK signal with wavelength multicasting using DRA-PC and HNLF is realized. DRA-PC compresses the inline RZ-DPSK signal which then interacts with two continuous waves (CWs) based on FWM effect in the HNLF. The pulsewidths of the multicast signals were compressed in the range of 12.5 and 4.27 ps after wavelength multicasting. Power penalties of the multicast RZ-DPSK signals with various pulsewidths within 3 dB compared to the input back-to-back signal before compression are obtained at BER of  $10^{-9}$ .

##### 4.2.2.2 Concept of Operation Principle

The concept of wavelength multicasting of RZ-DPSK signal with tunable pulsewidth using a DRA-PC and an HNLF-based FWM switch is shown in Fig. 4.11(a). The improved feature of the proposed scheme in comparison with the past works is on the use of DRA-PC to get RZ-DPSK signal with short-pulsewidths at picosecond tuning range before wavelength multicasting. Figure 4.11(b) illustrates the temporal profiles of all signals in the conversion processes. Fig. 4.11(c) shows the conceptual spectra of the proposed scheme. In the HNLF, the RZ-DPSK signal at frequency  $f_s$  compressed by DRA-PC interacts with the multiwavelength CW pumps at frequencies  $f_{p1}$ ,  $f_{p2}, \dots$ , and  $f_{pN}$  over FWM process. The input RZ-DPSK signal is multicast to many RZ signals with different wavelengths at FWM products generally given by the following expressions [24]

$$f_{ch2} = 2f_{p1} - f_s = f_{p1} + \Delta f \quad (4.3)$$

## 4.2 Application of Pulse Compression of RZ-DPSK Signal

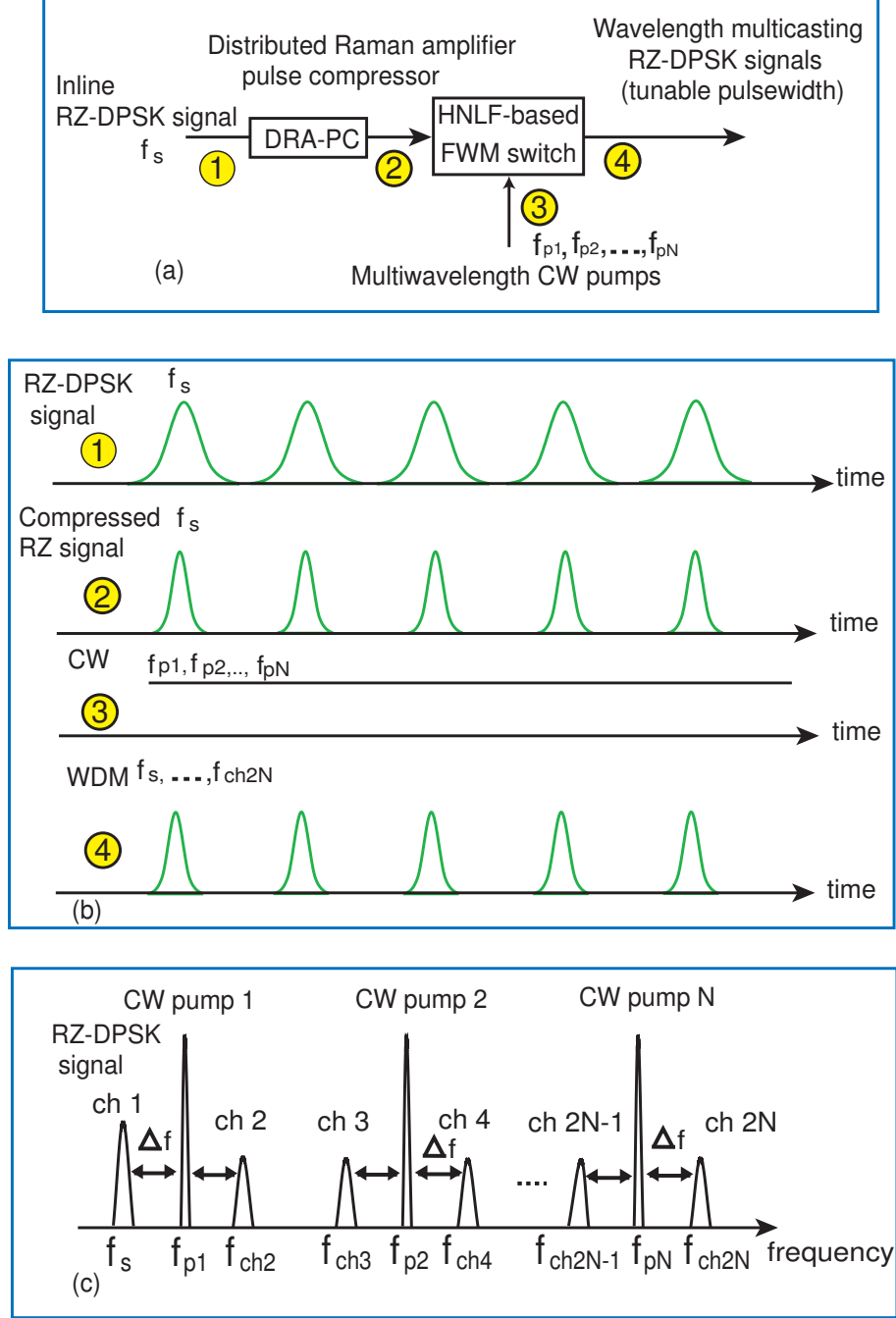


**Figure 4.11:** (a) Operation principle of wavelength multicasting for RZ-DPSK signal with tunable pulsewidth using DRA-PC.  
(b) Temporal profiles of all signals in the process.  
(c) Conceptual spectra of wavelength multicasting of RZ-DPSK signal after FWM process.

#### 4. PULSE COMPRESSION AND WAVELENGTH MULTICASTING OF AN INLINE RZ-DPSK SIGNAL

---

For  $N \geq 2$

$$f_{ch2N-1} = f_{pN} + f_s - f_{p1} = f_{pN} - \Delta f \quad (4.4)$$

$$f_{ch2N} = f_{pN} + f_{p1} - f_s = f_{pN} + \Delta f \quad (4.5)$$

where  $\Delta f$  is the frequency spacing between CW pump 1 and RZ-DPSK signal ( $\Delta f = f_{p1} - f_s$ );  $N$  is the number of CW pumps. After FWM process, the electric field amplitude of each multicast signal at the output is governed by expressions [24]

$$E_{ch2}(t) \propto E_{pump1}^2 E_{signal}^*(t), \quad (4.6)$$

$$E_{ch2N-1}(t) \propto E_{pump1}^* E_{signal}(t) E_{pumpN}, \quad (4.7)$$

$$E_{ch2N}(t) \propto E_{pump1} E_{signal}^*(t) E_{pumpN}, \quad (4.8)$$

where  $E_{pump1}$ ,  $E_{pumpN}$ , and  $E_{signal}(t)$  are the electric fields of pump 1, pump  $N$  and the compressed RZ-DPSK signal, respectively;  $*$  denotes the complex conjugate of electric field amplitude. Therefore, the multicast RZ-DPSK signals are simultaneously generated in the scheme using multiple pumps in both phase-conjugating and non-phase-conjugating in wavelength multicasting. The FWM products inherit the data of the RZ-DPSK signal and their pulsewidths follow that of the RZ-DPSK signal compressed by DRA-PC. Hence, the tunable pulsewidths of the converted RZ-DPSK signals are obtained by changing Raman pump power.

##### 4.2.2.3 Experimental Setup

The experimental setup is shown in Fig. 4.12. A 10 Gb/s RZ-DPSK signal at the wavelength of 1560.61 nm with pulsewidth of 20 ps is compressed by DRA-PC. The configure of DRA-PC has been illustrated in Fig. 4.1. After compression, the RZ-DPSK signal with short-pulsewidth and two CWs, which are set as the probe and pumps, respectively, interact together over FWM process. An EDFA followed by an OBPF and a variable optical attenuation (VOA) are used to adjust powers of the compressed RZ-DPSK signal and two CWs, respectively to obtain good output waveforms. Two polarization controllers (PCs) is used to obtain the largest conversion efficiency. The 320 nm HNLF has the parameters shown in

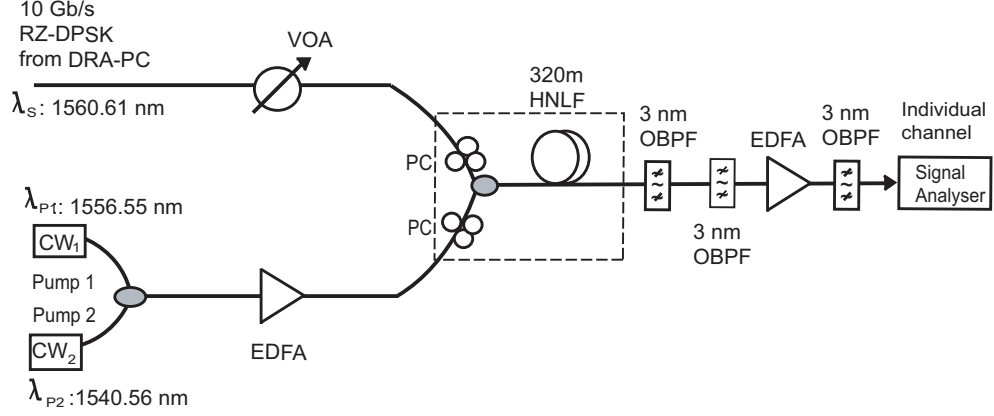


**Figure 4.12:** Experimental setup of wavelength multicasting of RZ-DPSK signal with tunable short-pulsewidth using distributed Raman amplifier-based pulse compressor (DRA-PC).

Table 3.2. The multicast RZ-DPSK signals with tunable short-pulsewidths are filtered to get the spectra, waveforms, eye patterns, and BER measurements.

### 4.2.2.4 Experimental Results and Discussions

Figures 4.13(a), (b) and (c) illustrates the spectra at the output of HNLF after wavelength multicasting of the inline compressed RZ-DPSK signal corresponding to different values of Raman pump power ( $P_r$ ) of 0.45, 0.64 and 0.82 W, respectively. By increasing  $P_r$ , the spectra of the RZ-DPSK signals were broaden at the output of DRA-PC, resulting in spectral broadening of multicast signals at the output of HNLF-based FWM switch. The reason comes from the facts that the increase in the peak power of the input RZ-DPSK signal made its spectrum broaden. The multicast signals at the wavelength of 1560.61 nm (channel 1), 1552.52 nm (channel 2), 1544.53 nm (channel 3), and 1536.61 nm (channel 4) were separately filtered. With different values of Raman pump power, there was always an existence of the undesired FWM product which was near the wavelength of the input signal (the same wavelength with channel 1) due to FWM interaction between pump 1 and channel 1. The phase information was not preserved in this undesired signal, thus, it could not be used as a converted signal.

#### 4. PULSE COMPRESSION AND WAVELENGTH MULTICASTING OF AN INLINE RZ-DPSK SIGNAL

---

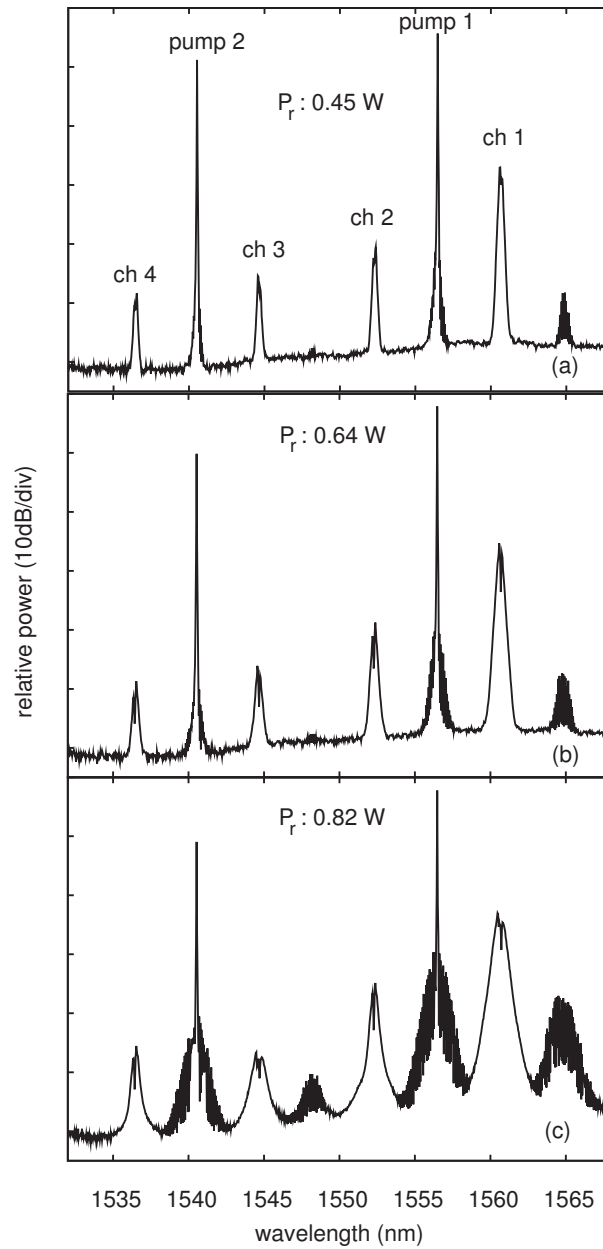


**Figure 4.13:** Spectra at the output of HNLF corresponding to different values of Raman pump powers ( $P_r$ ) of (a) 0.45, (b) 0.64, and (c) 0.82 W.

With the increase of  $P_r$ , the pulsewidth of input RZ-DPSK signal was shorter and its spectrum is more broader. As shown in Fig. 4.13(c), the other undesired FWM product occurred at the wavelength of around 1548.53 nm. The reason is

## 4.2 Application of Pulse Compression of RZ-DPSK Signal

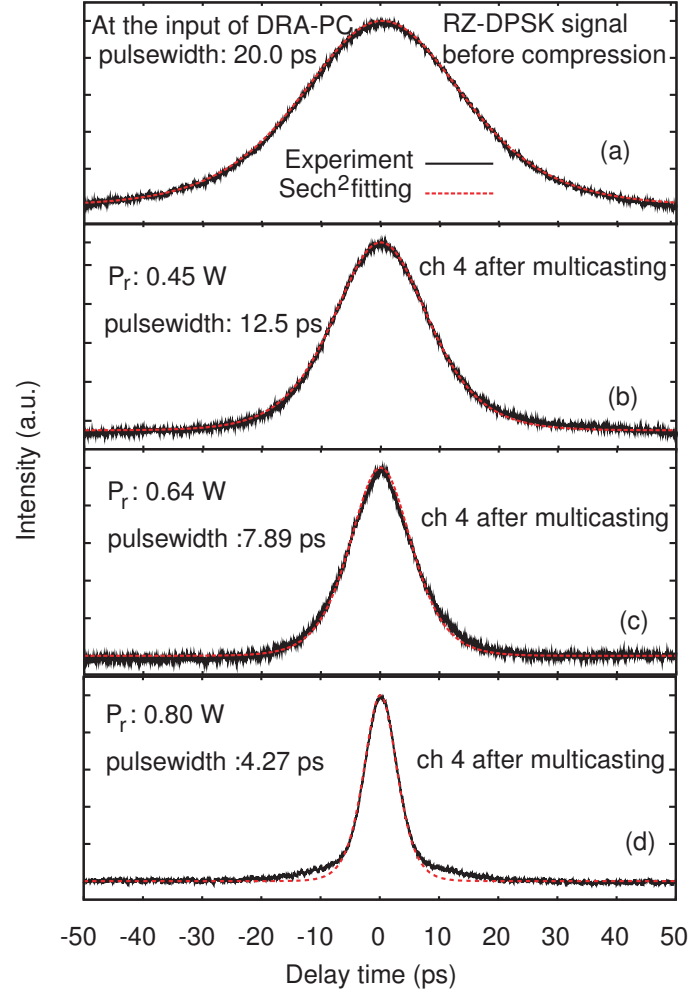


**Figure 4.14:** Autocorrelation traces of the RZ-DPSK signal (a) at the input of compressor (before compressing) and multicast signal at channel 4 (ch 4) with pulsewidths of (b) 12.5, (c) 7.89 and (d) 4.27 ps corresponding to Raman pump power ( $P_r$ ) of 0.45, 0.64, and 0.80 W, respectively.

due to the higher power of RZ-DPSK signal from DRA-PC at high pump power. The unwanted signal took up power from the system and reduce conversion efficiency of the multicast outputs. The autocorrelation traces of RZ-DPSK signal at the input DPA-PC before compression and the multicast signals at channel 4 (ch 4) with various pulsewidths of 12.5, 7.89 and 4.27 ps were performed in Fig. 4.14. This scheme provided the number of output channels which was double

#### 4. PULSE COMPRESSION AND WAVELENGTH MULTICASTING OF AN INLINE RZ-DPSK SIGNAL

---

compared to that of CW pumps. The increase of  $P_r$  made the RZ-DPSK signal be compressed over the adiabatic soliton compression. Therefore, the pulsewidths of multicast signals were also compressed to 12.5, 7.89, and 4.27 ps corresponding to  $P_r$  of 0.45, 0.64, and 0.8 W, respectively. It is notable to know that the pulse waveforms after wavelength multicasting with low pedestals were well-matched to  $\text{sech}^2$  function as shown in Fig. 4.14.

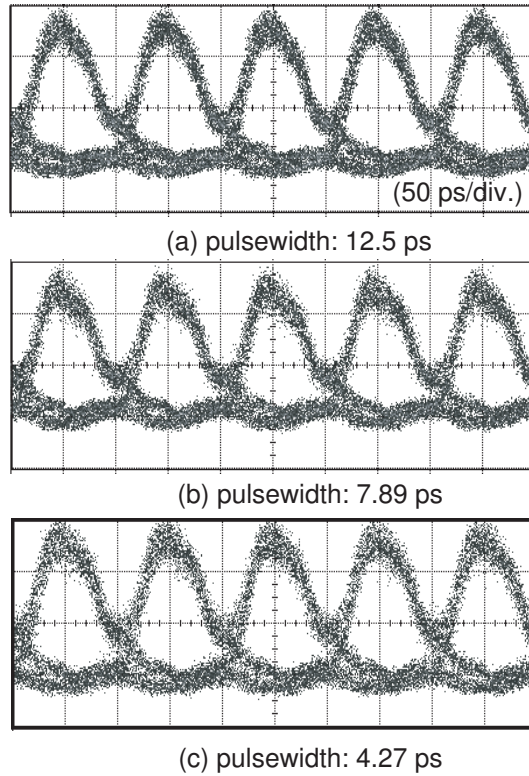


**Figure 4.15:** Eye patterns of the demodulated multicast RZ-DPSK signal at channel 4 (ch 4) with various pulsewidths of 12.5 (a), 7.89 (b) and 4.27 ps (c).

The clear-opened eye patterns of demodulated RZ-DPSK signal at channel 4 (1536.61 nm) with pulsewidths of 12.5, 7.89, and 4.27 ps are shown in Fig. 4.15 (a), (b), and (c), respectively. Due to the limitation of 30 GHz bandwidth of the sampling oscilloscope, eye patterns of RZ-DPSK signal with different pulsewidths were observed almost the same. To investigate the achievement of multicast

## 4.2 Application of Pulse Compression of RZ-DPSK Signal

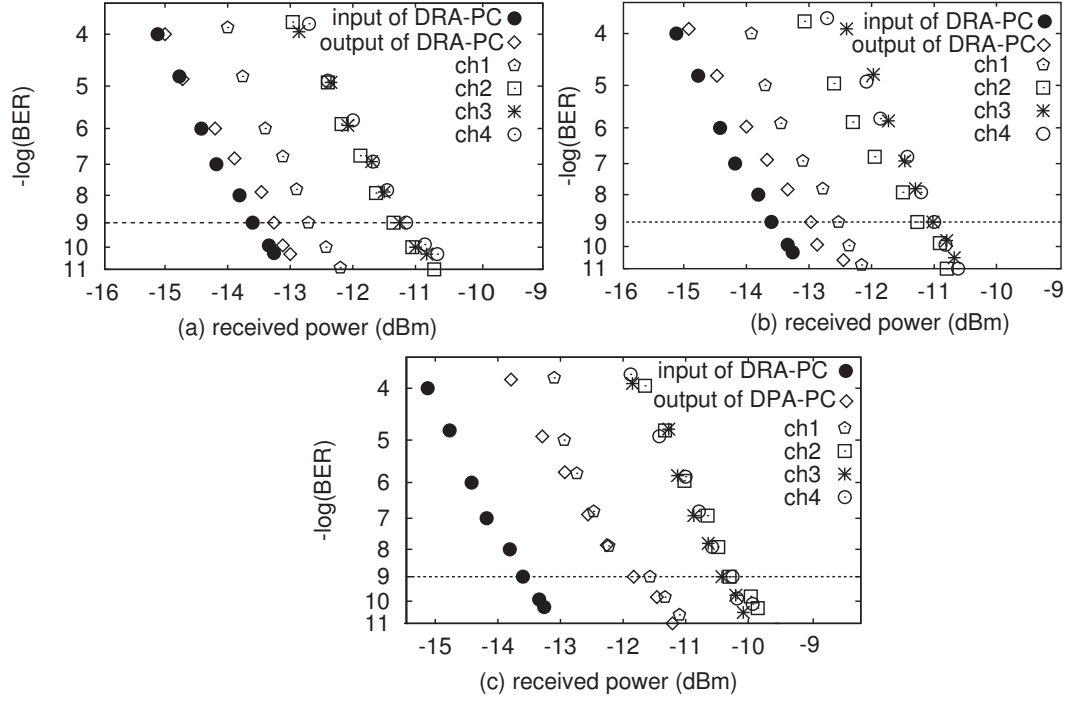


**Figure 4.16:** BER measurement of multicast RZ-DPSK signals with the pulsewidth around of 12.5, 7.89, and 4.27 ps at different values of Raman pump power ( $P_r$ ) of (a) 0.45, (b) 0.64 and (c) 0.80 W, respectively.

RZ-DPSK signal after wavelength multicasting processes, BER measurement of multicast RZ-DPSK signals with various pulsewidths of 12.5, 7.89 and 4.27 ps were taken as a function of received power as shown in Figs. 4.16 (a), (b) and (c), respectively. At each value of Raman pump power, receiver power of channel 1 was the best and the receiver power of channel 2 was very slightly better than those of channels 3 and 4. Channel 1 was the best because channel 1 was not a generated signal with new frequency, therefore, it remained the highest power compared to the other multicast signals. There was very a few variation in amount of power among channels 2, 3 and 4. Main concerns would be noises attributed by DPA-PC and EDFAs used for compression and FWM processes, in additional, by differences in powers and polarizations of CW pumps. The receiver sensitivities of converted signals at different pulsewidths corresponding to various values of Raman pump power are shown in Fig. 4.17. There were the differences



#### 4. PULSE COMPRESSION AND WAVELENGTH MULTICASTING OF AN INLINE RZ-DPSK SIGNAL

---

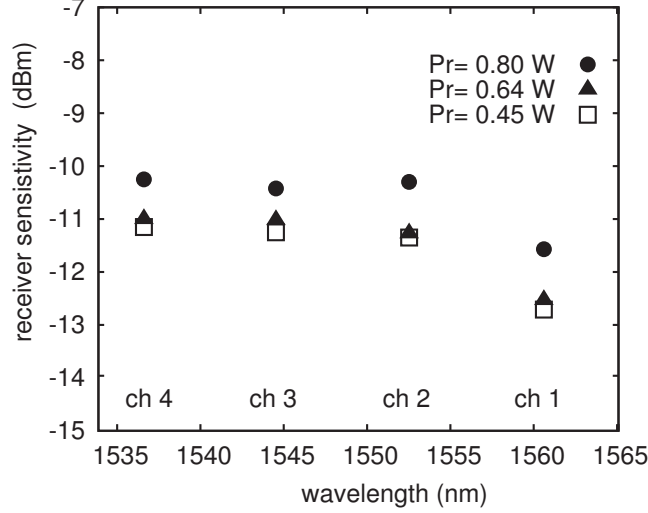


**Figure 4.17:** Receiver sensitivities of all converted RZ-DPSK signals with many pulsewidths corresponding to different values of Raman pump power at  $\text{BER} = 10^{-9}$ .

in amount of the received power of each signal with three different pulsewidths. For example, at channel 4, receiver power of RZ-DPSK signal with pulsewidth of 4.27 ps was 0.8 and 0.9 dB larger than that of RZ-DPSK signal with pulsewidths of 7.89 and 12.5 ps, respectively. The reason is that the received power increased as the pulsewidth of RZ-DPSK signal was shorter during compression process as explanation in the demonstration of the inline RZ-DPSK signal compression in section 4.1.4. In this scheme, the multicast signals were considered in only C band because the available EDFAs provided the efficient gain amplification in C band. The frequency channel between the RZ-DPSK signal and CW (pump 1) was set at the value of 500 GHz. The number of CW pumps was two pumps, leading the four converted channels in C band with 1 THz frequency spacing between adjacent channels. However, the channel bandwidth of the RZ-DPSK signal was around 123 GHz. Thus, the frequency channel between the data signal and the CW (pump 1) could be reduced to the value of 200 GHz, leading 400 GHz frequency spacing between adjacent converted channels. The estimated maximum number of multicast channels is ten channels with frequency spacing of 400 GHz

## 4.2 Application of Pulse Compression of RZ-DPSK Signal

---

(3.2 nm) in which the channel 10 is at the wavelength of 1531.9 nm in C band. The number of multicast channels is twice as that of CW pumps. The number of multicast channel depends on the conversion bandwidth which was determined by the nonlinearity and fiber dispersion induced phase mismatch among the signals. The frequency spacing between the data signal and the CW (pump 1) determine the packing density of the converted signals which is related to the bit-rate and the spectral efficiency. The spectral efficiency of each 10 Gb/s multicast signal with 1 THz frequency spacing between adjacent channels was only 0.01 b/s/Hz. If the frequency spacing between adjacent multicast channels is reduced to the value of 400 GHz, the spectral efficiency of each 10 Gb/s multicast signal is 0.025 b/s/Hz. However, the pulsewidth of each multicast signal was on the order of some picoseconds so that the multicast signals could be multiplexed to a higher OTDM signal up to 80 Gb/s. For example, with the frequency spacing of 400 GHz between adjacent multicast channels, the spectral efficiency of each expected 80 Gb/s OTDM signal is 0.2 b/s/Hz.

Similarly, as the aforementioned discussion in section 3.2.4, if a lot of multicast channels are required such as 100 multicast channels with channel spacing between adjacent channels of 400 GHz are required, the total required frequency spacing is over 39.6 THz. Therefore, it is obvious that our scheme could not satisfy for this requirement. So far, the demonstration in Ref. [109] has shown the conversion bandwidth which is obtained over 10 THz for wavelength multicasting of 320 Gb/s RZ-DPSK signal. Therefore, it is challenging for the demonstration of 100 multicasting wavelengths of 10 Gb/s RZ-DPSK signal with frequency spacing of 400 GHz between adjacent multicast channels. It is expected that there is a special nonlinear device with very small dispersion in wide band of frequency operation and the high nonlinearity is used to demonstrate 100 multicasting wavelengths of 10 Gb/s RZ-DPSK signal. In this scheme, the multicast 4x10 Gb/s RZ-DPSK signals are obtained with the shortest pulsewidth which is less than 5 ps. Therefore, it is desirable that these multicast signals could be multiplexed into the higher bit-rate OTDM signals up to 80 Gb/s if the high bit-rate signals are required. The potential total capacity provided by this scheme is 4x80 Gb/s.

### 4.3 Summary

This chapter focuses on the inline RZ-DPSK signal compression and its application in the aggregate signal based on a lower bit-rate of compressed signals and wavelength multicasting. A substantial contribution is the first effort to directly compress RZ-DPSK signal for the inline applications. After compression, the RZ-DPSK signal is multicast into many signals with short-pulsewidths which is considerable in the next process of aggregating different higher speed OTDM channels depending on their expected bit-rate. It is important that at intermediate nodes, the pulsewidth of multicast data signals could be tuned directly to adapt to the distinct channels of different line-rates which require different pulsewidths depending on their bit-rate during transmissions. Moreover, these setups could be considered for the phase-modulated signals such as nPSK signals.

## Chapter 5

# OTDM-to-WDM Conversion of RZ-DPSK Signal with Multicast WDM Signals

This chapter focuses on the networking at the interface of optical time division multiplexing (OTDM) and wavelength division multiplexing (WDM) networks by an OTDM-to-WDM conversion of return-to-zero (RZ)-differential phase shift keying (DPSK) signal. Using wavelength multicasting technique in this conversion, a double number of WDM channels compared to the number of OTDM tributaries is obtained. The input 20 Gb/s OTDM signal is converted to 4x10 Gb/s WDM RZ signals at four four-wave mixing (FWM) products. The key success of this demonstration based on wavelength multicasting technique is that one tributary of OTDM signal is not only converted to WDM signal but also is multicast to two WDM RZ signals. This feature improves the flexibility of wavelength assignment and routing in WDM networks with multicast WDM RZ signals. This technique inherits the idea of wavelength multicasting of RZ-DPSK signal in chapter 4.

### 5.1 Introduction

Fiber-optic communication systems have been emerging by their extremely high capacity. With the huge growth traffic demand and on-demand services continuing to exploit, the core networks need significant improvements in capacity. Thus, the network usage may be optimized by efficiently sharing of such high bandwidth among lower rate lines. Two widely networking ways are optical wavelength multiplexing (OTDM) and wavelength division multiplexing (WDM) to increase the network capacity and minimize resource requirements. It is given that in WDM networks, particularly wavelength-routed network, different WDM signals are expected to connect each tributary of OTDM signal for providing the flexibility in routing and wavelength assignment. Therefore, it is beneficial to convert a high-rate OTDM signal to different lower-rate signals at different wavelengths using wavelength multicasting technique to obtain multicast WDM RZ signals.

The OTDM-to-WDM conversion has been implemented using different non-linear interaction [17]–[21], [110]. However, in these schemes, the multicasting of the converted WDM signal is not considered. In Refs. [111], and [112], the converted WDM RZ signal are multicast corresponding to only each tributary of OTDM signal. Therefore, it is impossible to convert all tributaries of OTDM signal simultaneously. Meanwhile, the scheme in Ref. [113] enables the wavelength tunability of WDM RZ signals. There are two sets of the converted WDM RZ signals. The first set, which is located at the higher wavelengths, enables modulation format transparency, whereas the location of the second set at the lower wavelengths in which modulation format transparency could not be obtained. Thus, this scheme could not use for the OTDM-to-WDM conversion of the phase-modulated signals to obtain multicast WDM RZ signals. On top of these, it is a lack of flexibility for the practical WDM applications in which modulation format transparency and wavelength selection are highly desirable. In this thesis, the improved feature of the proposed scheme compared to the previous setups [110]–[113] is on the use of wavelength multicasting technique to obtain multicast WDM RZ signals for all tributaries of OTDM signals. This scheme is possible for the phase-modulated signal, thus, it is also possible for amplitude-

modulated signals due to the modulation format transparent feature. This idea of this proposed scheme relies on the operation principle of wavelength multicasting using multiwavelength continuous waves (CWs) set as the pumps in FWM process in chapter 4. A pair of WDM RZ signals is obtained corresponding to one tributary of OTDM signal based on the wavelength multicasting technique. Hence, it is called OTDM-to-WDM conversion with multicast WDM RZ signals. Different from the pumps sources in the setup reported in chapter 4, to simultaneously convert OTDM signal to multicast WDM signals, the pumps sources consisting of WDM RZ clocks and one CW are required. The number of WDM RZ signal depends on the number of tributaries of OTDM signal. The WDM RZ pulses could be generated by spectrally slicing of spectral-broadened short pulses referred to the filtering of the broad spectrum of compressed femtosecond soliton pulses [114], the combination of an arrayed waveguide grating (AWG) and a fiber loop mirror [115], supercontinuum generation [116], mode-locked lasers (MLLs) [117], [118], or using a set of laser diodes (LDs), electro-absorption modulator (EAM) and Raman amplification-based multiwavelength pulse compressor (RAMPC) used in chapters 2 and 3. In this chapter, the multiwavelength RZ pulses are generated by two LDs and a LiNbO<sub>3</sub> modulator (LNM) and then compressed by fiber-compressor. This compression process is popular due to its simplicity in setup and operation.

In this proposed scheme, a 20 Gb/s OTDM RZ-DPSK signal is converted to 4x10 Gb/s WDM RZ channels. After wavelength multicasting and sampling at the same time in a highly nonlinear fiber (HNLF)-based four-wave mixing (FWM) switch, the phase of all tributaries could be preserved in the corresponding WDM idlers. One tributary of OTDM signal is converted to two WDM RZ signals. Good bit-error-rate (BER) operations are achieved for four WDM RZ-DPSK channels with small power penalties compared to the back-to-back 10 Gb/s baseband signal before multiplexing to 20 Gb/s OTDM signal at BER of  $10^{-9}$ . This feature brings in a new way for OTDM-to-WDM conversion of the phase-modulated signals with the flexibility of wavelength selection.

### 5.2 Concept of OTDM-to-WDM Conversion

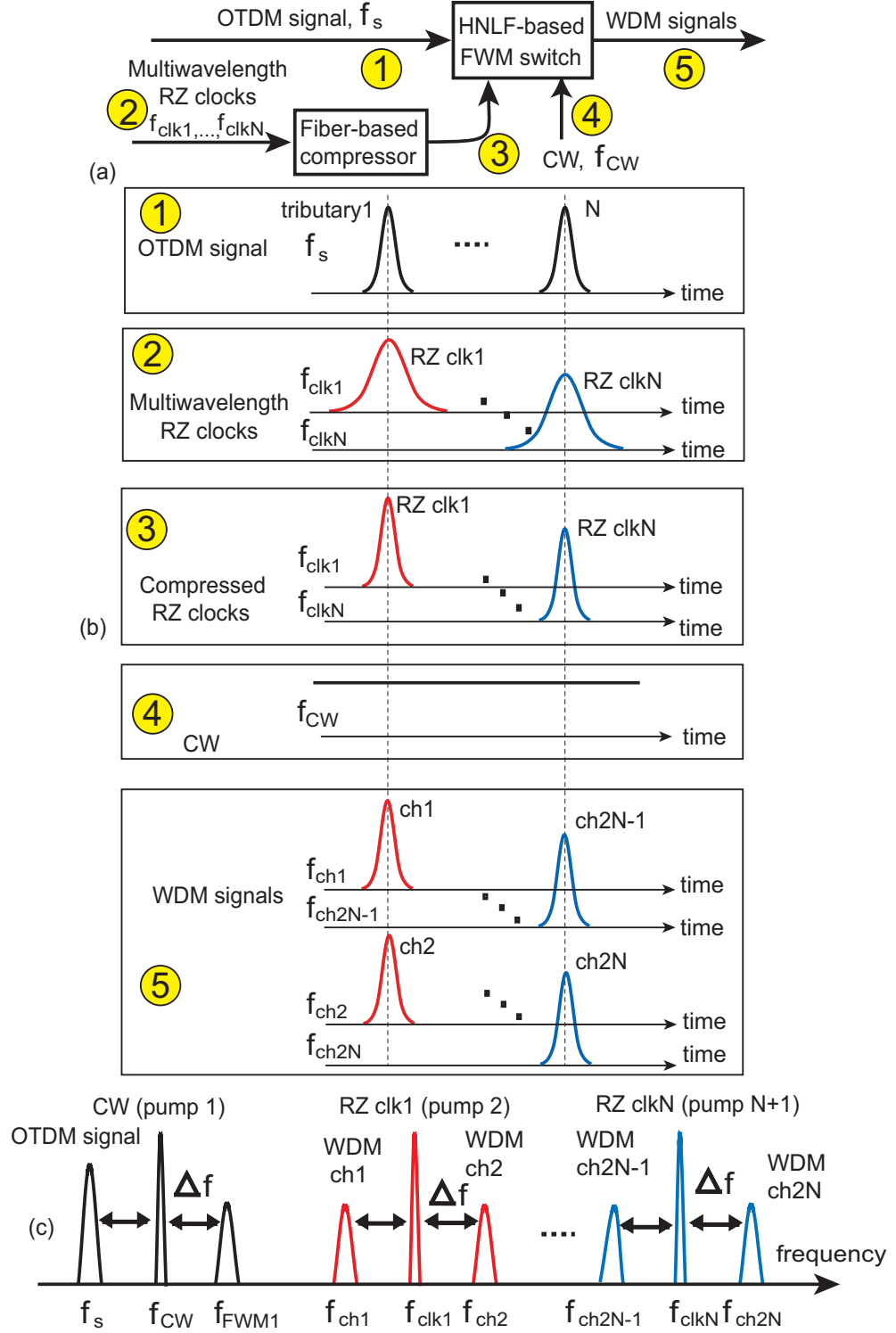
The concept of OTDM-to-WDM conversion using wavelength multicasting technique is shown in Fig. 5.1(a). The scheme consists of fiber-based compressor, which is a set of an HNLF and a standard single mode fiber (SSMF) which have been discussed and shown in Fig. 2.5, and a HNLF-based FWM switch. The notable feature of the proposed scheme compared to the previous setups is on the use of wavelength multicasting technique which simultaneously results in multicast WDM RZ signals, leading the flexibility of wavelength selection of WDM signals and increasing network capacity. A multiwavelength pulse compressor, which is based on HNLF and SSMF, generates WDM RZ clocks with short-pulsewidths to sample OTDM signal. The pulses could be chirped through SPM by a large amount in HNLF. The pulse compression occurs as SPM-induced chirped pulse propagates over an anomalous dispersion regime of SSMF. Figure 5.1(b) illustrates the temporal profiles of all signal in the conversion processes.

Fig. 5.1(c) shows the conceptual spectra of the proposed scheme. In the HNLF-based FWM switch, Nx10 Gb/s OTDM signal interacts with WDM RZ clocks over FWM process. A CW signal at the frequencies  $f_{CW}$  and multiwavelength WDM RZ clocks are set as pumps at the frequencies  $f_{clk1}$ ,  $f_{clk2}, \dots$ , and  $f_{clkN}$ , respectively and then interact with OTDM stream at the frequency of  $f_s$  in HNLF. The input RZ-DPSK OTDM signal is converted to many WDM-RZ signals with different wavelengths at FWM products. The frequencies of these new generated FWM signals are generally given by the following expressions [24]

$$f_{ch2N-1} = f_{clkN} + f_s - f_{CW} = f_{clkN} - \Delta f \quad (5.1)$$

$$f_{ch2N} = f_{clkN} + f_{CW} - f_s = f_{clkN} + \Delta f, \quad (5.2)$$

where  $\Delta f$  is the frequency separation between CW (pump 1) and OTDM signal ( $\Delta f = f_{CW} - f_s$ ), N is the number of RZ clocks set as pumps. After FWM, the electric field amplitude of WDM-RZ data outputs are governed by following



**Figure 5.1:** (a) Operation principle of the OTDM-to-WDM conversion using wavelength multicasting technique.

(b) Conceptual temporal profiles of all signals used in this conversion.

(c) Conceptual spectra of all signals in the OTDM-to-WDM conversion.



## 5. OTDM-TO-WDM CONVERSION OF RZ-DPSK SIGNAL WITH MULTICAST WDM SIGNALS

---

expression [22], [24]

$$E_{ch2N-1}(t) \propto E_{CW}^* E_s(t) E_{clkN}(t) \quad (5.3)$$

$$E_{ch2N}(t) \propto E_{CW} E_s^*(t) E_{clkN}(t) \quad (5.4)$$

where  $E_{CW}$ ,  $E_{clkN}(t)$ , and  $E_s(t)$  are the electric fields of the CW, RZ clock N and OTDM signal, respectively; \* denotes the complex conjugate of the electric field amplitude. Thus, the WDM RZ-DPSK signals are generated simultaneously in the multi-pumps scheme resulting in both phase-conjugating and non-phase-conjugating. The FWM products carry data information of the input OTDM signal corresponding to its tributaries.

### 5.3 Experimental Setup

The experimental setup of OTDM-to-WDM conversion with multicast WDM signals using wavelength multicasting is shown in Fig. 5.2. To generate a high-quality pulse for 20 Gb/s OTDM signals, an optical comb generator (OCG) is used. A continuous wave at 1556.17 nm from a laser diode (LD) is modulated by the OCG by 10 GHz radio frequency (RF) clock. The signal after OCG is boosted by an erbium-doped fiber amplifier (EDFA). Two 0.6 nm OBPFs is used to center OCG spectrum at the wavelength of 1558.17 nm to obtain 10 GHz RZ clock with short-pulsewidth. The pulse train is modulated in a DPSK modulator by a 10 Gb/s data with pseudorandom sequence of  $2^{31}-1$  bits from a pulse pattern generator (PPG) synchronized with a 10 GHz synthesizer. The generated 10 Gb/s RZ-DPSK signal with the pulsewidth of 8.06 ps is launched to a 2:1 bit-rate multiplexer to form a 20 Gb/s OTDM data stream. The OTDM signal is then amplified by an EDFA followed by a 3.0 nm BPF. Two WDM RZ clocks 1 and 2 at the wavelengths of 1546.12 and 1536.61 nm, respectively are generated by a LiNbO<sub>3</sub> modulator (LNM) driven by an electrical 10 GHz clock and is amplified by an EDFA. After LNM, two WDM RZ clocks are sent to an delay block consisting of an arrayed waveguide grating (AWG) and a tunable delay line (TDL) for ensuring 50 ps time spacing between two clocks. These

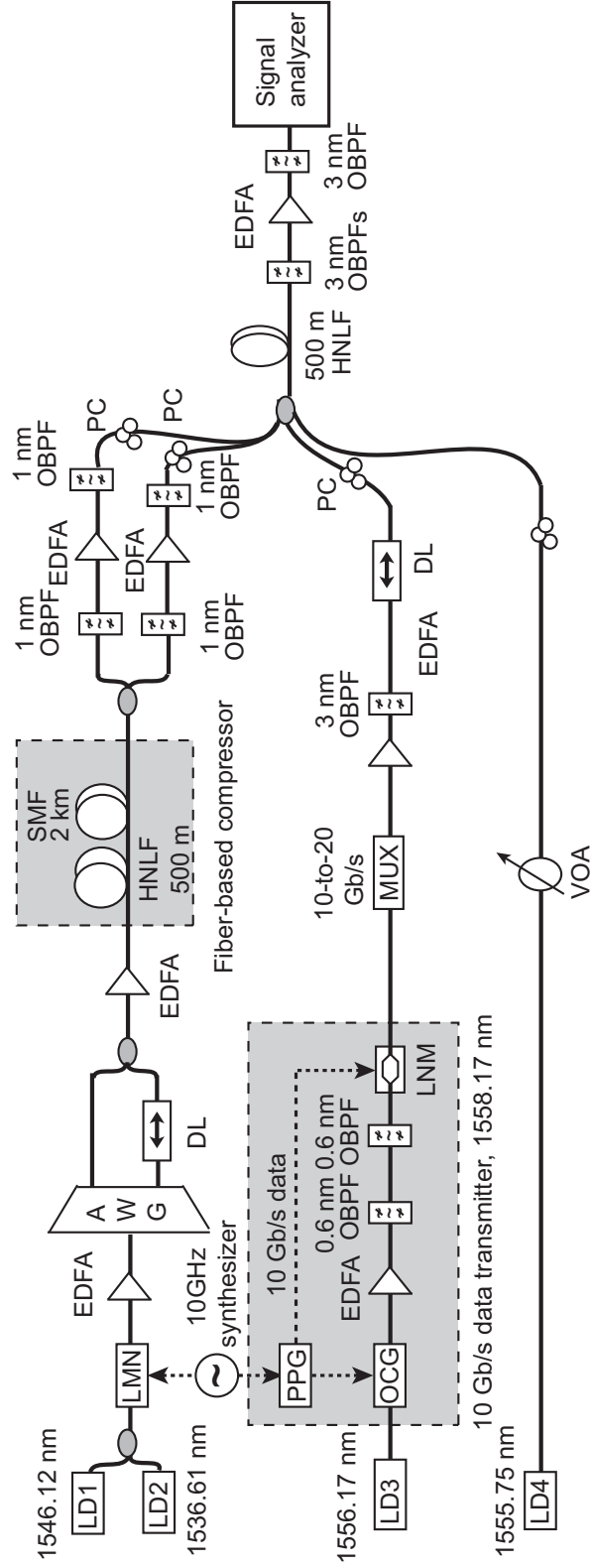


**Figure 5.2:** Experimental setup of OTDM-to-WDM conversion with multicast WDM RZ signals using wavelength multicasting technique.

## 5. OTDM-TO-WDM CONVERSION OF RZ-DPSK SIGNAL WITH MULTICAST WDM SIGNALS

---

two RZ clocks are combined by a coupler before being amplified by a EDFA and then sent to a fiber-based compressor consisted of 500 m HNLF and 2 km SSMF. The WDM RZ clocks are spectrally broadened by SPM in a 500 m HNLF whose parameters are shown in Table 5.1 and then compressed in a 2 km SSMF.

**Table 5.1:** Characteristics of 500 m highly nonlinear fiber (HNLF).

Parameter	Value	Unit
Length	500	m
Attenuation	0.47	dB/km
Dispersion at 1552 nm	-0.08	ps/nm/km
Dispersion slope at 1552 nm	0.032	ps/nm <sup>2</sup> /km
Nonlinear coefficient ( $\gamma$ )	12.6	W <sup>-1</sup> · km <sup>-1</sup>
Effective core area of fiber ( $A_{\text{eff}}$ )	11	$\mu\text{m}^2$

After compression, WDM RZ clocks are separately filtered and boosted by 1 nm OBPFs and EDFAs, respectively. These two RZ clocks and the continuous wave (CW) from LD 4 at the wavelength of 1555.75 nm are coupled with 20 Gb/s OTDM RZ-DPSK signal before being sent to HNLF-based FWM switch. The power of the CW is optimized by a variable optical attenuator (VOA) and the powers of the compressed WDM RZ, OTDM and CW signals are optimized by EDFAs and a VOA to obtain good output waveforms and the largest conversion efficiency. Four polarization controllers (PCs) are used before the coupler to optimize polarization state of these signals. The HNLF has the parameters shown in Table 3.2. After OTDM-to-WDM conversion based on wavelength multicasting technique, four converted WDM RZ signals corresponding two tributaries of 20 Gb/s OTDM signal are generated. They are filtered by 3 nm OBPFs and amplified by an EDFA to get spectra, waveforms, eye patterns, and BER measurement.

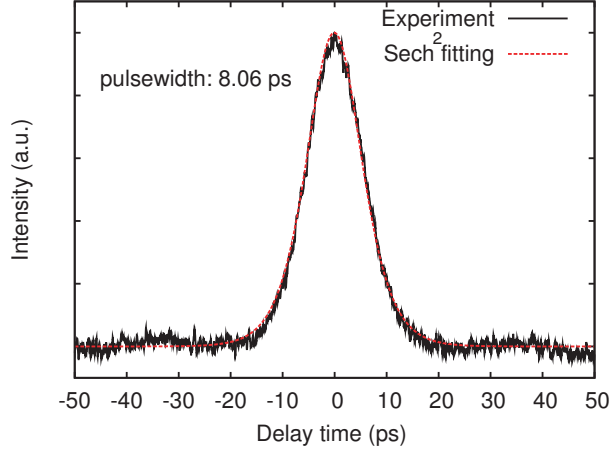


**Figure 5.3:** Autocorrelation trace of 10 Gb/s RZ-DPSK baseband signal

## 5.4 Experimental Results and Discussions

The autocorrelation trace of 10 Gb/s RZ-DPSK baseband signal with pulsewidth of 8.06 ps is shown in Fig. 5.3. The pulse compression is based on a set of 500 m HNLF and 2 km SSMF. The 500 m HNLF was used to induced large SPM-induced chirp and then followed by a 2 km SSMF for anomalous dispersive propagation. A high intensity pulse induces a shift variation in the local refractive index along the pulse, resulting a time-dependent phase-delay. An instantaneous frequency shift, or chirp is induced along the pulse. In SPM-induced chirp pulse, the high frequency (blue-shifted) components occur near the trailing edge of the pulse whereas the low-frequency components (red-shifted) occur near the leading edge. If the leading edge of the pulse is delayed so that the trailing edge catches up with the leading edge during propagation of the pulse through SSMF [22]. Therefore, RZ clock 1 (clk. 1), clock 2 (clk. 2) at the wavelengths of 1546.12 and 1536.61 nm with the pulsewidths of around 29.34 and 29.28 ps were compressed down to 12.68 and 12.63 ps, respectively. In this setup, RZ clocks 1 and 2 are synchronized with two tributaries of OTDM signal for conversion. In practice, by changing the order of WDM RZ clock, each tributary of OTDM signal could be mapped with the expected wavelength of WDM channels. Eye patterns of 10 Gb/s base band RZ-DPSK, 20 Gb/s OTDM RZ-DPSK and the compressed WDM

## 5. OTDM-TO-WDM CONVERSION OF RZ-DPSK SIGNAL WITH MULTICAST WDM SIGNALS

---

RZ clocks signals are shown in Figs. 5.4 (a), (b), and (c), respectively. In order to characterize the shape and width of the optical pulses, autocorrelation traces of RZ clock 1 (clk. 1) and clock 2 (clk. 2) before and after compression using fiber-compressor was measured as shown in Figs. 5.5(a) and (b), respectively.

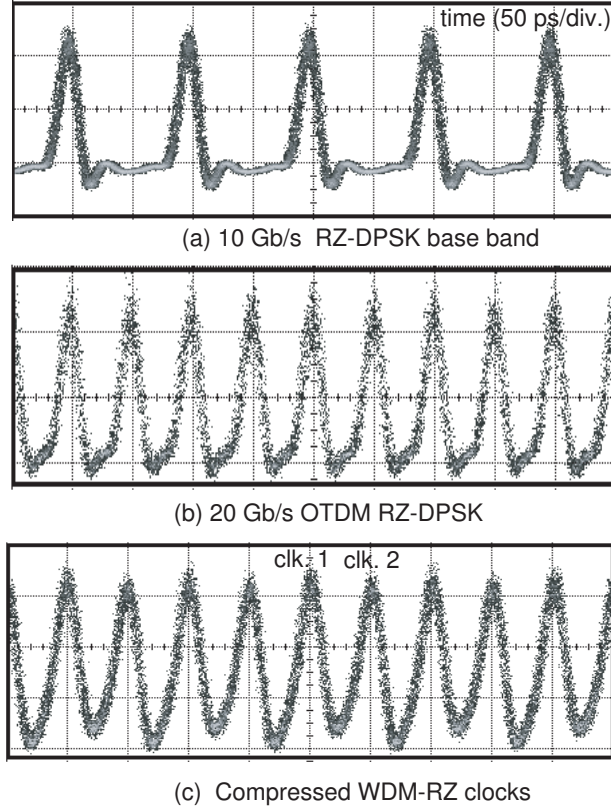


**Figure 5.4:** Eye patterns of 10 Gb/s baseband RZ-DPSK signal, 20 Gb/s OTDM RZ-DPSK signal and 2x10 Gb/s compressed WDM RZ clocks.

The spectra at the output of HNLF after conversion with multicast WDM signals are shown in Fig. 5.6. The 20 Gb/s OTDM signal at the wavelength of 1558.17 nm is converted to two pairs of WDM RZ signals, located at wavelength 1548.51 nm (channel 1), 1543.73 nm (channel 2), 1538.98 nm (channel 3) and 1534.25 nm (channel 4) corresponding to two tributaries of OTDM signal. The conversion efficiency defined as the power of multicast channel over the OTDM signal power is about -15 dB. From Eqs. (5.1) and (5.2), the frequencies of multicast WDM RZ signals depend on frequency spacing among OTDM signal, CW

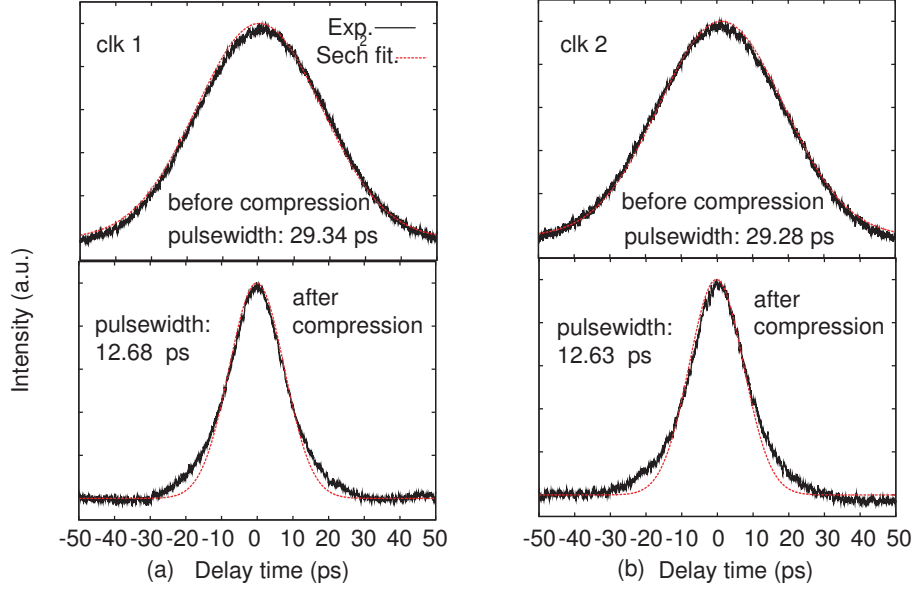


**Figure 5.5:** Autocorrelation traces of RZ clock 1 (clk.1) and clock 2 (clk.2) before and after compression.

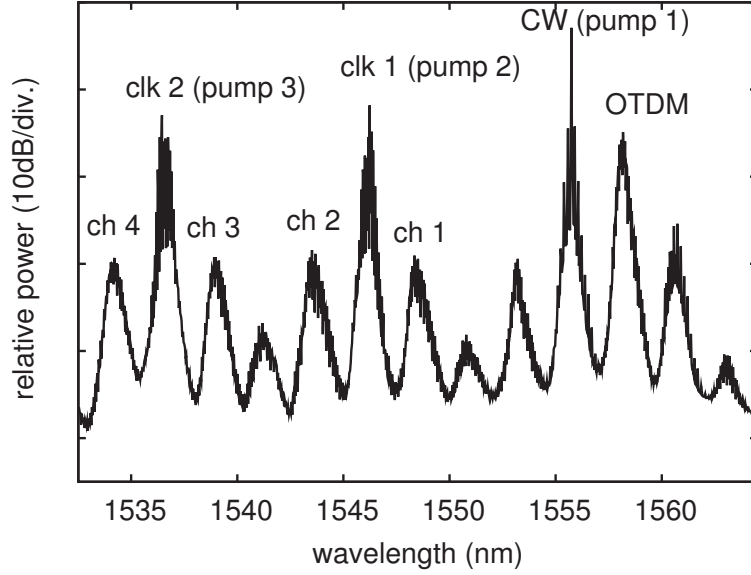


**Figure 5.6:** Spectra at the output of HNLF after conversion.

(pump1), clock 1 (pump 2) and clock 2 (pump 3). Figures 5.7(a), (b), (c), and (d) and 5.8(a), (b), (c), and (d) show autocorrelation traces and eyes patterns

## 5. OTDM-TO-WDM CONVERSION OF RZ-DPSK SIGNAL WITH MULTICAST WDM SIGNALS

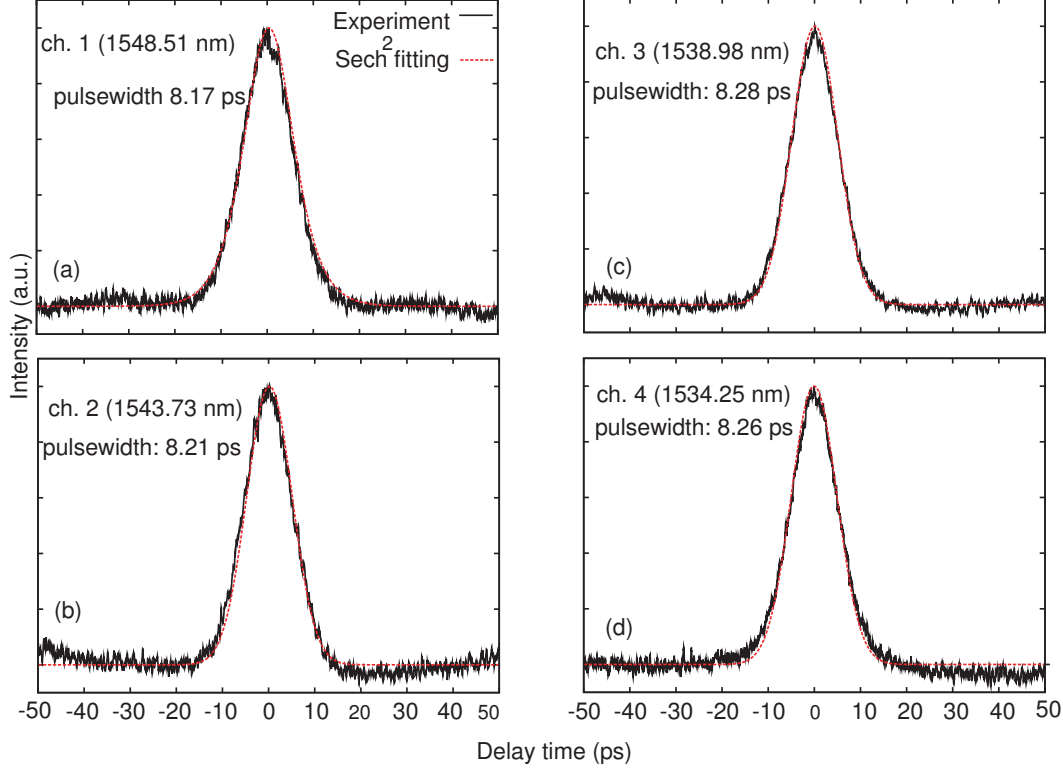


**Figure 5.7:** Autocorrelation traces of multicast WDM RZ-DPSK after conversion (a) at channel 1, (b) channel 2, (c) channel 3 and (d) channel 4.

of multicast WDM signals at channels 1, 2, 3 and 4, respectively after conversion. BER characteristics of all WDM RZ channels and the 10 Gb/s RZ-DPSK signal before multiplexing to 20 Gb/s OTDM signal are shown in Fig. 5.9. Error-free operations were achieved for four WDM channels with small power penalties within 2 dB compared the 10 Gb/s baseband signal. The penalty was probably caused by the amplified spontaneous emission (ASE) noise from EDFAs, and optical signal-to-noise ratio (OSNR) degradation of the multicast signals. At BER of  $10^{-9}$ , the received power of channel 1 was quite same as that of channel 2. Similarly, the received power of channel 3 was quite same as that of channel 4. Meanwhile, a small received power variations within 0.5 dB among WDM RZ channels probably originated from the imperfect multiplexing process in OTDM multiplexer and nonoptimal filtering by tunable filter under investigation of each

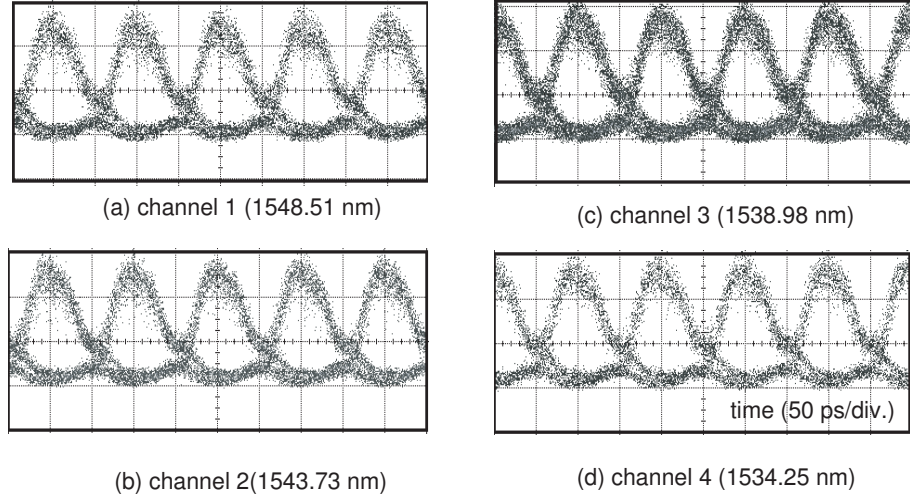


**Figure 5.8:** Eye patterns of demodulated WDM RZ-DPSK signals after conversion (a) at channel 1, (b) channel 2, (c) channel 3 and (d) channel 4.

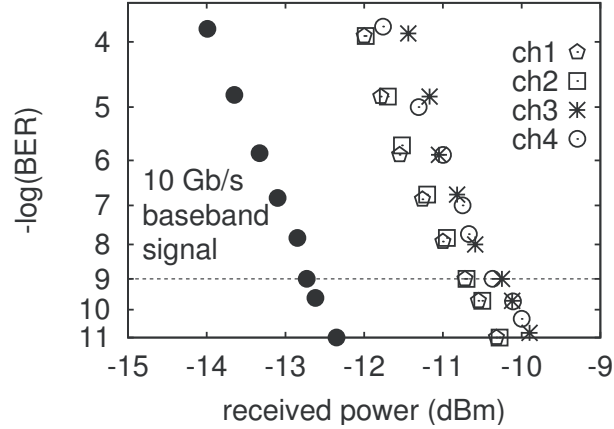


**Figure 5.9:** BER characteristics of multicast WDM RZ signals compared 10 Gb/s RZ-DPSK baseband signal.

channel.

When more than two multicast signals are required for converting one tributary of OTDM signal, this scheme could not be used because this conversion focuses two functions. The first function is that the all tributaries of OTDM signal are converted to WDM RZ signals. The second function is that the one WDM



## 5. OTDM-TO-WDM CONVERSION OF RZ-DPSK SIGNAL WITH MULTICAST WDM SIGNALS

---

converted signals are multicast to two channels corresponding to one tributary of OTDM signal. If more than two multicast channels are needed, the additional wavelength multicasting converter should be used after OTDM-to-WDM conversion. With the frequency arrangement of all signals in this demonstration, the four converted WDM RZ signals have equal frequency spacing which is twice as frequency spacing between OTDM signal and CW (pump 1). Moving to the conversion of the higher bit-rate OTDM such as beyond 40 Gb/s, spacing of frequencies among OTDM signals, the CW and RZ clocks as well as their frequencies also need to rearrange for getting high conversion efficiency. So far, in Ref. [109], 320 Gb/s OTDM RZ-on-off-keying (OOK) signal is demultiplexed to 8x40 Gb/s WDM signal with two stages of HNLFs with the complexity of controlling process. It is expected that the setup in Ref. [109] could be used for OTDM-to-WDM conversion of phase-modulated signal. Therefore, for converting the higher bit-rate of OTDM signal, the scheme in Ref. [109] could be considered. The other feature is that the scheme in Ref. [109] could only convert 320 Gb/s to 8x40 Gb/s WDM signals corresponding to eight tributaries of 320 Gb/s signal without multicast WDM signals. It is necessary to use the additional wavelength multicasting converters when the multicast WDM signals are needed.

### 5.5 Summary

This chapter focuses on OTDM-to-WDM conversion with multicast WDM RZ signals, especially supporting wavelength-routed network by flexible wavelengths selection of converted RZ signals. After conversion, all tributaries of OTDM signal are multicast into many WDM RZ signals. The number of multicast output is double compared that of tributaries of OTDM signal. This proposed scheme enables converting all OTDM tributaries to WDM channels and could be used for DPSK and/or OOK signals.

## Chapter 6

# Conclusion and Future Development

The advanced technologies applied in many telecommunications services have been leading a rapid growth of data traffic. In this thesis, all demonstrations using optical wavelength multicasting technique combined with pulse compression to generate multicast signals with short-pulsewidths during waveform conversion, waveform sampling, wavelength multicasting and optical time division multiplexing (OTDM)-to-wavelength division multiplexing (WDM) conversion. The purpose of these works aims to increase network capacity and flexibly optimize the utilized capacity of different links and test signals in WDM and OTDM networks. The initial signals which are converted and multicast into many signals with different features make the applications be more scalable as clearly mentioned in the previous chapters. Through all this thesis, wavelength multicasting technique uses four-wave mixing (FWM) effect in a highly nonlinear fiber (HNLF). In addition, short-pulsewidths are required flexibly to optimize the utilized capacity of different links, thus, the pulse compression of return-to-zero (RZ) clocks or RZ-differential phase-shift-keying (DPSK) data signal is also realized to support the generation of multicast signals with short-pulsewidths. In this chapter, the achieved results are concluded as follows

## 6. CONCLUSION AND FUTURE DEVELOPMENT

---

- So far, in the past works, for demonstrations of nonreturn-to-zero (NRZ)-to-RZ conversion and wavelength multicasting, it is very challenging to obtain multicast signals with the pulsewidth which is on the order of some picoseconds. This short-pulsewidth is required for the higher bit-rate signals aggregated from lower multicast signals. Therefore, chapter 3 has realized an all-optical NRZ-to-RZ conversion and wavelength multicasting with tunable short-pulsewidths in a large range from 12.17 to 4.68 ps using HNLF and Raman amplification-based multiwavelength pulse compressor (RA-MPC). Error-free operations are obtained for all multicast channels with better power penalties compared with the NRZ signal and small received power different among the converted RZ channels at bit-error-rate (BER) of  $10^{-9}$ . The WDM throughput is increased with the flexible wavelength assignment which supports wavelength-routed networks whereas these multicast signals could be used for aggregating the higher bit-rate OTDM signals.

The other work in chapter 3 is all-optical waveform sampling in real-time is also improved. Indeed, for sampling waveform of high-bandwidth signals such as military radar, it is desirable to use sampling short pulses so that the waveform does not change significantly through the sampling window. The key feature of this proposed sampler is the use of multiwavelength sampling clocks compressed by RA-MPC with short-pulsewidths which are less than 3 ps. Four compressed pulses interact with the input signal using FWM effect in HNLF. Four sampled signals based on multicasting wavelength conversion with short-pulsewidth at picosecond range are obtained, thus, leading a sampling rate of 40 GSample/s. The reconstructed waveforms are well-matched with the input waveforms.

- In addition, the phase-modulated signal, especially DPSK signal with the larger robustness compared to its counterpart OOK signal concerning a higher optical signal-to-noise ratio (OSNR), and the tolerance of some fiber nonlinearities effects, is attractive. From the desirable generation of an aggregate high-speed data rate based on optical time multiplexing of many

---

channels with lower speed data rates, an inline RZ-DPSK signal with pulsewidth compressed by a distributed Raman amplifier pulse compressor (DRA-PC). An investigation on the quality of a 40 Gb/s OTDM signal aggregated by an inline 10 Gb/s compressed RZ-DPSK signal is realized. A higher bit-rate OTDM signal is aggregated from the lower data-rate of the compressed RZ-DPSK signal with the short-pulsewidth of 3.2 ps and then demultiplexed by a HNLF-based FWM switch. The other application of this compressor is its use in wavelength multicasting of the RZ-DPSK signal, leading 4x10 Gb/s multicast RZ-DPSK signals with tunable short-pulsewidths in the range of 12.5 and 4.27 ps. These achieved results in chapter 4 give a new application, particularly inline signal processing compared to the other past works which could process the signals at the transmitters.

- At the exchanged gateway of WDM and OTDM networks, all-optical conversion OTDM-to-WDM is necessary. So far, there have been many demonstrations of WDM-to-OTDM conversions using a variety of techniques. However, these conversions only map out one WDM channel corresponding to one tributary of OTDM signal. This is a limitation in wavelength selection of converted WDM signals when optical networks required the variable wavelength for routing or increase wavelength resources. Therefore, to provide WDM-to-OTDM conversion with the flexibility in wavelength selection and the number of converted WDM signals, wavelength multicasting technique is used in OTDM-to-WDM conversion in chapter 5. The benefit of this methods is that the conversion and the multicast process occur simultaneously in a single FWM-based HNLF switch. The number of converted WDM RZ signals is double compared to that of tributaries of OTDM signal. This is the first effort in OTDM-to-WDM conversion of the phase-modulated signal with multicast WDM RZ signals. This technique inherits the idea of wavelength multicasting of RZ-DPSK signal in chapter 4. A OTDM-to-WDM conversion using wavelength multicasting to obtain 4x10 Gb/s WDM RZ channels from a 20 Gb/s RZ-DPSK OTDM signal is realized. Error-free operations are achieved for all converted WDM channels with power penalties

## 6. CONCLUSION AND FUTURE DEVELOPMENT

---

less than 2.5 dB compared 10 Gb/s baseband signal.

Through all the thesis, in the achieved result evaluations, besides eye pattern, spectral characteristics, autocorreclation traces, the most parameter is investigated by measuring BER with respect to the received power. The purpose is to find whether a quantitative experimental receiver sensitivity improvement or degradation of multicast RZ signals compared with the back-to-back signal after conversions as well as among multicast RZ signals under different pulsewidths investigation. The clear explanation is also mentioned for all results. The achievements in the realization such as optical wavelength multicasting for WDM and OTDM networks bring in the potential solutions in optical fiber communication systems in terms of the increase of network capacity, wavelength resource in routing and wavelength assignment as well as signal monitoring. Finally, there are some ideas in which further investigations could be considered. For future optical networks employing higher baud-rate, one of the solutions is the use of advanced format modulation with support high spectral efficiency. A desirable effort in future is that studying the application of optical signals with advanced format modulations.

# References

- [1] J. Gantz and D. Reinsel, “The digital universe in 2020: Big data, bigger digital shadows, and biggest growth in the far east,” *IDC IVIEW, EMC Corporation, Hopkinton, MA, USA*, 2012.
- [2] T. Koonen, “Fiber to the home/fiber to the premissis: what, where and when?,” in *Proceeding of the IEEE*, vol. 94, no. 5, pp. 911-934, May 2006.
- [3] P. E. Green, “Fiber to the home: The next big broadband thing,” *IEEE Communications Magazine*, vol. 42, no. 9, pp. 100-106, Sep. 2004.
- [4] N. J. Frigo, P. P. Iannone, and K. C. Reichmann, “A view of fiber to the home economics,” *IEEE Communications Magazine*, vol. 42, no. 8, pp. S16-S23, Aug. 2004.
- [5] I. Kaminow, T. Li, and A. E. Willner, “*Optical Fiber Telecommunications VB: Systems and Networks*,” 5 th Ed., Elsevier Inc, 2008.
- [6] G. K. P. Lei and C. Shu, “4x10 Gb/s wavelength multicasting with tunable NRZ-to-RZ pulse format conversion using time- and wavelength-interleaved pulses, *Opt. Commun.*, vol. 258, pp. 2525-2529, May 2012.
- [7] S. Liu, S. Fu, M. Tang, P. Shum and D. Liu, “4x10 Gb/s wavelength multicasting with tunable NRZ-to-RZ format conversion using nonlinear polarization rotation in an SOA,” *Laser Phys.*, vol. 23, pp. 085–103, Jun. 2013.

## REFERENCES

---

- [8] M. P. Fok, K. L. Lee, and C. Shu, “4x2.5 GHz repetitive photonic sampler for high-speed analog-to-digital signal conversion,” *IEEE Photon. Technol. Lett.*, vol. 16, pp. 876–878, Mar. 2004.
- [9] G. K. P. Lei, Mable P. Fok, and Chester Shu, “40-GS/s all-optical sampling using four-wave mixing with a time-and wavelength-interleaved laser source,” *Optical Society America (OSA) /Conference on Lasers and Electro-Optics(CLEO)/Quantum Electronics and Laser Science Conference (QELS)*, CTuH6, 2008.
- [10] C. -S. Bres, N. Alic, A. H. Gnauck, R. M. Jopson, and S. Radic, “Multicast parametric synchronous sampling,” *IEEE Photon. Technol. Lett.*, vol. 20, no. 14, pp. 1222–1224, Jul. 2008.
- [11] M. Skold, M. Westlund, H. Sunnerud, and P. A. Andrekson: “100 GSample/s optical real-time sampling system with Nyquist-limited bandwidth,” *Post-Deadline Papers, the 33rd European Conference on Optical Communications*, 2007.
- [12] M. Matsuura, B. P. Samarakoon, and N. Kishi, “Wavelength-shift-free adjustment of the pulsewidth in return-to-zero on-off keyed signals by means of pulse compression in distributed Raman amplification,” *IEEE Photon. Lett.*, vol. 21, no. 9, May 2009.
- [13] H. N. Tan, Q. Nguyen-The, M. Matsuura, and N. Kishi, “40-fold 4-channel sub-picosecond pulse compression by Raman amplification and self-phase modulation,” *37th The Optical Fiber Communication Conference and Exposition and The National Fiber Optic Engineers Conference (OFC/NFOEC 2012)*, OM2C.2, Los Angeles, USA, Mar. 2012.
- [14] M. P. Fok and C. Shu, “Performance investigation of one-to-six wavelength multicasting of ASK-DPSK signal in a highly nonlinear bismuth oxide fiber,” *J. Lightwave Technol.*, vol. 27, no. 15, pp. 2953–2957, 2009.
- [15] Y. Dai and C. Shu, “Polarization-insensitive wavelength multicasting of RZ-DPSK signal based on four-wave mixing in a photonic crystal fiber

- with residual birefringence,” in *Proc. of Optical Fiber Communication Conference and Exposition (OFC)*, OWP7, 2010.
- [16] C.-S. Bres, A. O. J. Wiberg, B. P.-P. Kuo, E. Myslivets, and S. Radic, “320 Gb/s RZ-DPSK data multicasting in self seeded parametric mixer,” in *Proc. of Optical Fiber Communication Conference and Exposition (OFC)*, OThC7, 2011.
- [17] G. Lei, C. Shu, and M. Fok, “All-optical OTDM-to-WDM signal conversion using cross-absorption modulation with time-and wavelength-interleaved short pulses,” *IEEE Photon. Technol. Lett.* vol. 22, no. 8, pp. 571-573, 2010.
- [18] H. Sotobayashi, W. Chujo and T. Ozeki, “80 Gbit/s simultaneous photonic demultiplexing based on OTDM-to-WDM conversion by four-wave mixing with supercontinuum light source,” *Electron. Lett.*, vol. 37, no. 10, pp. 640-642, 2001.
- [19] H. Nguyen Tan, Q. Nguyen-The, M. Matsuura, and N. Kishi, “Reconfigurable all-optical OTDM-to-WDM conversion using a multiwavelength ultrashort pulse source based on Raman compression, *J. Lightwave Technol.*, vol. 30 , no. 6, pp. 853–863, Mar. 2012.
- [20] A. H. Gnauck, R. M. Jopson, R. W. Tkach, C. J. McKinstrie, and S. Radic, “Serial-to-parallel demultiplexing using WDM sampling pulses,” *IEEE Photon. Technol. Lett.*, vol. 21, no. 2, Jan. 2009.
- [21] C. -S. Bres, A. O. J. Wiberg, B. P. -P. Kuo, J. M. Chavez-Boggio, C. F. Marki, N. Alic, and S. Radic, “Optical demultiplexing of 320 Gb/s to 8x40 Gb/s in single parametric gate,” *J. Lightwave Technol.*, vol. 28, no. 4, pp. 434-442, Feb. 2010.
- [22] G. P. Agrawal, *Nonlinear Fiber Optics*, Second Ed., Academic Press, 2001.



## REFERENCES

---

- [23] B. J. Ainslie and C. R. Day, “A review of single-mode fibers with modified dispersion characteristics,” *IEEE/OSA J. Lightwave Technol.*, vol. 4, no. 8, pp. 967–979, Aug. 1986.
- [24] A. E. Willner, S. Khaleghi, M. R. Chitgarha, and O. F. Yilmaz, “All-optical signal processing,” *IEEE J. Lightwave Technol.*, vol. 32, no. 4, pp. 660–679, Feb. 2014.
- [25] O. Aso, M. Tadakuma and S. Namiki, “Four-wave mixing in optical fibers and its applications,” *Furukawa Review*, no. 19, pp. 63–68, 2000.
- [26] N. Shibata, R. P. Braun, and R. G. Waarts, “Phase-mismatch dependence of efficiency of wave generation through four-wave mixing in a single-mode optical fiber,” *IEEE J. Quant. Electron.* , vol. QE-23, no. 7, pp. 1205–1210, Jul. 1987.
- [27] M. W. Maeda, W. B. Sessa, W. I. Way, A. Yi-Yan, L. Curtis, R. Spicer, and R. I. Laming , “The effect of four-wave mixing in fibers on optical frequency-division multiplexed systems,” *J. Lightwave Technol.*, vol. 8, no. 9, pp. 1402–1408, Sep. 1990.
- [28] A. Bogris, and D. Syvridis, “Regenerative properties of a pump-modulated four-wave mixing scheme in dispersion-shifted fibers,” *J. Lightwave Technol.*, vol. 21, no. 9, pp. 1892–1902, Sept. 2003.
- [29] R. Ramaswami, K. N. Sivarajan and G. H. Sasaki, *Optical network*, Third Edition, Elsevier, 2010.
- [30] C. Headley, and G. P. Agrawal, *Raman Amplification in Fiber optical communication systems*, Academic Press, 2005.
- [31] S. Namiki, K. Seo, N. Tsukiji, and S. Shikii, “Challenges of Raman amplification,” *in Proc. the IEEE*, vol. 94, no. 5, pp. 1024-1035, May 2006.
- [32] T. D. Vo, H. Hu, M. Galili, E. Palushani, J. Xu, L. K. Oxenlowe, S. J. Madden, D.-Y. Choi, D. A. P. Bulla, M. D. Pelusi, J. Schroder, B.

- Luther-Davies, and B. J. Eggleton, "Photonic chip based transmitter optimization and receiver demultiplexing of a 1.28 Tbit/s OTDM signal," *Opt. Express*, vol. 18, no. 16, pp. 17252-17261, Aug. 2010.
- [33] T. Sudmeyer, F. Brunner, E. Innerhofer, R. Paschotta, K. Furusawa, J. C. Baggett, T. M. Monro, D. J. Richardson, and U. Keller, "Nonlinear femtosecond pulse compression at high average power levels of a large-mode-area holey fiber," *Opt. Lett.*, vol. 28, pp. 1951-1953, 2003.
- [34] G. McConnell and E. Riis, "Ultra-short pulse compression using photonic crystal fibre," *Appl. Phys. B* vol. 78, no. 557, pp. 557-563, 2004.
- [35] F. Druon and P. Georges, "Pulse-compression down to 20 fs using a photonic crystal fiber seeded by a diode-pumped Yb:SYS laser at 1070 nm," *Opt. Express*, vol 12, no. 15 , pp. 3383-3396, Jul. 2005.
- [36] H. N. Tan, M. Matsuura, T. Katafuchi and N. Kishi, "Multi-channel optical processing with wavelength-waveform conversions, pulse duration tunability, and signal regeneration," *Opt. Express*, vol. 17, no. 25, pp. 22960-22973, Dec. 2009.
- [37] Y. Yu, X. Zhang, and D. Huang, "Pulse-width tunable multi-channel NRZ-to-RZ conversion with duplicate output," *Opt. Commun.*, vol. 285, no. 2, pp. 109-112, Jan. 2012.
- [38] L. H. Sahasrabuddhe and B. Mukherjee, "Light-trees: Optical multicasting for improved performance in wavelength-routed networks," *IEEE Commun. Mag.*, vol. 37, no. 2, pp. 67-73, Feb. 1999.
- [39] G. N. Rouskas, "Optical layer multicast: rationale, building blocks, and challenges," *IEEE Netw.*, vol. 17, no. 1, pp. 60-65, Jan./Feb. 2003.
- [40] S. B. Jun, K. J. Park, H. Kim, H. S. Chung, J. H. Lee, and Y. C. Chung, "Passive optical NRZ-to-RZ converter," in *Proc. Optical Fiber Communication Conference (OFC)*, ThN1, Feb. 2004.

## REFERENCES

---

- [41] G. W. Lu, L. K. Chen, and C. K. Chan, “Novel NRZ-to-RZ format conversion with tunable pulsewidth using phase modulator and interleaver,” in *Proc. Optical Fiber Communication Conference (OFC)*, JThB32, 2006.
- [42] Q. Nguyen-The, M. Matsuura, H. N. Tan, and N. Kishi, “All-optical NRZ-to-RZ data format conversion with picosecond duration-tunable and pedestal suppressed operations,” *IEICE on Trans. Electron.*, vol. E94-C, no. 7, pp. 1160–1166, Jul. 2011.
- [43] H. N. Tan, M. Matsuura, and N. Kishi, “Transmission performance of a wavelength and NRZ-to-RZ format conversion with pulsewidth tunability by combination of SOA-and fiber-based switches,” *Opt. Express*, vol. 16, no. 23, pp. 19063–19071, Nov. 2008.
- [44] Y. Yu, X. Zhang, J. B. Rosas-Fernandez, D. Huang, R. V. Penty, and I. H. White, “Single SOA based 16 DWDM channels all-optical NRZ-to-RZ format conversions with different duty cycles,” *Opt. Express*, vol. 16, no. 20, pp. 16166–16171, Sep. 2008.
- [45] H. N. Tan, M. Matsuura, and N. Kishi, “Parallel WDM signal processing in mixed NRZ and RZ transmission networks using a single optical gate with multiple switching windows,” *J. Lightwave Technol.*, vol. 18, no. 2, pp. 926–934, Mar./Apr. 2012.
- [46] Z. Q. Hui, “All-Optical NRZ-to-RZ format conversion with dual channel wavelength multicasting functions exploiting cross-phase modulation in a dispersion-flattened nonlinear photonic crystal fiber,” *Laser Phys.*, vol. 21, no. 7, pp. 1219–1229, Jul. 2011.
- [47] L.-S. Yan, A.-L. Yi, W. Pan, B. Luo, and J. Ye, “Simultaneous NRZ-to-RZ format conversion and one-to-six error-free channel multicasting using a single pump in a highly nonlinear fiber,” *Opt. Express*, vol. 18, no. 20, pp. 21404–21409, Sep. 2010.

- 
- [48] T. Richter, E. Palushani, C. Schmidt-Langhorst, R. Ludwig, L. Molle, M. Nolle, and C. Schubert, "Transmission of single-channel 16-QAM data signals at Terabaud symbol rates," *J. Lightwave Technol.*, vol. 30, no. 4, pp. 504-511, Feb. 2012.
- [49] H. N. Tan, T. Inoue, T. Kurosu, and S. Namiki, "Transmission and pass-drop operations of mixed baudrate Nyquist OTDM-WDM signals for all-optical elastic network," *Opt. Express*, vol. 21, no. 17, pp. 20313-20321, Aug. 2013.
- [50] E. P. Ippen, D. J. Eilenberger, and R. W. Dixon, "Picosecond pulse generation by passive mode locking of diode lasers," *Appl. Phys. Lett.*, vol. 37, no. 3, pp. 267-269, Aug. 1980.
- [51] I. Ogura, H. Kurita, T. Sasaki, and H. Yokoyama, "Precise operation-frequency control of monolithic mode-locked laser diodes for high-speed optical communication and all-optical signal processing," *Opt. and Quant. Electron.*, vol. 33, no. 7, pp. 709-725, Jul. 2001.
- [52] Q. Nguyen-The, H. Nguyen Tan, M. Matsuura, and N. Kishi, "Generation of multiwavelength picosecond pulses with tunable pulsewidth and channel spacing using a Raman amplification-based adiabatic soliton compressor," *Opt. Express*, vol. 20, no. 2, pp. 1230-1236, Jan. 2012.
- [53] Q. Nguyen-The, H. N. Tan, M. Matsuura, and N. Kishi, "All-optical WDM-to-OTDM conversion using a multiwavelength picosecond pulse generation in Raman compression," *IEEE Photon. Technol. Lett.*, vol. 24, no. 24, pp. 2235-2238, Dec. 2012.
- [54] G. P. Agrawal, "Effect of intrapulse stimulated Raman scattering on soliton-effect pulse compression in optical fibers," *Opt. Lett.* vol. 15, no. 4, pp. 224-226, Feb. 1990.
- [55] A. Sano, Y. Miyamoto, T. Kataoka, and K. Hagimoto, "Long-span repeaterless transmission systems with optical amplifiers using pulse width

## REFERENCES

---

- management,” *J. Lightwave Technol.*, vol. 16, no. 6, pp. 977–985, Jun. 1998.
- [56] T. Matsuda, A. Naka, and S. Saito, “Comparison between NRZ and RZ signal formats for in-line amplifier transmission in the zero-dispersion regime,” *J. Lightwave Technol.*, vol. 16, no. 3, pp. 977–985, Mar. 1998.
- [57] P. J. Winzer and A. Kalmar, “Sensitivity enhancement of optical receivers by impulsive coding,” *J. Lightwave Technol.*, vol. 17, no. 2, pp. 171–177, Feb. 1999.
- [58] M. Pauer, P. J. Winzer and W. R. Leeb, “Bit error probability reduction in direct detection optical receivers using RZ coding,” *J. Lightwave Technol.*, vol. 19, no. 9, pp. 1255–1262, Sept. 2001.
- [59] J. M. C. Boggio, J. R. Windmiller, M. Knutzen, R. Jiang, C. Bres, N. Alic, B. Stossel, K. Rottwitt, and S. Radic, “730-nm optical parametric conversion from near- to short-wave infrared band,” *Opt. Express*, vol. 16, no. 8, pp. 5435–5443, Apr. 2008.
- [60] C. -S. Bres, N. Alic, E. Myslivets, and S. Radic, “Scalable multicasting in one-pump parametric amplifier,” *J. Lightwave Technol.*, vol. 27, no. 3, pp. 356–363, Feb. 2009.
- [61] C. Schmidt -Langhorst and H. -G. Weber, “Optical sampling techniques,” *J. of Optical and Fiber Commun. Report*, vol. 2, no. 14, pp. 86–114, Mar. 2005.
- [62] P. A. Andrekson and M. Westlund, “Nonlinear optical fiber based high resolution all-optical waveform sampling,” *Laser Photon. Rev.* 1, no. 3, pp. 231–248, Nov. 2007.
- [63] T. Kanada and D. L. Franzen, “Optical waveform measurement by optical sampling with a mode-locked laser diode,” *Opt. Lett.*, vol. 1, no. 1, pp. 4–6, Jan. 1986.

- 
- [64] J. Li, J. Hansryd, P. O. Hedekvist, P. A. Andrekson, and S. N. Knudsen, "300 Gbit/s eye-diagram measurement by optical sampling using fiber based parametric amplification," *IEEE Photon. Technol. Lett.*, vol. 13, no. 9, pp. 987-989, 2001.
- [65] J. Li, M. Westlund, H. Sunnerud, B. E. Olsson, M. Karlsson, and P. A. Andrekson, "0.5 Tbit/s eye-diagram measurement by optical sampling using XPM-induced wavelength shifting in highly nonlinear fiber," *IEEE Photon. Technol. Lett.*, vol. 16, no. 2, pp. 566-568, Feb. 2004.
- [66] S. Diez, R. Ludwig, C. Schmidt, U. Feiste, and H. Weber, "160 Gbit/s optical sampling by a novel ultra-broadband switch based on four-wave mixing in a semiconductor optical amplifier," in *Proc. Optical Fiber Communication Conference and the International Conference on Integrated Optics and Optical Fiber Communication (OFC/IOOC99)*, San Diego, CA, Feb. 1999.
- [67] H. Ji, M. Pu, H. Hu, M. Galili, L. K. Oxenlwe, K. Yvind, J. M. Hvam, and P. Jeppesen "Optical waveform sampling and error-free demultiplexing of 1.28 Tb/s serial data in a nanoengineered Silicon waveguide," *J. Lightwave Technol.*, vol. 29, no. 4, pp. 426-431, Feb. 2001.
- [68] M. Westlund and P. A. Andrekson, "High-performance optical-fiber-nonlinearity-based optical waveform monitoring," *J. Lightwave Technol.*, vol. 23, no. 6, pp. 2012-2022, Jun. 2005.
- [69] T. Richter, E. Palushani, C. Schmidt-Langhorst, R. Ludwig, L. Molle, M. Nolle, and C. Schubert, "Transmission of single-channel 16-QAM data signals at Terabaud symbol rates," *J. Lightwave Technol.*, vol. 30, no. 4, pp. 504-511, Feb. 2012.
- [70] H. N. Tan, T. Inoue, K. Tanizawa, T. Kurosu, and S. Namiki, "Optical Nyquist filtering for elastic OTDM signals: Fundamentals and demonstrations," *IEEE/OSA J. Lightwave Technol.*, vol. 33, no.5, pp. 1014-1026, Mar. 2015.

## REFERENCES

---

- [71] S. V. Chernikov, D. J. Richardson, E. M. Dianov, and D. N. Payne, “Picosecond soliton pulse compression based on dispersion decreasing fiber,” *Electron. Lett.*, vol. 28, no. 19, pp. 1842–1844, Sep. 1992.
- [72] J. H. Lee, T. Kogure, and D. J. Richardson, “Wavelength tunable 10-GHz 3-ps pulse source using a dispersion decreasing fiber-based a non-linear optical loop mirror,” *IEEE J. Sel. Top. Quantum Electron.*, vol. 10, no. 1, pp.181–185, Jan./Feb. 2004.
- [73] S. V. Chernikov, J. R. Taylor and R. Kashyap, “Experimental demonstration of step-like dispersion profiling in optical fiber for soliton pulse generation and compression,” *Electron. Lett.*, vol. 30, no. 5, pp. 433–435, Mar. 1994.
- [74] T. Inoue, H. Tobioka, K. Igarashi, and S. Namiki, “Optical pulse compression based on stationary rescaled pulse propagation in a comb-like profiled fiber,” *J. Lightwave Technol.*, vol. 24, no. 7, pp. 2510–2522, Jul. 2006.
- [75] M. Nakazawa, E. Yoshida, H. Kubota, and Y. Kimura, “Generation of a 170 fs, 10 GHz transform-limited pulse train at 1.55  $\mu\text{m}$  using a dispersion-decreasing, erbium-doped active soliton compressor,” *Electron. Lett.*, vol. 30, no. 24, pp. 2038–2040, Nov. 1994.
- [76] K. Iwatsuki, K. Suzuki, and S. Nishi, “Adiabatic soliton compression of gain-switched DFB-LD pulse by distributed fiber Raman amplification,” *IEEE Photon. Technol. Lett.*, vol. 3, no. 12, pp. 1074–1076, Dec. 1991.
- [77] Q. N. Q. Nhu, Q. Nguyen-The, H. N. Tan, M. Matsuura, and N. Kishi, “Waveform conversion and wavelength multicasting with pulsewidth tunability using Raman amplification multiwavelength pulse compressor,” *IEICE Trans. on Electron.*, vol. E98-C, no. 8, pp. 824–831, Aug. 2015.
- [78] S. Ferber, R. Ludwig, C. Boerner, A. Wietfeld, B. Schmauss, J. Berger, C. Schubert, G. Unterboersch and H.G. Weber, “Comparison of DPSK

- and OOK modulation format in 160 Gbit/s transmission system,” *Electron. Lett. 2nd*, vol. 39, no. 20, Oct. 2003.
- [79] A. H. Gnauck and P. J. Winzer, “Optical phase-shift-keyed transmission,” *J. Lightwave Technol.*, vol. 23, no. 1, pp. 115–130, 2005.
- [80] W. A. Atia and R. S. Bondurantet, “Demonstration of return-to-zero signaling in both OOK and DPSK formats to improve receiver sensitivity in an optically preamplified receiver,” in *Proced. IEEE Lasers and Electro-Optics Society 12th Annual Meeting*, TuM3, vol. 1, 1999.
- [81] A. H. Gnauck, S. Chandrasekhar, J. Leuthold, and L. Stulz, “Demonstration of 42.7-Gb/s DPSK receiver with 45 photons/bit sensitivity,” *IEEE Photon. Technol. Lett.*, vol. 15, no. 1, pp. 99–101, Jan. 2003.
- [82] C. Xu, X. Liu, and X. Wei, “Differential phase-shift keying for high spectral efficiency optical transmissions,” *IEEE J. Sel. Topic in Quant. Electron.*, vol. 20, no. 2, pp. 281–293, 2004.
- [83] A. H. Gnauck and P. J. Winzer, “Optical phase-shift-keyed transmission,” *J. Lightwave Technol.*, vol. 23, no. 1, pp. 115–130, Jan. 2005.
- [84] F. Zhang, C.-A. Bunge, and K. Petermann, “Analysis of nonlinear phase noise in single-channel return-to-zero differential phase-shift keying transmission systems,” *Optic Lett.*, vol. 31, no. 8, pp. 1038–1040, Apr. 2006.
- [85] X. Liu, “Nonlinear effects in phase shift keyed transmission,” Optical Fiber Communication Conference (OFC), ThM4, Feb. 2004.
- [86] A. Hasegawa and Y. Kodama, “Guiding-center soliton in optical fibers,” *Opt. Lett.*, vol. 15, no. 24, pp. 1443–1445, Dec. 1990.
- [87] K.-P. Ho, *Phase-Modulated Optical Communication System*, Springer Science Business Media, Technology Engineering, 2005.



## REFERENCES

---

- [88] P. V. Mamyshev and N. A. Mamysheva, "Pulse-overlapped dispersion-managed data transmission and intrachannel four-wave mixing," *Opt. Lett.*, vol. 24, no. 21, pp. 1454–1456, Nov. 1999.
- [89] X. Wei and X. Liu, "Analysis of intrachannel four-wave mixing in differential-phase-shift-keyed transmission with large dispersion," *Opt. Lett.*, vol. 28, no. 23, pp. 2300–2302, Dec. 2003.
- [90] F. Zhang, C.-A. Bunge, and K. Petermann, "Analysis of nonlinear phase noise in single-channel return-to-zero differential phase-shift keying transmission systems," *Optic Lett.*, vol. 31, no. 8, pp. 1038–1040, Apr. 2006.
- [91] X. Liu, "Nonlinear effects in phase shift keyed transmission," *Optical Fiber Communication Conference (OFC)*, ThM4, Feb. 2004.
- [92] H. Kim and A. H. Gnauck, "Experimental investigation of the performance limitation of DPSK systems due to nonlinear phase noise," *IEEE Photon. Technol. Lett.*, vol. 15, no. 2, pp. 320–322, Feb. 2003.
- [93] T. T. Lee, "Nonblocking copy networks for multicast packet switching," *IEEE J. Sel. Areas Commun.*, vol. 6, no. 9, pp. 1455–1467, Dec. 1988.
- [94] R. K. Pankaj, "Wavelength requirements for multicasting in all-optical networks," *IEEE/ACM Trans. Netw.*, vol. 7, no. 3, pp. 414–424, Jun. 1999.
- [95] W. Wang, L. G. Rau, and D. J. Blumenthal, "160 Gb/s variable length packet/10 Gb/s-label all-optical label switching with wavelength conversion and unicast/multicast operation," *J. Lightw. Technol.*, vol. 23, no. 1, pp. 211–218, Jan. 2005.
- [96] L. Gong, X. Zhou, X. Liu, "Efficient resource allocation for all-optical multicasting over spectrum-sliced elastic optical networks," *Optical Communications and Networking*, vol. 5, no. 8, pp. 836–847, Aug. 2013.

- 
- [97] F. Zhang, W.D. Zhong, Z. Xu, T.H. Cheng, C. Michie, and I. Andonovic, "A broadcast/multicast-capable carrier-reuse WDM-PON," *J. Lightwave Technol.*, vol. 29, no. 15, pp. 2276-2284, Aug. 2011.
- [98] W. Lim, Y. Yang, and M. Milosavljevic. "Multicast polling for 10G-EPON," *Electron. Lett.*, vol. 48, no. 9, pp. 513-514, Apr. 2012.
- [99] Y. Wang, C. Yu, T. Luo, L. Yan, Z. Pan, and A. E. Willner, "Tunable all-optical wavelength conversion and wavelength multicasting using orthogonally polarized fiber FWM," *J. Lightwave Technol.*, vol. 23, no. 10, pp. 3331-3338, 2005.
- [100] G. Contestabile, N. Calabretta, R. Proietti, and E. Ciaramella, "Double-stage cross-gain modulation in SOAs: an effective technique for WDM multicasting," *IEEE Photon. Technol. Lett.*, vol. 18, no. 1, pp. 181-183, Jan. 2006.
- [101] N. Yan, T. Silveira, A. Teixeira, A. Ferreira, E. Tangdiongga, P. Monteiro and A. M. J. Koonen, "40Gbit/s wavelength multicast via SOA-MZI and applications," *Electron. Lett.* vol. 43, no. 23, pp. 1300-1302, 2007.
- [102] G. Contestabile, M. Presi, and E. Ciaramella, "Multiple wavelength conversion for WDM multicasting by FWM in an SOA," *IEEE Photon. Technol. Lett.*, vol. 16, no. 7, pp. 1775-1777, 2004.
- [103] G. Contestabile, N. Calabretta, M. Presi, and E. Ciaramella, "Single and multicast wavelength conversion at 40 Gb/s by means of fast non-linear polarization switching in an SOA," *IEEE Photon. Technol. Lett.*, vol. 17, no. 12, pp. 2652-2654, Dec. 2005.
- [104] K. K. Chow, C. Shu., "All-optical wavelength conversion with multicasting at 6x10Gbit/s using electroabsorption modulator," *Electron. Lett.*, vol. 39, no. 19, pp. 1395-1397, Sept. 2003.

## REFERENCES

---

- [105] Z. Q. Hui, J. G. Zhang, "All-optical wavelength multicasting exploiting cross-phase modulation in a dispersion-flattened nonlinear photonic crystal fiber," *Laser Physics*, vol. 21, no. 3, pp. 512-518, Mar. 2011.
- [106] I. Ismail, Q. Nguyen-The, M. Matsuura, and N. Kishi, "One-to-six wavelength multicasting of RZ-OOK based on picosecond-width-tunable pulse source with distributed Raman Amplification," *IEICE Trans. on Electron.*, vol. E98-C, no. 8, pp. 816-822, Aug. 2015.
- [107] M. Matsumoto and K. Sanuki, "Performance improvement of DPSK signal transmission by a phase-preserving amplitude limiter," *J. of Opt. Express*, vol. 16, no. 15, pp. 11169-11175, Jun. 2008.
- [108] G. -W. Lu, K. S. Abedin, T. Miyazaki, and M. E. Marhic, "RZ-DPSK OTDM demultiplexing using fibre optical parametric amplifier with clock-modulated pump," *Electron. Lett.*, vol. 45, no. 4, pp. 221-222, Feb. 2009.
- [109] C. -S. Bres, A. O. J. Wiberg, B. P.-P. Kuo, J. M. Chavez-Boggio, C. F. Marki, N. Alic, and S. Radic "Optical demultiplexing of 320 Gb/s to 8 40 Gb/s in single parametric Gate," *J. Lightwave Technol.*, vol. 28, no. 4, pp. 434-441, Feb. 2010.
- [110] R. Morais, R. Meleiro, P. Monteiro, P. Marques, "TDM-to-WDM conversion based on wavelength conversion and time gating in a single optical gate," in *Proc. Optical Fiber Communication Conference (OFC08)*, OTuD5, Feb. 2008.
- [111] Y. Awaji, T. Miyazaki, F. Kubota, "40 Gb/s WDM-multicasting wavelength conversion from 160Gb/s OTDM signal," *Optical Networks and Technologies*, Springer, pp. 292-298, 2005.
- [112] Z. -Q. Hui and J. -G. Zhang, "Wavelength conversion, time demultiplexing and multicasting based on cross-phase modulation and four-wave

- mixing in dispersion-flattened highly nonlinear photonic crystal fiber,” *J. Opt. A: Pure and Applied Opt.*, vol. 14, pp. 1–8, May 2012.
- [113] M. V. Drummond, A. L. J. Teixeira, P. P. Monteiro, and R. N. Nogueira<sup>1</sup>, “Flexible OTDM-to-WDM converter enabled by a programmable optical processor,” *Opt. Express.*, vol. 20, no. 2, pp. 1783–1789, Jan. 2012.
- [114] M. J. Guy, S. V. Chernikov, J. R. Taylor, “A duration-tunable, multiwavelength pulse source for OTDM and WDM communications systems,” *IEEE Photon. Technol. Lett.*, vol. 9, no. 7, pp. 1017-1019, Jul. 1997.
- [115] I. Y. Khrushchev, J. D. Bainbridge, J. E. A. Whiteaway, I. H. White, and R. V. Penty, “Multiwavelength pulse source for OTDM/WDM applications based on arrayed waveguide grating,” *IEEE Photon. Technol. Lett.*, vol. 11, no. 12, pp. 1659-1661, Dec. 1999.
- [116] Y. Takushima and K. Kikuchi, “10-GHz, over 20-channel multiwavelength pulse source by slicing super-continuum spectrum generated in normal-dispersion fiber,” *IEEE Photon. Technol. Lett.*, vol. 11, no. 3, pp. 322-324, Mar. 1999.
- [117] St. Fischer, M. Duelk, M. Puleo, R. Girardi, E. Gamper, W. Vogt, W. Hunziker, E. Gini, and H. Melchior, “40-Gb/s OTDM to 4x10 WDM conversion in monolithic InP Mach-Zehnder interferometer module,” *IEEE Photon. Technol. Lett.*, vol. 11, no. 10, pp. 1262-1264, Oct. 1999.
- [118] B. S. Robinson, S. A. Hamilton, and E. P. Ippen, “Multiple wavelength demultiplexing using an ultrafast nonlinear interferometer,” in *Proc. Conference on Lasers and Electro-Optics (CLEO01)*, CThU5, May 2001.

## REFERENCES

---

# Publications

## Journal Papers related to this thesis

1. **Q. Nguyen Quang Nhu**, Q. Nguyen-The, H. Nguyen Tan, M. Matsuura, and N. Kishi, “Waveform conversion and wavelength multicasting with pulsewidth tunability using Raman amplification multiwavelength pulse compressor,” **IEICE Transaction on Electronics**, vol. E98-C, no. 8, pp. 824–831, Aug. 2015.
2. **Q. Nguyen Quang Nhu**, H. Nguyen Tan, Q. Nguyen-The, M. Matsuura, and N. Kishi, “Performance of an inline RZ-DPSK pulse compression using Raman amplifier and its application in OTDM tributary,” **IEICE Transaction on Electronics**, vol. E99-C, no. 2, pp. 227–234, Feb. 2016.

## Other Journal Papers

3. **Q. Nguyen Quang Nhu**, and T. Nguyen Van, “Proposing the design methods of logical topologies with consideration both Traffic Demand and hop Count of Physical Route in IP over WDM Networks”, **Journal of Science and Technology of The University of Danang**, no. 4[39], pp. 201–207, 2010.

### International Conference Papers

4. **Q. Nguyen Quang Nhu**, Q. Nguyen-The, H. Nguyen Tan, M. Matsuura, and N. Kishi, “All-optical waveform sampling using Raman amplification multiwavelength compressor,” **19th OptoElectronics and Communications Conference (OECC 2014)**, TUPS1-17, Australia, Jul. 2014.
5. **Q. Nguyen Quang Nhu**, Q. Nguyen-The, H. Nguyen Tan, M. Matsuura, and N. Kishi, “All-optical waveform sampling based on four wave mixing in a highly nonlinear fiber,” **Triangle Symposium on Advanced Information and Communication Technologies (ICT) 2014 (TriSAI 2014)**, Beijing, China, Sept. 2014.
6. **Q. Nguyen Quang Nhu**, Q. Nguyen-The, H. Nguyen Tan, M. Matsuura, and N. Kishi, “Parametric NRZ-to-RZ wavelength multicasting with pulsewidth tunability using Raman amplification multiwavelength pulse compressor,” **International Topical Meeting on Microwave Photonics/The 9th Asia-Pacific Microwave Photonics Conference 2014 (MWP/APMC 2014)**, TuEG-10, Sapporo, Japan, Oct. 2014.
7. **Q. Nguyen Quang Nhu**, Q. Nguyen-The, H. Nguyen Tan, M. Matsuura, and N. Kishi, “Wavelength multicasting of RZ-DPSK signal with tunable pulsewidth using Raman amplification pulse compressor,” **The 21st Asia-Pacific Conference on Communications 2015 (APCC 2015)**, 14-AM2-C.3, Kyoto, Japan, Oct. 2015.
8. Q. Nguyen-The, **Q. Nguyen Quang Nhu**, M. Matsuura, and N. Kishi, “All-optical OTDM-to-WDM conversion based on cross phase modulation in highly nonlinear fiber,” **19th OptoElectronics and Communications Conference (OECC 2014)**, TUPS1-18, Australia, Jul. 2014.
9. **Q. Nguyen Quang Nhu**, and T. Nguyen Van, “The design methods for logical topologies with consideration both traffic demand and hop count of physical route in IP over WDM networks”, **The 3rd International Conference on Communications and Electronics (ICCE)**, no. 978-1, pp. 51–55, Vietnam, 2010.

**IEICE Society Domestic Conference Paper**

**10. Q. Nguyen Quang Nhu, Q. Nguyen-The, H. Nguyen Tan, M. Matsuura, and N. Kishi** All-optical 410 Gb/s, “Ultra-short pulsewidth NRZ-to-RZ format conversion and wavelength multicasting using Raman amplifier muliwavelength pulse compressor,” **The Institute of Electronics, Information and Communication Engineers (IEICE) General Conference**, Japan, Mar. 2014.





# Curriculum Vitae

Mrs. Nguyen Quang Nhu Quynh was born in 1979. She received B.E. degree from Danang University of Technology, Danang, Vietnam in 2002, and M.E. degree from the University of Danang, Vietnam, in 2008. From 2003 to 2012, she joined the Faculty of Electronic and Telecommunication, Danang University of Technology, Danang, Vietnam as a Lecturer. She came to Japan for graduate studies at the University of Electro-Communications, Tokyo under Japanese Government (Monbukagakusho) Scholarship from April, 2012. Her present research is on all-optical signal processing technologies using nonlinearities. She received the Excellent Student Award from the University of Danang and Samsung scholarship from Samsung, electronic company in 2008 for the research achievement and the highest Grade Point Average (GPA) during M.E. study, respectively. Mrs. Quynh is a Student Member of the IEICE Communications Society. She is currently a Ph.D. student at the Department of Communication Engineering and Informatics, the University of Electro-Communications, Tokyo, Japan. She is a daughter of Nguyen Van Tao and Tran Thi Khanh. She is married to Huynh Hung Nam and has two daughters, Huynh Quynh Anh and Huynh Nguyen Minh Ngoc.